AN ABSTRACT OF THE DISSERTATION OF

Joseph Duggan Maurer for the degree of Doctor of Philosophy in Statistics presented on August 31, 2017.

Title: Turbine Induced Bird and Bat Fatalities at Wind Projects: Statistical Methods for Mortality Estimation Using Road and Pad Carcass Surveys

Abstract approved: _____

Claudio Fuentes Lisa Madsen

Turbines at wind projects pose a threat to birds and bats flying at altitudes within the rotor swept area. These animals die from colliding with the turbine blades. Estimating mortality, or the total number of bird or bat fatalities at a wind project, is critical to understanding environmental impacts of wind energy, and potential population effects to at-risk species.

Mortality is estimated by conducting carcass surveys, and then adjusting observed counts for carcasses that land outside the searched area, carcasses removed by scavengers, and imperfect detection. The goal of this research is to assess if and when mortality estimation can be achieved by only searching the roads that lead up to turbines and pads beneath turbines (R&P).

Accounting for unsearched area, or equivalently estimating the proportion of carcasses that land on R&P, is pivotal to the success of mortality estimation from R&P

searches. Methods based on previously proposed ideas to account for unsearched area are tested and compared using simulations to determine what situations and methods are the most appropriate for mortality estimation based on R&P carcass surveys under different spatial carcass distributions. Results of the simulations are utilized to develop an estimator of mortality based on R&P searches under isotropic carcass distributions. The theoretical properties of the estimator are derived, and utilized for standard error calculation and confidence interval creation. Because optimal methods differ for isotropic and anisotropic spatial carcass distributions, a hypothesis test is needed to determine if it is valid to assume an isotropic distribution.

Turbine Induced Bird and Bat Fatalities at Wind Projects: Statistical Methods for Mortality Estimation Using Road and Pad Carcass Surveys

by

Joseph Duggan Maurer

A DISSERTATION

submitted to

Oregon State University

in partial fulfillment of
the requirements for the
degree of

Doctor of Philosophy

Presented August 31, 2017
Commencement June 2018

Doctor of Philosophy dissertation of Joseph Duggan Maurer presented on August 31, 2017.

APPROVED:

Co-Major Professor, representing Statistics

Co-Major Professor, representing Statistics

Chair of the Department of Statistics

Dean of the Graduate School

I understand that my dissertation will become part of the permanent collection of Oregon State University libraries. My signature below authorizes release of my dissertation to any reader upon request.

Joseph Duggan Maurer, Author

ACKNOWLEDGEMENTS

I would like to take this opportunity to extend my gratitude and appreciation to everyone in the Oregon State Statistics Department that made this Ph.D. dissertation possible, my parents for their endless patience throughout my educational career, and my wife for her persistent support of my academic pursuit.

TABLE OF CONTENTS

TABLE OF CONTENTS (Continued)

LIST OF FIGURES

LIST OF FIGURES (Continued)

LIST OF FIGURES (Continued)

LIST OF FIGURES (Continued)

LIST OF TABLES

LIST OF TABLES (Continued)

LIST OF TABLES (Continued)

Turbine Induced Bird and Bat Fatalities at Wind Projects: Statistical Methods for Mortality Estimation Using Road and Pad Carcass Surveys

1 Introduction

1.1 Background

The report *Wind Vision: A New Era for Wind Power in the United States* (U.S. Department of Energy [2015]) outlines a course of action that increases the share of national end-use electricity generated by wind power to 35% by 2050. America relied on fossil fuels to produce 65.1% of the consumed electricity in 2016, while wind accounted for 5.6% (Table 1.1). In 2013, wind was credited with a range of environmental benefits including reductions in carbon dioxide by 115 billion metric tons; sulfur dioxide by

Table 1.1: Sources for national end-use electricity generation in the United States for 2016 (U.S. Department of Energy [2017]).

Source	2016 Share (%)	Source	2016 Share (%)
Fossil Fuels	65.1	Coal	30.4
		Natural Gas	33.8
		Petroleum	0.6
		Other	0.3
Nuclear	19.7	Nuclear	19.7
Renewable	14.8	Hydro	6.4
		Wind	5.6
		Biomass	1.5
		Solar	0.9
		Geothermal	0.4
Other	0.4	Other	0.4

157,000 metric tons; nitrous oxide by 97,000 metric tons; and water consumption by 36.5 billion gallons (U.S. Department of Energy [2015]).

Wind energy undeniably offers environmental benefits, especially when compared to current practices with fossil fuels; however, it is not free of environmental costs. Early wind projects, such as Altamont Pass, were constructed in the 1980s, and soon after the risk posed to raptors and other flying vertebrates was recognized (Howell and DiDonato [1991]). Today, wind turbine induced bird and bat fatalities are well documented in the literature (Kunz et al. [2007b], Arnett et al. [2008]), and post construction monitoring at wind projects is recommended for a minimum of one year to assess impacts on bird and bat populations (U.S. Fish and Wildlife Service [2012]).

Ecologists, statisticians, industry and policy makers are working together to estimate, understand, and reduce bird and bat fatalities at wind projects. Statistics is directly applied in this field when estimating mortality, the total number of turbine induced bird or bat fatalities at a wind project during a specified period (Shoenfeld [2004], Huso [2010], Korner-Nievergelt et al. [2011]). The purpose of this thesis is to identify the necessary conditions, and appropriate methods for mortality estimation using data from carcass surveys performed entirely on roads leading up to turbines and pads beneath turbines (R&P).

Section 1.2 discusses traditional mortality estimation methods. Section 1.3 discusses the potential advantages of estimating mortality based on data collected on roads and pads and provides a general outline of the chapters that follow.

1.2 Mortality Estimation

Integrated detection systems with vibration and visual surveillance methods designed for monitoring bird and bat activity and collisions with turbine blades and tower in real time have made advancements in the past decades (Kunz et al. [2007a], Suryan et al. [2016]), but have not been implemented or proven reliable for estimating mortality of all species of interest. Typically, mortality is estimated from data collected during ground searches, where human observers search predetermined areas at specific time intervals for carcasses (Gauthreaux [1995], U.S. Fish and Wildlife Service [2012]). Counts obtained from carcass surveys are extrapolated using an estimator to account for imperfect detection, carcasses carried off by scavengers, and unsearched areas (Huso [2010], Korner-Nievergelt et al. [2011]).

Searcher efficiency refers to the conditional probability that a searcher observes a carcass in the searched area, given it is present when the search is conducted. This quantity is commonly estimated using a binomial trial, where carcasses are placed in the field and searcher efficiency is estimated by the number of observed carcasses divided by total number of available carcasses (Wobeser and Wobeser [1992]). Morrison [2002] noted that studies often account for this quantity changing with the size of the animal; however, many studies neglect that searcher efficiency can be a function of vegetation types and height, time of year, weather conditions, and characteristics of the searcher such as eyesight, physical ability, training, or interest in the study. Failing to account for biases in the probability of detection can lead to biased results. Researchers such as Korner-Nievergelt et al. [2013] account for all of these factors by conducting searcher

efficiency trials throughout the entire searched area during the duration of the study.

Estimates of mortality must also account for carcass persistence, or the amount of time a carcass remains observable after falling into the searched area. Carcasses become unobservable if carried off by scavengers, buried by a plow, or decomposed past recognition (Morrison [2002]). Methods used to estimate carcass persistence differ between studies (Bispo et al. [2013]), but share the basic premise of placing carcasses in the field and monitoring until they become unobservable or until the pre-determined end of the study (Wobeser and Wobeser [1992]). Some authors (Kerlinger [2002], Anderson et al. [2004]) estimate the probability that a carcass persists during the interval between searches, by placing carcasses in the field and observing how many remain at the end of an interval. Under the assumption that a fatality is equally likely to occur any day between searches, Jain et al. [2007] estimated the probability a carcass persists through half the interval between searches. Some authors (Johnson et al. [2003], Erickson et al. [2004]) examine carcasses daily to estimate the average persistence time with the maximum likelihood estimate assuming persistence follows an exponential distribution with non-censored and right-censored observations.

Bispo et al. [2013] observed that carcass persistence is the time to an event and thus a classic survival analysis application. The estimator proposed by Huso [2010] assumes an exponential survival model for persistence, and can be adapted for any parametric survival model (e.g. Weibull, log-logistic, log-normal, etc.). The Huso [2010] estimator can also be applied using a non-parametric survival model (Kaplan and Meier [1958]) as long as the persistence trials are longer than the time between searches or conducted until less than 1% of the trial carcasses remain. Bispo et al. [2013] outlines a method to decide

which parametric model provides the best fit, and provides evidence that persistence can depend on carcass size and time of year.

Adjusting for searcher efficiency and persistence allows extrapolation of carcass counts to mortality in the searched area, but in order to obtain an estimate of mortality for the entirety of the project researchers must account for unsearched areas. Under ideal circumstances, researchers can take a representative random sample of turbines, search the entirety of the fall zone of the sampled turbines, and extrapolate to the entire project or report the estimated number of fatalities per turbine. Thick vegetation, crop fields, dangerous steep terrain, rivers or lakes sometimes result in unsearched areas forcing researchers to estimate the proportion of carcasses that fell into searched areas at sampled turbines. Some researchers have achieved this by dividing the estimated number of carcasses in the searched area by the proportion of area searched (Gruver et al. [2009], Drake et al. [2012]). Jain [2005] partitioned the area under turbines into ten meter concentric annuli, divided the number of observed carcasses in each annulus by the percentage of its area searched and summed. In a study at Fowler Ridge, located on a corn and soy farm, Good et al. [2011] searched the road and pad of 100 turbines and removed the vegetation at an additional nine turbines to employ a ratio estimator of mortality (Lohr [2009]). Huso and Dalthorp [2014] proposed modeling the carcass distribution with a generalized linear model and dividing the estimated mortality in the searched area by the proportion of carcasses expected to fall into the searched area.

Searcher efficiency, carcass persistence, and unsearched areas must be accounted for when estimating mortality from ground searches. Statistically based methods have been, and continue to be, developed in order to get the most accurate and precise estimates

possible, making statistics a vital part of inference on mortality at wind projects.

1.3 Mortality Estimation from Road and Pad Surveys

Previously proposed methods (Jain [2005], Good et al. [2011], Huso and Dalthorp [2014]) designed to account for areas that go unsearched during a carcass survey can be utilized to estimate mortality at an individual wind project based primarily, or solely, from data collected on roads leading to turbines and pads beneath turbines associated with erection and construction (R&P). R&P searches are attractive from both a statistical and implementation perspective, and may be capable of producing more desirable results than the traditional method of sampling turbines and searching an area of predetermined size.

Searcher efficiency is often maximized on R&P (Kerns et al. [2005], Good et al. [2012]). Higher searcher efficiency decreases variability in mortality estimates, so estimates based on R&P have potential to be more precise relative to searches conducted on an equivalent amount of area obtained by searching the entirety of some turbines and adjusting for visibility classes (e.g. road, grass, thick vegetation, etc.).

R&P searches only require researchers to conduct searcher efficiency and carcass persistence trials in a single visibility class instead of several. This would increase the number of trial carcasses that can be used to estimate the probability (G) a carcass is observed given it landed on R&P. As the number of trial carcasses for a single visibility class increases, so does the precision in the estimate of G, leading to less variability in mortality estimates.

Estimation from R&P searches may also increase the precision of mortality estimates by mitigating or eliminating sampling variability derived from variation in fatality rates at individual turbines, which has been observed by some researchers (Arnett et al. [2008]). For instance, at Mountaineer and Meyersdale facilities where turbines are arranged in linear arrays, Kerns et al. [2005] found higher fatality rates at the end or center of arrays at both sites. While the results were not statistically significant, Fiedler et al. [2007] observed the estimated average fatalities per turbine at Buffalo Mountain facilities was highest along the northernmost ridge ($\bar{x} = 29.0$) and lowest along the southernmost ridge ($\bar{x} = 11.6$). R&P searches would lower the area searched at individual turbines, allowing more turbines to be sampled or potentially censused, assisting with sampling challenges posed by turbine to turbine variation.

A R&P search protocol also allows researchers to extend the searched area further from the turbine without extravagant increases in resources. Configurations of searched areas vary greatly between studies (Hull and Muir [2010], Huso and Dalthorp [2014]), with square or circular plots used most commonly (Gauthreaux [1995], U.S. Fish and Wildlife Service [2012]). When using square or circular plots, increases in the maximum linear distance searched from the turbine increases the total area searched at a squared rate. Under this circumstance, searching past the maximum distance a carcass can land from the turbine is costly, but not searching far enough can induce bias. Under a R&P search protocol, increasing the maximum distance searched will likely correspond to a linear increase in area searched as long as the width of the roads remains constant with distance from the turbine. So, increasing the maximum distance searched under a R&P search protocol may entail a trivial increase in resources while eliminating bias from not

searching far enough.

In principle, a R&P search protocol possesses many desirable properties, but the critical question is whether mortality can be accurately and precisely estimated from data primarily, or solely, collected on roads and pads. Chapter 2 addresses this question by comparing methods based on the ideas of the models proposed by Jain [2005], Good et al. [2011], and Huso and Dalthorp [2014]. These methods account for unsearched areas by estimating the probability a carcass lands within the searched area. Through the use of a simulation the methods are evaluated and compared on their performance in estimating the probability a carcass lands on R&P under various wind project R&P configurations, average carcass per turbine rates, spatial carcass distributions, and search protocols. In Chapter 3, the results of the simulations are utilized to develop an estimator of mortality based on R&P carcass surveys, along with the theoretical properties of the estimator and methods for calculating the standard error and confidence intervals. In Chapter 4, novel methods for identifying and accounting for unsearched areas under anisotropic spatial carcass distributions are proposed and compared via simulations. Chapter 5 concludes the thesis with a discussion of the findings, limitations of R&P surveys, and future research.

2 Adjusting Mortality Estimates for Unsearched Areas Under a Road and Pad Search Protocol

2.1 Introduction

When estimating mortality, the total number of turbine-induced bird and bat fatalities at a wind project during a specified period, researchers adjust the number of carcasses observed by the proportions expected to fall in the searched area (Jain [2005], Huso and Dalthorp [2014]), persist scavenged (Bispo et al. [2013]), and be discovered by a searcher (Wobeser and Wobeser [1992]). This chapter focuses on methods used to adjust for unsearched areas to develop estimators of mortality based on data primarily, or solely, collected on roads leading to the turbines and pads beneath the turbines associated with erection and construction (R&P).

Accurate estimation of mortality from R&P searches requires accounting for the unsearched area (i.e. non-R&P). Therefore, the performance of a mortality estimator based on R&P searches hinges on its ability to accurately estimate the probability (a) a carcasses lands on R&P. Rather than developing a novel method for estimating a, four methods were examined that have been proposed in public reports and peer reviewed journals to account for areas within the fall distribution of carcasses, but outside of the searched area.

In Section 2.2 the previously suggested methods of adjusting for unsearched areas

are introduced. Section 2.3 outlines the simulations used to compare the methods. The results are provided in Section 2.4, and a general conclusion is given in Section 2.5.

2.2 Adjusting for Unsearched Areas

Some authors (Gruver et al. [2009], Drake et al. [2012]) account for unsearched areas by simply dividing the estimated mortality in the searched area by the proportion of area searched. Under this method the estimate for the probability (a) a carcass lands in the searched area, is the raw proportion of area searched within the assumed fall zone. Huso and Dalthorp [2014] refer to this technique as the naïve estimator and point out this approach is only valid if the carcass density is uniform and the fall zone is known exactly, "an implausible assumption when turbine-induced mortality occurs." It is widely accepted that carcass density decreases with distance (Figure 2.1). Therefore, any method used to account for unsearched area must take into account the relationship between carcass density and distance.

Jain [2005] accounted for the relationship between density and distance by partitioning the area beneath turbines into concentric annuli, ten meters wide. For each annulus (indexed by i), the number of observed carcasses (C_i) and proportion (A_i) of area searched are used to estimate mortality (M) as

$$\widehat{M} = \frac{1}{\hat{G}} \sum_i \frac{C_i}{A_i}, \tag{2.1}$$

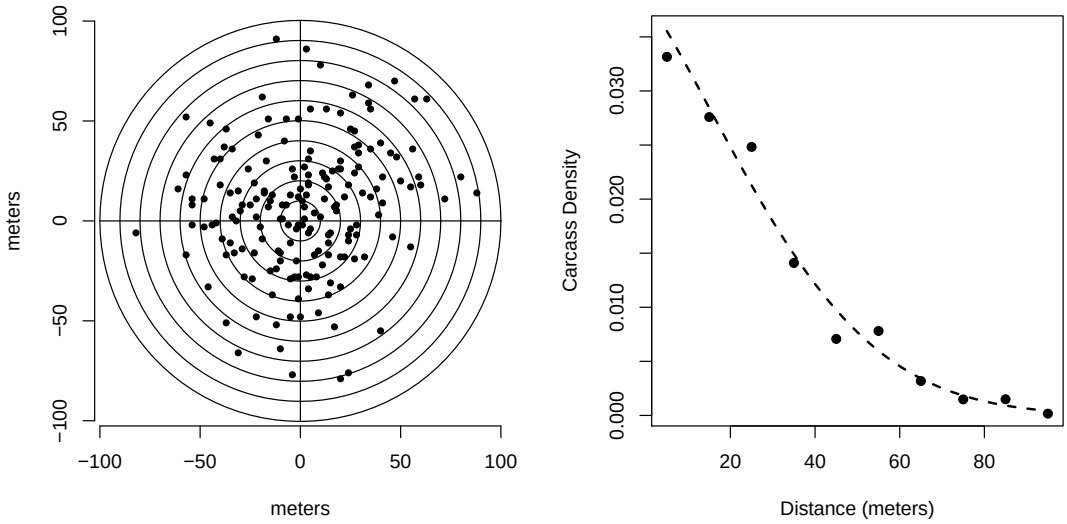

Figure 2.1: (Left) Location of 182 carcasses with respect to the nearest turbine observed from data collected from April to November of 2013 at an anonymous wind project in Ohio. (Right) Observed and estimated carcass density for each annulus. Poisson regression was used to obtain the fitted curve assuming the log mean carcass density follows a quadratic function of distance.

where $\hat{G}$ is the estimated probability that a carcass is observed, given it landed in the searched area; a function of both searcher efficiency and carcass persistence; and assumed constant across annuli. Unlike the other methods of accounting for unsearched areas described below, the estimator proposed by Jain [2005] estimates mortality (M) directly. Assuming searches were conducted to the maximum distance a carcass can land from the turbine, the estimate of a can still be obtained as

$$\hat{a} = \frac{\frac{C}{\hat{G}}}{\hat{M}} = \frac{C}{\sum_i \frac{C_i}{A_i}}, \tag{2.2}$$

where C ($= \sum_i C_i$) is the total number of observed carcasses. Note that (2.2) is independent of G.

Jain developed this method with guidance from the statistics department at Iowa State University (personal communication). This model accounts for the relationship between carcass density and distance empirically by allowing carcass density to differ by distance, but assumes carcass density is homogeneous within a ten meter annulus. This assumption is an improvement to the naïve estimator, but still questionable considering the rate that density decreases between 40 and 70 meters in Figure 2.1 (Right).

Results in Chapter 3 show that under a set of conditions (2.2) produces unbiased estimates of a. One of those conditions is homogeneous carcass density within an annulus. For reasons discussed in Chapter 3, this assumption becomes more reasonable if the area of individual annuli is decreased. The *cake* method utilizes the same approach to account for unsearched areas as Jain [2005], with annuli that have a one meter difference between inner and outer radii instead of ten meters. $\widehat{M}_{cake}$ and $\hat{a}_{cake}$ are given by (2.1) and (2.2) where the annuli, indexed by i, have one meter buffers. The name "cake" is given because this method divides the fall zone into annuli or rings. Rings closest to the turbine tend to have the highest density of carcasses, yielding a wedding cake appearance when plotted in three dimensions.

Huso and Dalthorp [2014] proposed accounting for unsearched areas by modeling the spatial distribution of carcasses with a generalized linear model (glm). This can be achieved by partitioning the area beneath turbines into one meter square cells indexed by the distance, r, and direction, θ, from the nearest turbine (Figure 2.2).

Huso and Dalthorp [2014] introduced their method using logistic regression. Warton

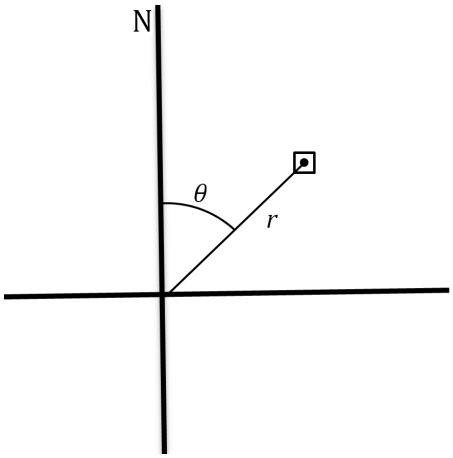

Figure 2.2: Example of a single cell in the partition of the fall zone under the *glm* method proposed by Huso and Dalthorp [2014]. Cells are index by the distance (r) from the turbine and the angle (θ), clockwise from due north.

et al. [2010] demonstrated that a Poisson point process model produces similar coefficient estimates and standard errors as a logistic regression when modeling presence-only data as long as the grid used to fit the models is sufficiently dense. Presence-only data refers to data consisting only of observations of the organism but with no reliable data on where the species was not found (Pearce and Boyce [2006]). Observations from ground searches at wind facilities qualifies as presence-only data, because surveys only provide information on where carcasses were found. Due to imperfect detection, it cannot be concluded that carcasses were absent from any location. In the simulations described in Section 2.3, a one-meter dense grid was used, and results for the logistic and Poisson regression models were similar. The Poisson model is advantageous in this setting as it allows for more than one carcass to occupy a grid cell.

The method to account for unsearched areas developed by Huso and Dalthorp [2014]

in the context of a Poisson process model assumes the number of observed carcasses in a grid cell ($C_{r,\theta}$) follows a Poisson distribution with mean $\lambda_{r,\theta}$ modeled as a function of distance from the turbine,

$$C_{r,\theta} \sim \text{Poisson}(\lambda_{r,\theta}) \qquad \log(\lambda_{r,\theta}) = \beta_0 + \beta_1 r + \beta_2 r^2 + \log(O_{r,\theta}),$$

where $O_{r,\theta}$ is the offset for the cell indexed by (r,θ), and is equal to the number turbines where that cell is searched. The fitted Poisson regression model can be utilized to estimate the spatial carcass distribution, $\hat{f}(r,\theta)$, as

$$\hat{f}(r,\theta) = \frac{\exp(\hat{\beta}_0 + \hat{\beta}_1 r + \hat{\beta}_2 r^2)}{\sum_{r,\theta} \exp(\hat{\beta}_0 + \hat{\beta}_1 r + \hat{\beta}_2 r^2)}. \tag{2.3}$$

The estimate of a is obtained by integrating $\hat{f}(r,\theta)$ over the searched area. When a one meter dense grid is used, the integral can be calculated numerically as

$$\hat{a}_{glm} = \sum_{r,\theta} \hat{f}(r,\theta) \frac{O_{r,\theta}}{T}, \tag{2.4}$$

where T is the total number of turbines at the wind facility. Given the estimated proportion of carcasses that land on R&P, mortality is estimated as

$$\widehat{M}_{glm} = \frac{\frac{C}{\hat{G}}}{\hat{a}_{glm}}. \tag{2.5}$$

Good et al. [2011] used ratio estimation (Lohr [2009]) at Fowler Ridge Wind Farm in Indiana to account for unsearched areas. The roads and pads (R&P) of 109 turbines were

searched, and then a square, 80x80 meter plot was cleared of vegetation and searched at nine of the 109 turbines. Assuming the proportion of carcasses that fall on the R&P is similar for each of the 109 turbines, a is estimated using the number of observed carcasses on R&P and non-R&P at cleared turbines ($C_{R\&P,clr}$ and $C_{nonR\&P,clr}$), and the probability a carcass is observed given it landed on R&P or non-R&P (G and G_{clr}), as

$$\hat{a}_{ratio} = \frac{\frac{C_{RP,clr}}{\hat{G}}}{\frac{C_{RP,clr}}{\hat{G}} + \frac{C_{nonRP,clr}}{\hat{G}_{clr}}}. \tag{2.6}$$

Similar to the glm estimator, the ratio estimator estimates mortality with

$$\widehat{M}_{ratio} = \frac{\frac{C}{\hat{G}}}{\hat{a}_{ratio}}, \tag{2.7}$$

where C is the total number of carcasses observed on R&P.

2.3 Simulations

Simulations were used to evaluate the performance of the cake, glm, and ratio methods presented in Section 2.3. The simulations were designed to (1) determine if mortality estimation of turbine induced bird and bat fatalities is possible based on data collected primarily or solely on R&P, (2) understand what conditions influence the accuracy and precision of each method, and (3) compare the methods to each other. Simulations considered two R&P configurations of actual wind projects, four carcass rates per turbine, four spatial carcass distributions, and three search protocols differing by the maximum

distance searched.

Simulations were performed in R 3.2.0 (R Core Team [2015]). 1000 trials were performed for every combination of settings. Each trial simulated a data set of observed carcasses designed to mimic the random process observed in practice. Each trial in the same set of simulations assigned a turbine number and relative location to the same number of carcasses (M). Turbine number was assigned based on the discrete uniform distribution, and location was assigned to a one-meter dense grid based on one of the four spatial carcass distributions discussed below. Given the turbine and location, an indication to determine if the carcass landed on R&P was assigned to each carcass based on the R&P configurations of the wind facility used in that trial. Carcasses were then assigned an indication to determine whether or not they were observed by the searcher. This value was determined by a Bernoulli trial, with probability of success 0.85 for carcasses on R&P (G), and 0.32 for carcasses on non-R&P (G_{clr}) at turbines cleared of vegetation. The values for G and G_{clr} were based on the Good et al. [2011] report.

The cake, glm, and ratio methods were applied in every trial, or simulated data set, to obtain the estimated proportion, $\hat{a}$, of carcasses that land on R&P using (2.2), (2.4) and (2.6) and a pseudo estimate of mortality ($\widetilde{M}$). The notation and use of the word "pseudo" are used to emphasize that these estimates were not obtained using true mortality estimators. $\widetilde{M}_{cake}$, $\widetilde{M}_{glm}$, and $\widetilde{M}_{ratio}$ differ from (2.1), (2.5) and (2.7) as $\hat{G}$ is replaced with G. In practice G is unknown, and therefore must be estimated. Given the vast array of field methods, sample sizes, and estimators used to estimate G (Shoenfeld [2004], Huso [2010], Korner-Nievergelt et al. [2011], Bispo et al. [2013]), it was decided that including the variation of $\hat{G}$ to produce true morality estimates, distracted from the

research objectives. Instead the pseudo estimates of M are provided to focus attention on how various factors that affect accuracy and precision of $\hat{a}$ influence mortality estimates.

The cake and *glm* methods were based only on observed carcasses on R&P. In addition to the carcasses observed on R&P the ratio estimator also requires observed carcass counts on non-R&P at turbines where the vegetation is cleared. The number of cleared turbines differed for the two R&P configurations considered.

R&P Configurations

The R&P configurations of two wind energy facilities, referred to as WP2 and WP3, were used to determine if a carcass landed on R&P (Figure 2.3). At WP2 there are 355 turbines, and R&P orientation is predominately aligned with cardinal directions. WP3 consists of 23 turbines and is built along a ridge line, therefore the R&P have more twist and turns with no unifying patterns. The R&P configurations for both fa-

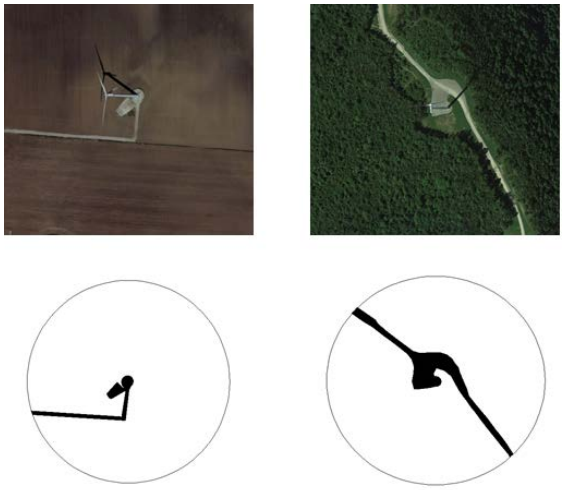

Figure 2.3: Google Earth images (top) and R polygon plots (bottom) of a typical R&P configuration at WP2 (left) and WP3 (right).

cilities where obtained using Google Earth, mapped in ArcGIS, and imported into R as polygons (Figure 2.3 (bottom)). After carcasses were assigned a turbine number and location, the polygon for the specified turbine and the inout() function in the R package *splancs* (Rowlingson and Diggle [1993]) were used to determine whether or not the carcass landed on the R&P.

When Good et al. [2011] conducted their study at WP2, nine of the 355 turbines were cleared of vegetation to employ the ratio estimator. Therefore, in the simulations nine turbines are cleared and searched at WP2. Mortality estimation at WP3 was not done using the ratio estimator. Clearing the same percent of turbines at WP3 as WP2 only corresponds to clearing 0.6 of a turbine. After discussing this topic with professional statisticians in the field of turbine-induced bird and bat fatalities, it was decided to clear three of 23 turbines at WP3 when employing the ratio estimator (Manuela Huso and Daniel Dalthorp, personal communications). The turbines selected for clearing differed in each trial, and were selected using a simple random sample.

Carcass per turbine rate

In each simulation an average of either 2, 10, 25, or 70 carcasses per turbine are distributed. A rate of 70 carcasses per turbine was obtained by taking the average of the two highest estimates of mortality per turbine reported in the literature review for this research. BHE Environmental [2010] estimated 50.5 (90% CI: 36.1-70.3) bat fatalities per turbine at Cedar Ridge Wind Farm in Wisconsin, and Hein et al. [2014] estimated 90 (95% CI: 57-153) fatalities per fully operational turbine at Pinnacle Wind Farm in West Virgina. A rate of 2 carcasses per turbine is used to avoid generating instances where zero carcass are observed, as these trials provide no information on how the meth-

ods compare to each other, and complicate the interpretation of the results if excluded. With an average rate of two carcasses per turbine the average number of observed carcasses per trial at WP3 is a mere 8.01, and the probability zero carcasses are observed is 0.00015. Averages of 10 and 25 carcasses per turbine were selected arbitrarily to assess the performance of the methods when the rate is between 2 and 70.

At WP2 rates of 2, 10, 25, and 70 equate to 710; 3,550; 8,875; and 24,850 total fatalities respectively. Under these four mortality rates it is expected that 87; 435; 1,086; and 3,042 fatalities are observed on R&P in a given trial. At WP3 the four rates correspond to 46, 230, 575, and 1610 total fatalities, with the expected number of observed fatalities on R&P of 8, 40, 100, and 281. The expected numbers of carcasses was calculated using the fitted spatial carcass distribution discussed below.

Spatial Carcass Distribution

Four spatial carcass distributions are used to assign carcass location. Three of the distributions are isotropic (Figure 2.4), meaning the distribution is only a function of distance from the turbine, not angle, and one is anisotropic (Figure 2.5). The isotropic distributions are referred to as the fitted, empirical, and circular distributions.

The fitted distribution was obtained using the distance to the nearest turbine of the 182 carcasses observed at WP1 (Figure 2.1), and (2.3) associated with the *glm* method. The empirical distribution is the observed fraction of the 182 carcasses in each one meter annulus. The circular distribution was calculated assuming that carcasses are struck uniformly in the rotor swept area, and fall straight down after colliding with the blades. Under the circular distribution, the probability a carcass lands between distances r_1 and r_2 is proportional to amount of rotor swept area above r_1 and r_2. Fifty meter turbine

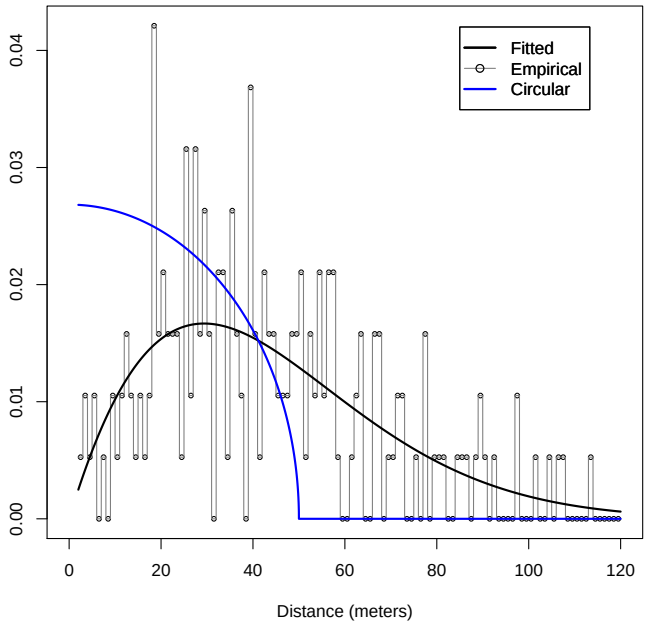

Figure 2.4: Probability density functions (pdf) of the distributions used for assigning carcass distance from the turbine tower. The fitted and empirical functions are based on data collected at WP1. The circular distribution was calculated under the implausable assumption that carcasses are struck uniformly in the rotor swept area, and fall straight down after colliding with the blades.

blades were used when calculating this distribution, so the probability a carcass lands beyond 50 meters is zero.

To understand how the methods of adjusting for unsearched areas are affected by various isotropic carcass distributions, it was necessary to use distributions significantly different from one another. The empirical or circular distributions may not be perfect, or even reasonable models for describing the distribution of carcass distance, but these distributions were not included to claim that carcass distance follows either of these

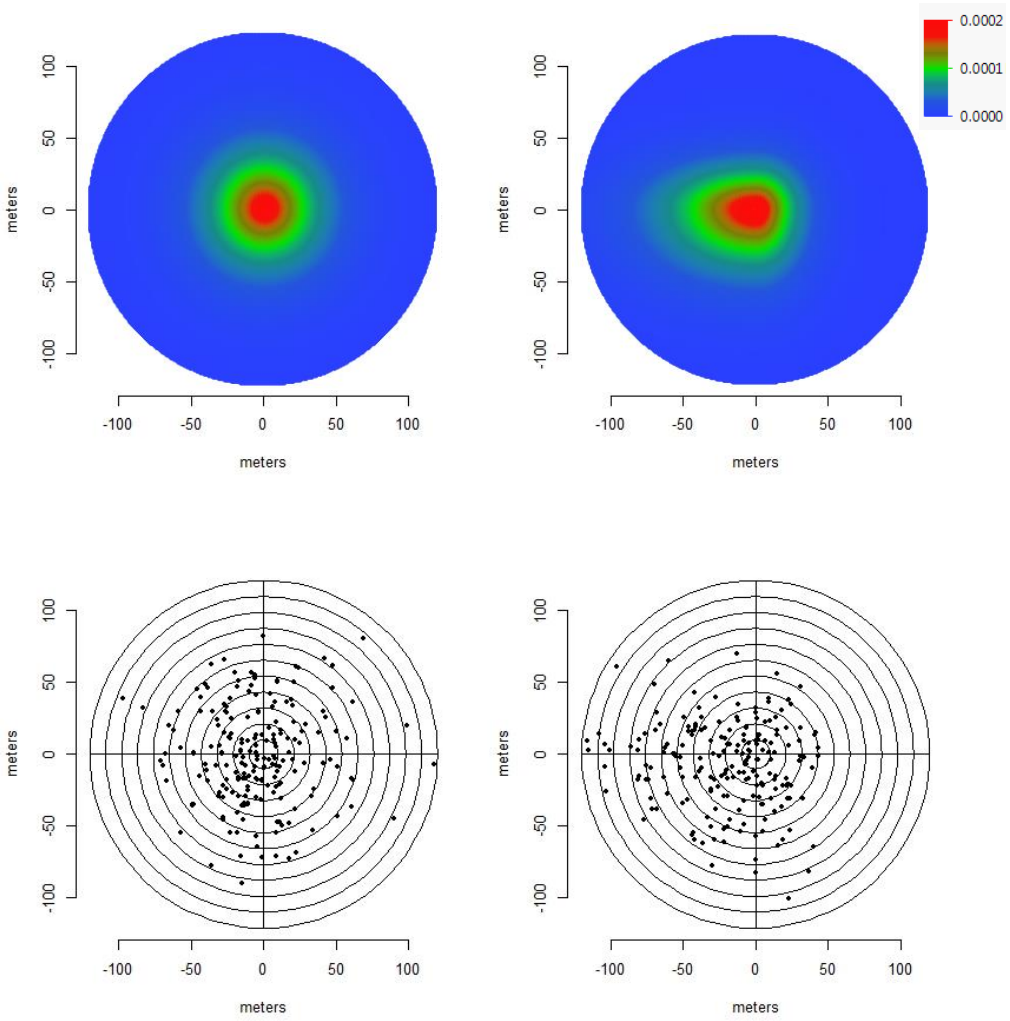

Figure 2.5: Carcass density (top) and a simulated sample of 200 carcasses (bottom) for isotropic (left) and anisotropic (right) spatial carcass distributions.

functions. Instead, they are used as a tool to examine how the methods perform under different isotropic spatial distributions.

Under an anisotropic spatial carcass distribution, carcass density changes with both distance and direction (Figure 2.5). In the context of turbine induced bird and bat fatalities, it seems reasonable to suspect that carcasses are more likely to fall with the wind than against it, making the assumption of isotropy dubious at wind projects with little variation in wind direction. The anisotropic spatial carcass distribution is utilized to study the effects an anisotropic carcass distribution has on each method. The anisotropic distribution was constructed to be strong enough to examine the effects anisotropy has on the methods being considered, while still being realistic (Huso and Dalthorp personal communications). This distribution mimics a circumstance where wind predominately originates from the east. Carcasses are twice as likely to fall west of the turbine, where they also tend to be more dispersed relative to carcasses east of the turbine.

Maximum Distance Searched

The maximum distance assigned to carcasses is determined by the spatial carcass distribution. Under the fitted, empirical, and anisotropic distributions, carcasses can land 120 meters from the turbine, while under the circular distribution the maximum assignable distance is 50 meters. In each simulation, however, carcass searches are performed to either 60, 90, or 120 meters.

When searches are conducted short of the maximum distance a carcass can land from the turbine, the cake and ratio methods have no obvious adjustments to account for this; however, the *glm* method can be fit to data from any size area and then extrapolated to the entire assumed fall zone. In each simulation, the Poisson regression in the *glm* method is fit with data collected on the grid within the maximum distance searched (60, 90 or 120 meters), and the proportion of carcasses that land in the searched area using

(2.4) is calculated based on a grid that extends 120 meters from the turbine.

2.4 Simulation results

Only a subset of the simulations are discussed, because all of the findings from this research can be summarized in reference to nine simulations (Table 2.1 and Table 2.2), and challenges in presenting meaningful results from each of the 96 simulation combinations (2 R&P configurations, 4 rates, 4 fall distributions, and 3 search protocols) in a reasonable number of pages. The simulations where results are provided are grouped into the Goldilocks, Rate Per Turbine, Fall Distribution, and Max Distance Searched simulations (Figure 2.6).

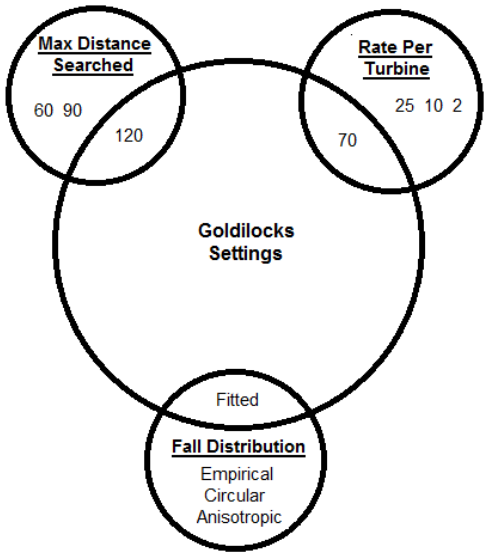

Figure 2.6: Venn Diagram to show the settings and grouping of the nine simulations used to discuss the results.

Table 2.1: Mean (and standard deviation) for estimates obtained in the Goldilocks Simulation and Rate Per Turbine Simulations at WP2 and WP3. Settings were determined by the average number of fatalities per turbine (Rate), spatial carcass distribution used to simulate carcass location (Distribution), and the maximum distance searched (Distance). For each setting, 1000 trials were performed to estimate the probability (a) a carcass lands on R&P and the average rate of carcasses per turbine using the cake, *glm*, and ratio methods. The estimate for the average rate was calculated as $\bar{M} = \frac{\widetilde{M}}{T}$, where T is the number of turbines ($T = 355$ at WP2, and $T = 23$ at WP3).

		Goldilocks	Rate Per Turbine		
	Rate	70	25	10	2
	Distribution	Fitted	Fitted	Fitted	Fitted
	Distance	120	120	120	120
WP2	a	0.144	0.144	0.144	0.144
	$\hat{a}_{cake}$	0.143 (0.004)	0.143 (0.007)	0.144 (0.011)	0.146 (0.026)
	$\bar{M}_{cake}$	70.4 (2.5)	25.1 (1.4)	10.0 (0.9)	2.01 (0.41)
	$\hat{a}_{glm}$	0.144 (0.004)	0.144 (0.007)	0.145 (0.011)	0.148 (0.026)
	$\bar{M}_{glm}$	70.0 (2.4)	25.0 (1.4)	10.0 (0.9)	1.99 (0.40)
	$\hat{a}_{ratio}$	0.145 (0.021)	0.143 (0.032)	0.149 (0.050)	0.166 (0.129)*
	$\bar{M}_{ratio}$	71.1 (10.5)	26.4 (6.0)	11.1 (6.7)	2.23 (1.47)*
WP3	a	0.205	0.205	0.205	0.205
	$\hat{a}_{cake}$	0.205 (0.009)	0.205 (0.015)	0.207 (0.024)	0.221 (0.070)
	$\bar{M}_{cake}$	70.0 (5.0)	25.1 (3.0)	10.0 (1.8)	2.00 (0.82)
	$\hat{a}_{glm}$	0.205 (0.009)	0.205 (0.014)	0.207 (0.022)	0.217 (0.066)
	$\bar{M}_{glm}$	70.0 (5.0)	25.1 (3.0)	10.0 (1.8)	2.00 (0.78)
	$\hat{a}_{ratio}$	0.207 (0.046)	0.210 (0.069)	0.218 (0.111)*	0.307 (0.339)*
	$\bar{M}_{ratio}$	72.6 (16.4)	27.2 (10.0)	12.3 (8.6)*	1.65 (1.22)*

*$\hat{a}_{ratio}$ was either 0 or undefined for 103 trials at WP2 with average rate of two, and 9 and 341 trials at WP3 with average rate of ten and two respectively.

Table 2.2: Mean (and standard deviation) for estimates obtained in the Fall Distribution Simulations and Max Distance Searched Simulations at WP2 and WP3. Settings were determined by the average number of fatalities per turbine (Rate), spatial carcass distribution used to simulate carcass location (Distribution), and the maximum distance searched (Distance). For each setting, 1000 trials were performed to estimate the probability (a) a carcass lands on R&P and the average rate of carcasses per turbine using the cake, glm, and ratio methods. The estimate for the average rate was calculated as $\bar{M} = \frac{\widetilde{M}}{T}$, where T is the number of turbines ($T = 355$ at WP2, and $T = 23$ at WP3).

		Fall Distribution			Max Distance Searched	
	Avg carcs per turbine	70	70	70	70	70
	Fall Distribution	Empirical	Circular	Anisotropy	Fitted	Fitted
	Max distance searched	120	120	120	90	60
WP2	a	0.134	0.360	0.149	0.143	0.139
	$\hat{a}_{cake}$	0.134 (0.004)	0.361 (0.006)	0.131 (0.004)	0.150 (0.004)	0.181 (0.004)
	$\bar{M}_{cake}$	69.9 (2.4)	70.3 (1.3)	80.1 (2.7)	67.0 (2.3)	54.0 (1.6)
	$\hat{a}_{glm}$	0.139 (0.004)	0.376 (0.007)	0.131 (0.004)	0.0143 (0.005)	0.139 (0.012)
	$\bar{M}_{glm}$	68.0 (2.3)	67.6 (1.3)	79.8 (2.7)	70.0 (2.9)	67.3 (9.5)
	$\hat{a}_{ratio}$	0.135 (0.019)	0.364 (0.031)	0.150 (0.022)	0.152 (0.021))	0.183 (0.026)
	$\bar{M}_{ratio}$	71.0 (10.0)	70.1 (6.0)	71.1 (10.6)	67.3 (9.5)	56.0 (7.8)
WP3	a	0.200	0.383	0.200	0.202	0.187
	$\hat{a}_{cake}$	0.200 (0.009)	0.383 (0.012)	0.201 (0.010)	0.213 (0.009)	0.244 (0.009)
	$\bar{M}_{cake}$	70.2 (4.8)	70.1 (3.3)	69.5 (5.0)	66.3 (4.7)	53.7 (3.4)
	$\hat{a}_{glm}$	0.203 (0.009)	0.375 (0.012)	0.202 (0.010)	0.202 (0.012)	0.181 (0.034)
	$\bar{M}_{glm}$	69.1 (4.7)	71.7 (3.4)	69.2 (5.0)	70.3 (5.8)	76.2 (21.0)
	$\hat{a}_{ratio}$	0.202 (0.046)	0.387 (0.062)	0.202 (0.050)	0.212 (0.047)	0.245 (0.060)
	$\bar{M}_{ratio}$	72.7 (16.9)	71.0 (11.0)	73.6 (20.0)	69.6 (15.3)	56.1 (13.5)

Goldilocks Simulation

In the Goldilocks Simulation an average of 70 carcasses per turbine are simulated from the isotropic fitted spatial carcass distribution, and searches are conducted to the maximum distance a carcass can land from turbine, 120 meters. Under these conditions the cake, *glm* and ratio methods of accounting for unsearched areas perform at their relative best (Figure 2.7); meaning each estimator appears relatively unbiased and the variation is minimal relative to all other settings. This simulation acts as a reference, as all other simulations only differ from it in one setting (i.e. rate, spatial carcass distribution, distance searched), appearing in every figure used to summarize simulation results in this section.

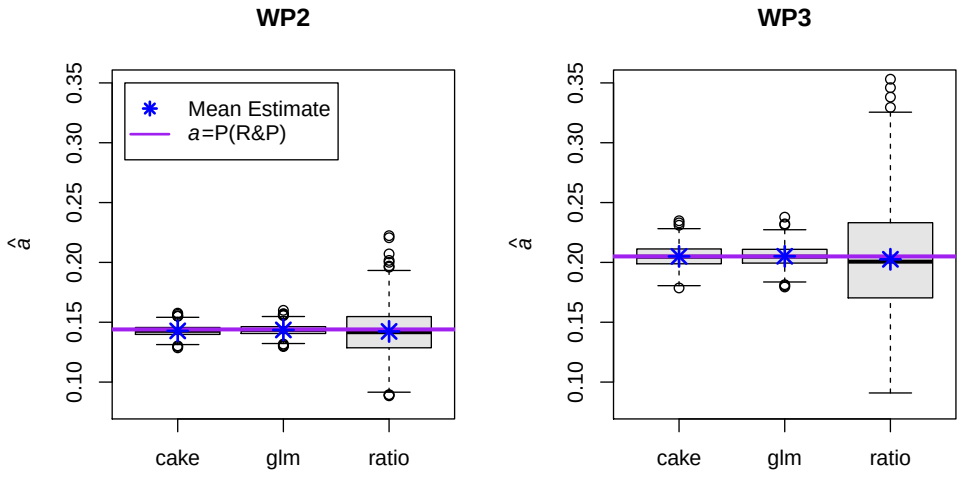

Figure 2.7: Estimates for the probability (a) that a carcass lands on R&P using the cake, *glm*, and ratio methods, under the R&P configurations at WP2 and WP3, in the Goldilocks Simulation.

The Goldilocks Simulation also displays the performance of each method under ideal, yet realistic conditions (Figure 2.7). Under these conditions all methods appear relatively unbiased, with mean estimates of a, the probability a carcass lands on R&P, within 0.5% of the true value for each method at both WP2 and WP3 (Table 2.1). The standard deviation of the cake and glm estimates of a are similar (0.004 at WP2 and 0.009 at WP3) and considerably less than the standard deviation of the ratio estimates (0.020 at WP2 and 0.046 at WP3).

Rate Per Turbine Simulations

The Rate Per Turbine Simulations consider the effect of reducing the average number of carcasses per turbine from 70 in the Goldilocks Simulation to 25, 10 and 2. Carcass location is simulated from the fitted isotropic spatial carcass distribution and searches are conducted to 120 meters. Unsurprisingly, the standard deviation of each method increases as the rate of carcasses per turbine decreases (Table 2.1 and Figure 2.8). Again, the standard deviations of both $\hat{a}$ and $\bar{M}$ are similar for the cake and glm method, and much less than the standard deviation of the ratio method. As the average number of carcasses per turbine decreases the cake and glm methods still produce relatively unbiased estimates, with pseudo mortality estimates within 1% of the truth, even with just eight expected observed carcasses on R&P at WP3 when the rate is 2 (Table 2.3). The bias of the ratio method increases as the average rate of carcasses per turbine decreases. In fact, ratio estimation is always biased (Lohr [2009]). In the context of mortality estimation of turbine-induced bird and bat fatalities at wind projects, the bias of the ratio method becomes more apparent as the average rate of carcasses per turbine, or number of observed carcasses, decreases.

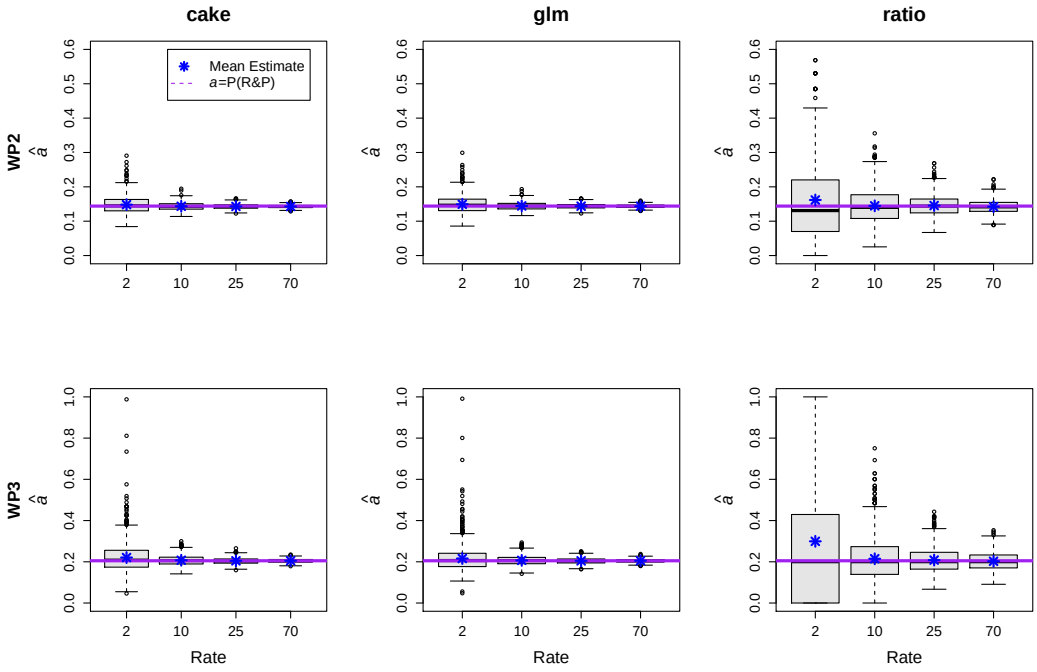

Figure 2.8: Estimates for the probability (a) that a carcass lands on R&P using the cake, *glm*, and ratio methods, under the R&P configurations at WP2 and WP3, in the Rate Per Turbine Simulations. Settings differ by the average number of fatalities per turbine (Rate).

Table 2.3: Expected number of observed carcasses at WP2 (355 turbines) and WP3 (23 turbines) under the four average number of fatalities per turbine rates in the Rate Per Turbine Simulations.

	Rate			
	2	10	25	70
WP2	87	435	1086	3042
WP3	8	40	100	281

The Rate Per Turbine Simulations also demonstrate another pitfall of the ratio method: it can fail to provide an estimate of mortality even when the there are observed fatalities. In every trial, at both wind facilities, at least one carcass was observed, yet the ratio method was unable to produce estimates in 103 and 341 at WP2 and WP3 respectively when the average number of carcasses per turbine was two. This is because mortality cannot be estimated by the ratio method if no carcasses are observed on the R&P at the turbines cleared of vegetation.

Fall Distribution Simulations

The isotropic fitted fall distribution used in the Goldilocks Simulation and Rate Per Turbine Simulations gives a slight advantage to the *glm* method. Recall this distribution was obtained by fitting a Poisson point process to data collected at WP1. This means that carcass location, in these simulations, is assigned from the same type of function the *glm* method uses to model the spatial carcass distribution. The purpose of the Fall Distribution Simulations is to understand how each method is affected by differences in the spatial carcass distribution used to assign carcass location. To make the effect as strong as possible, distributions were chosen that substantially differed from the distribution in the Goldilocks Simulation (Figure 2.4).

As the function used to assign carcass location changes, so does the the probability (a) a carcasses lands on R&P (Table 2.2). Therefore, the pseudo estimates for the estimated number ($\bar{M}$) of carcasses per turbine are used to compare the methods (Figure 2.9), as mortality (M) remained constant throughout the Fall Distribution Simulations. Unsurprisingly, the *glm* method is the most affected, and the effect of the carcass distribution on the *glm* estimates depends on the R&P configurations. When the empirical

distribution from WP1 is used to assign location, $\bar{M}_{glm}$ on average underestimates the rate by 2.6% and 1.3% at WP2 and WP3 respectively. Under the circular distribution, where the *glm* method is fit to a grid that extends 70 meters past the 50 meter maximum assignable distance, $\bar{M}_{glm}$ underestimates the rate by 2.9% at WP2 and overestimates by 2.6% at WP3. The slight bias in $\bar{M}_{glm}$ occurs because a logistic quadratic function of distance provides a poor approximation of empirical and circular marginal carcass

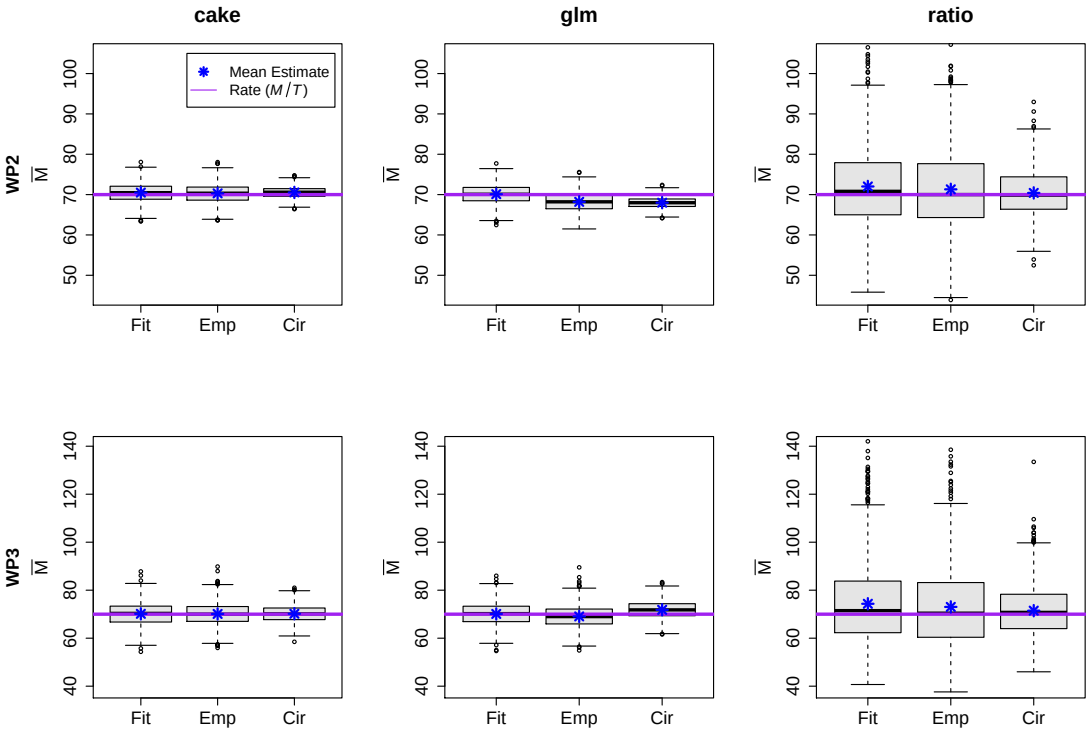

Figure 2.9: Estimates for the average ($\bar{M}$) number of carcasses per turbine using the cake, *glm*, and ratio methods, under the R&P configurations at WP2 and WP3, in the Fall Distribution Simulations. $\bar{M} = \frac{\widetilde{M}}{T}$, where T is the number of turbines $T = 355$ at WP2, and $T = 23$ at WP3. Settings differ by the isotropic distribution used to simulation carcass location.

distance distributions (Figure 2.10).

The cake and ratio methods are relatively unaffected by the various isotropic fall distributions. Both methods are slightly more precise under the circular distribution, likely because under this distribution the probability a carcass lands on the pad increases, which increases a. At WP2 a increases from 0.144 under the fitted distribution to 0.360 under the circular distribution. Similarly, at WP3 a increases from 0.205 to 0.383. The cake estimator does appear to be slightly less accurate under the circular distribution at WP2 with a 0.8% bias in $\bar{M}_{cake}$. This is probably due to the steep descent of the probability density function for the circular distribution near 50 meters, which noticeably violates the assumption of homogeneous carcass density within an annulus necessary for unbiased estimates using the cake method.

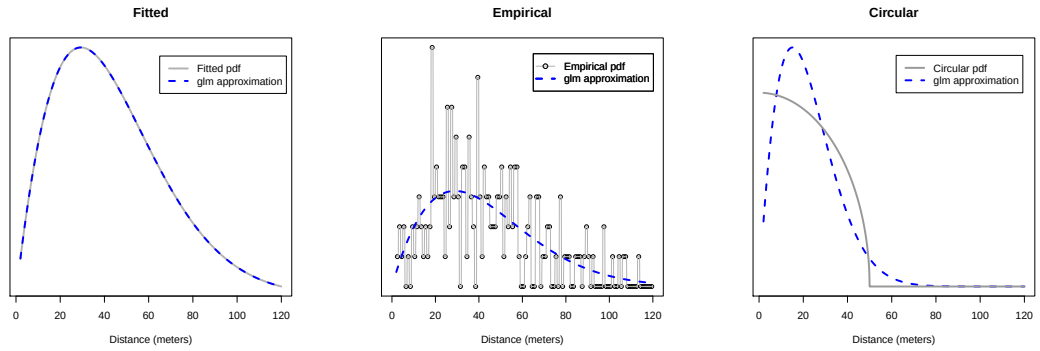

Figure 2.10: *glm* approximation to the three isotropic carcass distance probability density functions considered in the Fall Distribution Simulations.

The fitted, empirical, and circular carcass distributions are all isotropic, meaning that carcass density is only a function of distance from the turbine. Under the anisotropic distribution, density changes with direction and distance. The anisotropic distribution

in this simulation was designed to mimic a carcass distribution that would result from a eastern originating wind direction on average. Carcasses are twice as likely to land west of the turbine, where they are more dispersed relative to carcasses that fall east of the turbine (Figure 2.5). As with the other spatial carcass distributions, a differs between isotropy and anisotropy, therefore comparisons consider the estimates of $\bar{M}$ (Figure 2.11).

The ratio method produced relatively similar results under both the anisotropic and

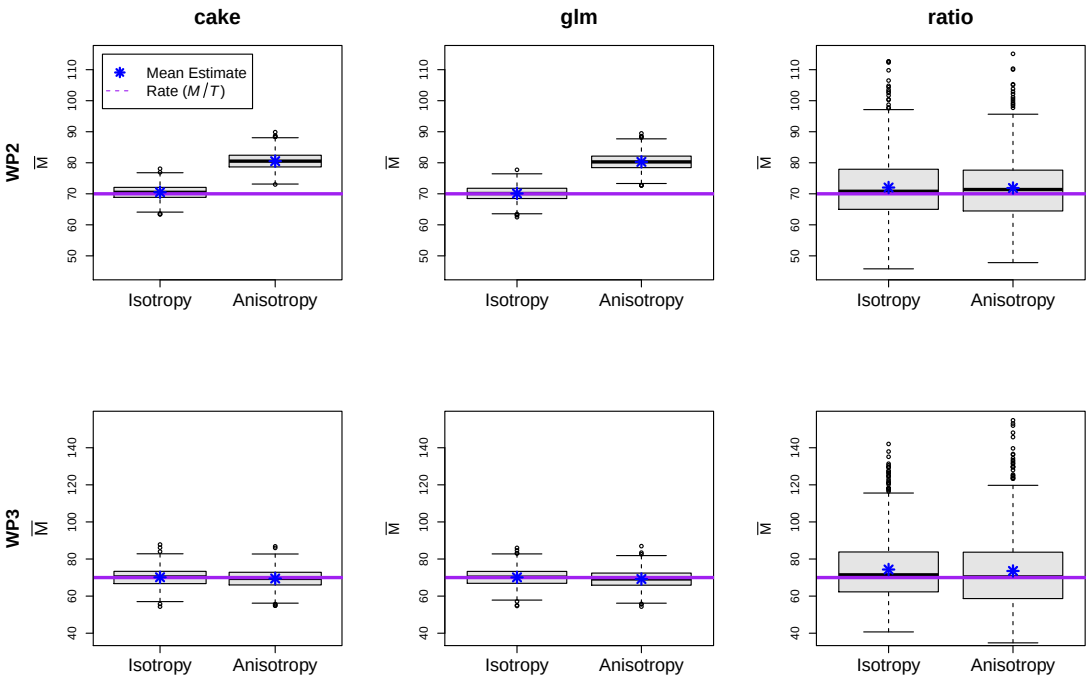

Figure 2.11: Estimates for the average ($\bar{M}$) number of carcasses per turbine using the cake, *glm*, and ratio methods, the R&P configurations at WP2 and WP3, under the fitted and anisotropic distributions in the Fall Distribution Simulations. $\bar{M} = \frac{\widetilde{M}}{T}$, where T is the number of turbines $T = 355$ at WP2, and $T = 23$ at WP3.

fitted spatial carcass distributions. The cake and *glm* methods, however, are affected by anisotropy and the effect depends on the R&P configurations. At WP2, $\bar{M}_{cake}$ and $\bar{M}_{glm}$ overestimate by about 15% on average; while at WP3, the bias of both pseudo estimates is a mere 1%. It was expected that anisotropy would affect both the cake and *glm* methods, so the results at WP3 in this simulation were unanticipated.

The cake and *glm* methods implicitly assume the spatial carcass distribution is isotropic. The cake method estimates the number of carcasses in an annulus, or ring, by dividing the number of observed carcasses in that ring by the proportion of area searched. This is reasonable when carcasses are distributed uniformly throughout a ring, which is not the case under anisotropy. The *glm* method, used in this analysis, fits the a Poisson regression on carcass density as a function that only depends on distance, meaning this method does not account for distributions where carcass density also changes with direction.

So, why is it that $\bar{M}_{cake}$ and $\bar{M}_{glm}$, or equivalently $\hat{a}_{cake}$ and $\hat{a}_{glm}$, produce relatively unbiased estimates under anisotropy at WP3? To answer this question, consider the R&P configurations at WP2 and WP3 (Figure 2.12). At WP2 the roads are predominantly aligned with the cardinal directions (e.g. north, east, south and west), and the largest proportion of roads were built due west of the turbine. The cake and *glm* methods are fit assuming that points at similar distances from the turbine will behave similarly in terms of carcass abundance or density, and therefore categorize observations by distance when estimating the number or density of carcasses. With the R&P configurations at WP2 the majority of observations for any distance greater than 15 meters from the turbine are recorded west of the turbine. Therefore, the most weight, when calculating the number or density of carcasses, will be given to the western direction at this wind

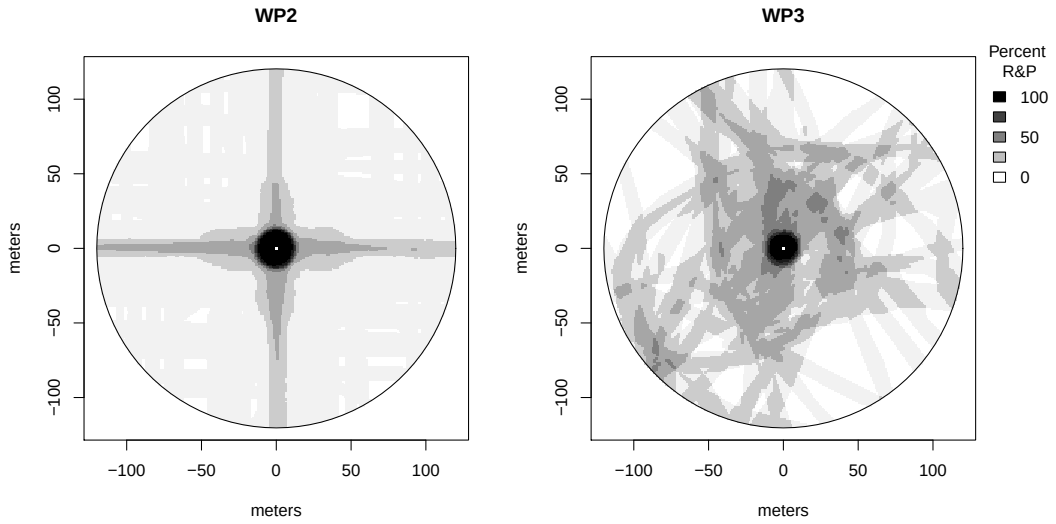

Figure 2.12: Composite of R&P configurations of all 355 turbines at WP2 (left) and 23 turbines WP3 (right). The shading for a given point is determined by the proportion of individual turbine R&P configurations that contain that point in the R&P. Points that are black are contained in the R&P at every turbine, and points that are white are not contained in the R&P of any turbine.

facility. Under the anisotropic distribution, more carcasses fall in the western direction than any other direction (Figure 2.5). Therefore the combination of giving the most weight to observations west of the turbine, and the highest number of carcasses falling west of the turbine creates an over estimate of the number or density of carcasses at most distances, leading to an overestimate of mortality for the cake and *glm* methods. When the anisotropic carcass distribution is rotated 180^{o}, causing the lowest number of carcasses to fall in the west, M is underestimated to a similar extent.

Now consider the R&P configurations of WP3 (Figure 2.12). While this configuration does provide equal representation of every direction, there are no general patterns.

So for a given distance, the distribution of points, with respect to angle, contained in R&P is roughly uniform, providing an estimate of carcasses or density based off similar weights across every direction. This yields reasonable estimates for the marginal density of carcasses at a given distance, because fatalities are equally likely to occur at any turbine; which leads to reasonable estimates using the cake and *glm* methods, and accounts for the negligible bias in $\bar{M}_{cake}$ and $\bar{M}_{glm}$.

To understand why the cake and *glm* methods are not affected by anisotropy when R&P configurations provide equal representation of each angle for a given distance, consider estimation based off n of N turbines with constant probability (G) of observing a carcass at all points in the fall zone. If the entire area was searched under the n turbines and C carcasses are observed, then the cake and *glm* estimates of M are equivalent to the total estimate from a simple random sample ($\frac{N}{n}\frac{C}{G}$). Obviously, this estimate will not be affected by any type of anisotropy. This implies that if each point is searched at the same proportion of turbines, anisotropy will not affect the cake and *glm* methods. Furthermore, our research indicates that anisotropy will not affect these methods as long as, for a given distance, each angle is searched the same number of times. This allows for points closer to the turbine to be searched more intensively than those further away. Of course, in practice no wind facility is going to have R&P configurations that explicitly satisfy this condition, but WP3 provides a configuration that is close enough such that the anisotropy considered in this study does not have a strong effect on the cake and *glm* methods.

Maximum Distance Searched Simulations

In the Maximum Distance Searched Simulations the number of carcasses and carcass

location is assigned using the same settings as the Goldilocks Simulation, but searches were only conducted to 60 or 90 meters. Under the fitted distribution, which was based on data collected at WP1, 4.8% of carcasses land past 90 meters and 23.6% land past 60 meters. The cake and the ratio methods are incapable of estimating the number of carcasses that land outside the searched area, and therefore produce relatively unbiased estimates for $(1-0.048)M$ and $(1-0.236)M$ when searches are conducted to 90 and 60 meters respectively (Table 2.2 and Figure 2.13).

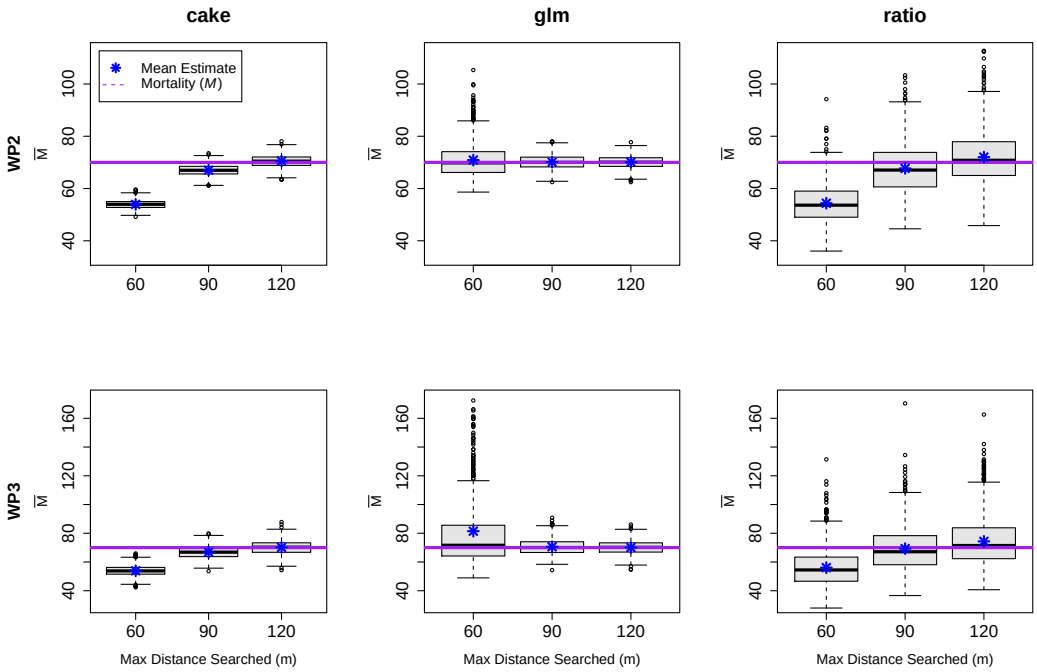

Figure 2.13: Estimates for the average ($\bar{M}$) number of carcasses per turbine using the cake, *glm*, and ratio methods, under the R&P configurations at WP2 and WP3, in the Maximum Distance Searched Simulations. $\bar{M} = \frac{\widetilde{M}}{T}$, where T is the number of turbines $T = 355$ at WP2, and $T = 23$ at WP3. Settings differ by the maximum distance from the turbine that searches are conducted.

The *glm* method, on the other hand, can be used to estimate the number of carcasses that land outside the searched area. Carcass density is modeled as a function of distance and the model can be used to extrapolate estimated carcass density beyond the maximum distance searched. Therefore the *glm* method estimates of a using (2.4) were still based on the grid that extends 120 meters from the turbine. When searches are only conducted to 90 meters the *glm* method produces estimates as accurate as searches conducted to 120 meters with a menial increase in standard error of $\hat{a}_{glm}$ from 0.0043 to 0.0051 at WP2 and 0.0085 to 0.0114 at WP3. When searches were conducted to 60 meters, $\hat{a}_{glm}$ was still unbiased for a, but the variation substantially increased. In 23 of the 1000 trials the leading coefficient for distance squared was positive, which lead to an increase in carcass density as distance increased from the turbine. These produced estimates of M that were so large they had to be excluded from Figure 2.13.

Admittedly, we had the advantage of knowing the true maximum distance a carcass could land from the turbine. In practice the maximum distance will be unknown, but the *glm* method produced similar results when applied to grids that extended 150 and 200 meters from the turbine, even when the maximum assignable carcass distance was held constant at 120 meters.

2.5 Conclusions

The research in this chapter examines the use of methods that have been previously proposed to account for unsearched areas, in the context of estimating bird or bat mortality at an individual wind project using data primarily, or solely, collected on roads lead-

ing up to turbines and pads beneath turbines (R&P). Three methods were considered: an empirical approach based on ideas from Jain [2005], referred to as the cake method; a generalized linear model (glm) method based on ideas from Huso and Dalthorp [2014]; and a ratio method which was applied by Good et al. [2011]. The performance of these three methods was examined and compared via a simulation which considered various R&P configurations, average carcass per turbine rates, spatial carcass distributions, and search protocols.

While the ratio method appears robust to different fall distributions including those that are anisotropic, its sensitivity to the average rate of carcasses per turbine and high variation yield undesirable results. With the exception of the results using the anisotropy fall distribution at WP2, the cake and glm methods outperformed the ratio method in every setting considered in this analysis. The Low Rate Simulations demonstrated that as the average rate of carcasses per turbine decreases, $\hat{a}_{ratio}$ becomes less accurate, more variable, and occasionally fails to even produce an estimate for mortality. Good et al. [2011] encountered this issue when estimating mortality for individual species at WP2. Zero carcasses were observed on the R&P at cleared turbines for three of the seven bat species found while monitoring the facilities, and therefore the probability that these three species land on R&P could not be estimated.

The results from any simulation are dependent on the settings that were used. In this analysis, the performance of the ratio method would have improved if the probability (G_{clr}) of detection in cleared areas was increased or if more turbines were cleared. Under the Goldilocks settings, however, increasing G_{clr} to 0.85 (=$G_{R\&P}$) only decreased the standard deviation in $\widetilde{M}_{ratio}$ by about 9% at WP2 and WP3; and in order to be com-

petitive with cake and *glm* methods 90 of 355 turbines at WP2, or 13 of 23 turbines at WP3, would have to be cleared.

Not only are the statistical properties less attractive when compared to the cake and *glm* methods, the ratio method is also more expensive and not always possible to implement. All methods require searching the R&P of every turbine. The cake and *glm* methods also require that the facility be mapped in a GIS program before estimation. The ratio method, though, requires data from plots that are cleared of vegetation. When the vegetation is dense, terrain is treacherous, or if bodies of water are within the carcass fall zone, obtaining counts for cleared turbines is impractical or even impossible. When clearing beneath turbines is possible, researchers must pay for the excavation. On top of the excavation fees, Good et al. [2011] also had to compensate a farmer for the loss of land at WP2, as this facility is located on a corn and soy farm. Then, when plots are cleared, these areas have to be searched. At WP2 the area comprising the R&P of all 355 turbines is equivalent to 13 turbines cleared to 120 meters. i.e., at WP2, the area searched for the cake and *glm* methods was only 60% of the area that was searched for ratio method.

The cake and *glm* methods performed similarly throughout most simulations. The cake method is relatively unbiased under isotropic fall distributions regardless of the marginal distribution used to assign carcass distance. When the distribution used to assign carcass distance is poorly modeled by a Poisson regression, the *glm* method becomes biased, but still produces estimates well within the range of the ratio method. In practice, the adequacy of the Poisson model can and should be examined using Pearson or deviance residuals (McCullagh [1984]). The only real data considred in the chap-

ter came from WP1, and the Poisson point process provided a very reasonable fit (see Figure 2.1 in Section 2.2)

When the fall distribution becomes anisotropic, the cake and *glm* methods may produce biased results depending on the R&P configuration. At WP2 where some directions were searched at a higher intensity than others, the anisotropic distribution considered in this analysis yielded a 15% overestimate of mortality for both the cake and *glm* methods. However, at WP3, where the every angle is searched at a relatively similar intensity for a given distance, the cake and *glm* methods yield a 1% bias, while the ratio method had a 5% bias.

When searches are conducted short of the maximum distance a carcass can land from the turbine, the *glm* method is able to estimate the number of carcasses that land past the maximum distance searched, while the cake and ratio methods are only capable of estimating the number of carcasses that fell within the maximum searched distance. Even with the *glm* method, though, searches have to be conducted to a reasonable distance. When searches were only conducted to half the maximum distance, the *glm* estimates can greatly overestimate mortality, if the fitted model predicts carcass density will increase with distance, which can easily be identified by users.

Under isotropy, the precision of the cake and *glm* is affected by the total number of fatalities. It is not however, the average rate of carcasses per turbine that determines the accuracy. Notice in Table 2.1 that the standard deviation of $\hat{a}_{cake}$ and $\hat{a}_{glm}$ is less at WP2 when the average rate is 25 than at WP3 when the average rate is 70. These results suggests cake and *glm* estimates of a depend more on the number of observed carcasses, rather than the average rate per turbine.

Further research is necessary to determine the number of carcasses that need to be observed to ensure accurate estimation using the cake or *glm* methods. The research conducted in this analysis suggests the necessary number of carcasses will likely be a function of the R&P configurations and spatial carcass distribution.

Mortality estimation is achievable based on data solely collected from R&P searches. The results of the cake and *glm* methods in this analysis demonstrate their ability to accurately and precisely estimate the probability a carcass lands on R&P. As the results presented in this analysis show, the cake and *glm* methods' precision is a function of the R&P configurations, a, and the number of observed carcasses; and depending on R&P configurations, the accuracy can be influenced by anisotropy. In the next chapter the theoretical properties of the cake method are explored, and a method of estimating G is introduced to develop the cake estimator of mortality. Chapter 4 considers approaches to adjust the cake and *glm* methods to test and account for anisotropic spatial carcass distributions.

3 The Cake Estimator

3.1 Introduction

The simulations performed in Chapter 2 demonstrate that mortality, the total number of bird or bat fatalities at a wind project, can be estimated based on searches performed only on the roads leading up to turbines and pads beneath turbines (R&P). In this chapter the cake method of adjusting for unsearched areas (i.e. non-R&P), based on ideas suggested by Jain [2005], is utilized to develop the cake estimator of mortality. Section 3.2 provides the theoretical properties of the proposed estimator. In Section 3.3 a method to estimate the probability that a carcass is observed given it landed on R&P is suggested and compared to commonly used methods. Then, a closed form expression and bootstrap method are developed for standard error calculation and confidence interval creation (Sections 3.4, 3.5, and 3.6).

Let M be the true mortality, and G be the probability a carcass is observed given it landed on R&P. If the fall area beneath turbines is partitioned into concentric annuli, with C_i as the observed number of carcasses in the i^{th} annulus, and A_i as the proportion of area searched for the i^{th} annulus, then the cake estimator can be expressed as

$$\widehat{M}_{\text{cake}} = \frac{1}{\hat{G}} \sum_i \frac{C_i}{A_i}, \tag{3.1}$$

where $\hat{G}$ is an estimator for G.

3.2 Theoretical Results for the Cake Estimator

Lemma 1 *Assume the spatial distribution of carcass location, $f(r,\theta)$, does not vary between turbines, and is uniform within an annulus (i.e. for points (r_1,θ_1), (r_2,θ_2) in the same annulus , $f(r_1,\theta_1) = f(r_2,\theta_2)$). If either of the following hold:*

(i) fatalities are equally likely to occur at any turbine ($P(T_j) = \frac{1}{T}$), or

(ii) for any annulus the proportion of area searched is equal at all turbines ($A_{ij} = A_i$), then the probability a carcass lands on the R&P given it landed in the i^{th} annulus is equal to the proportion of area contained in R&P for the i^{th} annulus (i.e. $\mathrm{P}(RP_i|\mathcal{A}_i)$=$A_i$*).*

Proof. Refer to the notation given in Table 3.1. Observe that the probability a carcass lands on the R&P given it landed in the i^{th} annulus of the j^{th} turbine ($\mathrm{P}(RP_{ij}|\mathcal{A}_i \cap T_j)$) is equal to the proportion of area contained in R&P in the i^{th} annulus of the j^{th} turbine (A_{ij}), because $f(r,\theta)$ is uniform within an annulus.

Table 3.1: Notation for Lemma

r	Distance from the turbine in (2,∞)
θ	Angle in radians, clockwise from due north in [0,2π)
$f(r,\theta)$	Probabitly density function of the spatial carcass distribution
A_i	Proportion of area contained in R&P for the i^{th} annulus at the wind project
A_{ij}	Proportion of area contained in R&P for the i^{th} annulus at the j^{th} turbine
$\mathcal{A}_i$	Event a carcass lands in the i^{th} annulus
RP_i	Event a carcass lands on R&P in the i^{th} annulus at the wind project
RP_{ij}	Event a carcass lands on R&P in the i^{th} annulus at the j^{th} turbine
T	Number of turbines
T_j	Event a carcass is struck at the j^{th} turbine ($\sum_{j=1}^{T} T_j = 1$)

Case (i): Assume fatalities are equally like to occur at any turbine ($\mathrm{P}(T_j) = \frac{1}{T}$).

$$\begin{aligned}
\mathrm{P}(RP_i|\mathcal{A}_i) &= \sum_{j=1}^{T} \mathrm{P}(RP_{ij}|\mathcal{A}_i \cap T_j)\mathrm{P}(T_j) \\
&= \sum_{j=1}^{T} A_{ij}\frac{1}{T} \\
&= \frac{1}{T}\sum_{j=1}^{T} \frac{\mathrm{area}(\mathrm{R\&P}_{ij})}{\mathrm{area}(\mathrm{annulus}_{ij})} \\
&= A_i,
\end{aligned}$$

where $\mathrm{area}(\mathrm{annulus}_{ij})$ is the area of the i^{th} annulus at a single turbine, and $\mathrm{area}(\mathrm{R\&P}_{ij})$ is the area of the roads and pads contained in the i^{th} annulus at the j^{th} turbine.

Case (ii): Assume for any annulus the proportion of area contained in R&P is equal at all turbines (i.e. $\mathrm{area}(\mathrm{R\&P}_{ij}) = \frac{\mathrm{area}(\mathrm{R\&P}_i)}{T}$).

$$\begin{aligned}
\mathrm{P}(RP_i|\mathcal{A}_i) &= \sum_{j=1}^{T} \mathrm{P}(RP_{ij}|\mathcal{A}_i \cap T_j)\mathrm{P}(T_j) \\
&= \sum_{j=1}^{T} A_{ij}\mathrm{P}(T_j) \\
&= \sum_{j=1}^{T} \frac{\mathrm{area}(\mathrm{R\&P}_{ij})}{\mathrm{area}(\mathrm{annulus}_i)}\mathrm{P}(T_j) \\
&= \sum_{j=1}^{T} \frac{\frac{\mathrm{area}(\mathrm{R\&P}_i)}{T}}{\mathrm{area}(\mathrm{annulus}_i)}\mathrm{P}(T_j) \\
&= \frac{\mathrm{area}(\mathrm{R\&P}_i)}{T \cdot \mathrm{area}(\mathrm{annulus}_i)} \sum_{j=1}^{T} \mathrm{P}(T_j) \\
&= A_i
\end{aligned}$$

■

Theorem 2 *Let $\hat{G}$ be an estimate for G. Assume the location of each carcass is assigned independently, and detection of carcasses on R&P is determined independently. If the spatial distribution of carcass location is uniform within an annulus and constant across turbines, and either of the following hold:*

(i) fatalities are equally likely to occur at any turbine ($P(T_j) = \frac{1}{T}$), or

(ii) for any annulus the proportion of area searched is equal at all turbines ($A_{ij} = A_i$),

then

$$\mathrm{E}[\widehat{M}_{cake}] = \mathrm{E}\left[\frac{G}{\hat{G}}\right]M \qquad \textit{and} \qquad \mathrm{Var}[\widehat{M}_{cake}] = \mathrm{Var}\left[\frac{GM}{\hat{G}}\right] + \mathrm{E}\left[\frac{GM}{\hat{G}^2}\right]\sum_i \frac{(1-GA_i)f_i}{A_i}.$$

Table 3.2: Notation for Theorem

M	True mortality
G	Probability a carcass that lands on R&P is observed
i	Index for the annuli (1, ..., I)
f_i	Probability a carcass lands in the i^{th} annulus
$\mathcal{C}_i$	Number of carcasses in the i^{th} annulus
	$(\mathcal{C}_1, ..., \mathcal{C}_I) \sim \text{Multinomial}(M, f_1, ..., f_I)$
C_i	Observed number of carcasses in the i^{th} annulus
A_i	Proportion of the i^{th} annulus contained in R&P (known)

Proof. Observe that $C_i|\mathcal{C}_i \sim \text{Binomial}(\mathcal{C}_i, GA_i)$ as the probability a carcass lands on R&P given it landed in the i^{th} annulus equals A_i by Lemma 1, carcass location is assigned independently, and the detection of a carcass in the searched area is independent of location and any other carcass by assumption. Therefore, C_i given $\mathcal{C}_i$ is the sum of $\mathcal{C}_i$ independent Bernoulli trials with probability of success equal to the probability of

landing on R&P times the probability of being observed (GA_i).

$$
\begin{aligned}
\mathrm{E}[\widehat{M}_{\text{cake}}] &= \mathrm{E}\left[\frac{1}{\hat{\hat{G}}}\sum_i \frac{C_i}{A_i}\right] \\
&= \mathrm{E}\left[\frac{1}{\hat{\hat{G}}}\right]\mathrm{E}\left[\sum_i \frac{\mathrm{E}[C_i|\mathcal{C}_i]}{A_i}\right], \qquad \mathfrak{C} = [\mathcal{C}_1, ..., \mathcal{C}_n], \text{ Law of total expectation} \\
&= \mathrm{E}\left[\frac{1}{\hat{\hat{G}}}\right]\mathrm{E}\left[\sum_i \frac{GA_i\mathcal{C}_i}{A_i}\right], \qquad C_i|\mathcal{C}_i \sim \text{Binomial}(\mathcal{C}_i, GA_i) \\
&= \mathrm{E}\left[\frac{G}{\hat{\hat{G}}}\right]\mathrm{E}\left[\sum_i \mathcal{C}_i\right] \\
&= \mathrm{E}\left[\frac{G}{\hat{\hat{G}}}\right]\sum_i \mathrm{E}[\mathcal{C}_i] \\
&= \mathrm{E}\left[\frac{G}{\hat{\hat{G}}}\right]\sum_i Mf_i \\
&= \mathrm{E}\left[\frac{G}{\hat{\hat{G}}}\right]M
\end{aligned}
$$

$$
\begin{aligned}
\mathrm{Var}[\widehat{M}_{\text{cake}}] &= \mathrm{E}\left[\left(\frac{1}{\hat{\hat{G}}}\sum_i \frac{C_i}{A_i}\right)^2\right] - \left(\mathrm{E}\left[\frac{1}{\hat{\hat{G}}}\sum_i \frac{C_i}{A_i}\right]\right)^2 && (1) \\
&= \mathrm{E}\left[\left(\frac{1}{\hat{\hat{G}}}\right)^2\right]\mathrm{E}\left[\mathrm{E}\left[\left(\sum_i \frac{C_i}{A_i}\right)^2\middle|\mathfrak{C}\right]\right] - \left(\mathrm{E}\left[\frac{G}{\hat{\hat{G}}}\right]M\right)^2 && (2) \\
&= \mathrm{E}\left[\frac{1}{\hat{\hat{G}}^2}\right]\mathrm{E}\left[\mathrm{Var}\left[\sum_i \frac{C_i}{A_i}\right] + \left(\mathrm{E}\left[\sum_i \frac{C_i}{A_i}\right]\right)^2\middle|\mathfrak{C}\right] - \left(\mathrm{E}\left[\frac{GM}{\hat{G}}\right]\right)^2 && (3) \\
&= \mathrm{E}\left[\frac{1}{\hat{\hat{G}}^2}\right]\mathrm{E}\left[\sum_i \frac{\mathrm{Var}[C_i|\mathcal{C}_i]}{A_i^2} + \left(\sum_i \frac{\mathrm{E}[C_i|\mathcal{C}_i]}{A_i}\right)^2\right] - \left(\mathrm{E}\left[\frac{GM}{\hat{G}}\right]\right)^2 \\
&= \mathrm{E}\left[\frac{1}{\hat{\hat{G}}^2}\right]\mathrm{E}\left[\sum_i \frac{GA_i(1-GA_i)\mathcal{C}_i}{A_i^2} + \left(\sum_i \frac{GA_i\mathcal{C}_i}{A_i}\right)^2\right] - \left(\mathrm{E}\left[\frac{GM}{\hat{G}}\right]\right)^2 && (4) \\
&= \mathrm{E}\left[\frac{1}{\hat{\hat{G}}^2}\right]\left(G\sum_i \frac{(1-GA_i)\,\mathrm{E}[\mathcal{C}_i]}{A_i} + (GM)^2\right) - \left(\mathrm{E}\left[\frac{GM}{\hat{G}}\right]\right)^2
\end{aligned}
$$

$$= \mathrm{E}\left[\frac{G}{\hat{G}^2}\right]\sum_i \frac{(1-GA_i)(Mf_i)}{A_i} + \mathrm{E}\left[\left(\frac{GM}{\hat{G}}\right)^2\right] - \left(\mathrm{E}\left[\frac{GM}{\hat{G}}\right]\right)^2 \tag{5}$$
$$= \mathrm{Var}\left[\frac{GM}{\hat{G}}\right] + \mathrm{E}\left[\frac{GM}{\hat{G}^2}\right]\sum_i \frac{(1-GA_i)f_i}{A_i}$$

(1) and (3) hold because $\mathrm{Var}[\cdot] = E[\cdot^2] - (E[\cdot])^2$. (2) holds from the law of total expectation and the result of the expectation above. (4) holds because of the binomial distribution of $C_i|\mathcal{C}_i$. (5) holds because $\mathcal{C} \sim \text{multinomial}(M, f_1, ..., f_I)$. ■

Corollary 2.1 *If G is known and the conditions of Theorem 2 are satisfied, then* $\widehat{M}_{cake}$ *is unbiased for M with variance*

$$\frac{M}{G}\sum_i \frac{(1-GA_i)f_i}{A_i}. \tag{3.2}$$

Proof. The results follow immediately by substituting G for $\hat{G}$ in Theorem 2. ■

As a verification of these results, consider applying Corollary 2.1 to the results of the Distance Simulation in Chapter 2 where the empirical spatial carcass distribution was used to assign carcass location. Recall, this empirical distribution (Figure 3.1) was obtained using data from a carcass survey at WP1 in 2013 where the distance from the turbine was obtained for 182 carcasses to the nearest meter. Therefore, by construction, this distribution is uniform within an annulus as long as the buffer (distance between inner and outer diameter of the annuli) is less than or equal to one meter. Since the cake method considered in Chapter 2 used a one meter buffer, carcasses were equally likely to occur at any turbine, and G was assumed known, the conditions for Corollary 2.1 are

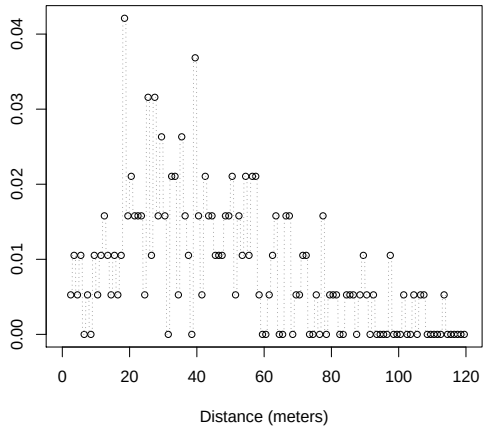

Figure 3.1: Marginal distribution of distance under the empirical spatial distribution of carcass location used in the Distance Simulations in Chapter 2. Based on the recorded distance of 182 carcasses observed at WP1.

explicitly satisfied. The Monte Carlo estimates for the mean and standard deviation from the simulation based on 10,000 trials (Table 3.3) are almost identical to those calculated using the results of Corollary 2.1.

Table 3.3: Results for the cake method from the Distance Simulations when carcass location was assigned according to the Empirical distribution in Figure 3.1, and the calculated mean and standard deviation given by Corollary 2.1.

Wind Project	Simulation mean (standard deviation)	Calculated mean	Calculated standard deviation
WP2	24,848 (849)	24,850	845
WP3	1,610 (112)	1,610	112

The values in Table 3.3 provide evidence that (3.2) yields an accurate estimate of $\mathrm{SD}[\widehat{M}_{\mathrm{cake}}]$, but it utilizes information that would not be available in practice. During

implementation of the results given above, M, G and f_i will all be unknown, and therefore must be estimated.

3.3 Estimating G

3.3.1 The Binomial Method

In the literature of turbine induced bird and bat fatalities, the most commonly used methods for estimating the probability (G) a carcass is observed given it landed in the searched area, were proposed by Shoenfeld [2004], Huso [2010] and Korner-Nievergelt et al. [2011]. All three of these methods model G as a function of carcass persistence, the distribution of the amount of time a carcass remains observable, and searcher efficiency, the probability a carcass is observed given it is present in the searched area when a search is conducted. To implement these methods independent experiments are conducted to estimate carcass persistence and searcher efficiency. The results from the two trials are combined to form an estimate of G.

Shoenfeld [2004], Huso [2010] and Korner-Nievergelt et al. [2011] have demonstrated the paradigm of independence between carcass persistence and searcher efficiency can be utilized to obtain reasonable estimates of G; however, G can also be estimated by a single binomial experiment, performed throughout a season, that accounts for carcass persistence and searcher efficiency. This can be accomplished by placing N carcasses in the searched area, and simply recording the number (X) of carcasses that

were observed. Under this protocol G is estimated as

$$\hat{G}_{binom} = \frac{X}{N}. \tag{3.3}$$

Trial carcasses should be placed in the searched area at times that mimic the arrival of the species of interest. If researchers assume that carcasses arrive uniformly at night or during the day, this can be accomplished using the discrete uniform distribution on all days in the period of interest, along with a Bernoulli($\frac{1}{2}$) distribution to decide if the carcass is placed at sunset or sunrise. Trial carcasses may go unobserved because they were carried off by scavengers, or because searchers never found the carcass. The reason why a carcass went unobserved is lost under this protocol, but when the goal of study is to estimate mortality (M), differentiating between carcass persistence and searcher efficiency is unnecessary.

Using a binomial trial to estimate G has both statistical and practical advantages. To domonstrate these advantages the methods proposed by Shoenfeld [2004], Huso [2010] and Korner-Nievergelt et al. [2011] are introduced (Subsection 3.3.2) and compared to $\hat{G}_{binom}$ via a simulation (Subsection 3.3.3).

3.3.2 Previously Proposed Methods for Estimating G

For a single visibility class (e.g. R&P, grass, thick vegetation, etc.) each of the estimators proposed by Shoenfeld [2004], Huso [2010] and Korner-Nievergelt et al. [2011] incorporate searcher efficiency into their models by assuming detection of carcasses is

independent for each carcass and follows a Bernoulli distribution with probability of success p. The three methods differ, though, by distributional assumptions about carcass arrival into to the searched area, and how carcasses become unobservable either due to scavengers or decay.

Shoenfeld [2004] assumes both carcass arrival into the searched area and removal of carcasses follow Poisson processes and models G as

$$G_{shoen} = \frac{\bar{t}p}{I}\left(\frac{e^{I/\bar{t}}-1}{e^{I/\bar{t}}-1+p}\right), \tag{3.4}$$

where $\bar{t}$ is the average carcass persistence time, p is the searcher efficiency, and I is the interval between searches. Huso [2010] assumes carcass arrival is uniform over the interval between searches, and carcass persistence follows an exponential distribution to develop the model

$$G_{huso} = \frac{pv\int_0^{Iv} e^{-x/\bar{t}}dx}{I}, \tag{3.5}$$

where $v = \min(1, \tilde{I}/I)$ for $\tilde{I} = -\bar{t}\cdot\log(0.01)$. Korner-Nievergelt et al. [2011] assumes that all carcasses arrive immediately after a search is conducted, and uses the probability a carcasses persists for at least a 24 hour period (s) to develop the model

$$G_{korner} = \frac{ps(1-s^I)}{nI(1-s)}\sum_{i=0}^{n-1}(n-i)\Big((1-p)s^I\Big)^i \tag{3.6}$$

where n is the number of searches conducted throughout the study.

Estimates of G using these three methods can be obtained using a Binomial trial for searcher efficiency (p), and survival analysis for carcass persistence. To estimate

Table 3.4: Notation for equations used to model G

$\bar{t}$	Average carcass persistence
p	Searcher efficiency
I	Interval between searches
s	Probability a carcass persist for at least 24 hours
n	Number of searches in the study

p, carcasses are placed in the searched area, and a carcass survey is conducted under standard protocol without alerting searchers to the trial carcasses. After the survey, researchers examine if unobserved trial carcasses were still present, and estimate p with the number of observed carcasses divided by the number of observable carcasses. The number of observable carcasses is the number of carcasses found plus the number of carcasses that remained in the field after the search was conducted.

In the carcass persistence trial, carcasses are placed in the field and monitored until they become unobservable. Carcasses are visited at most once per day, so all observations are interval censored. When using G_{shoen} or the form of G_{huso} presented above and in Huso [2010], $\bar{t}$ is estimated using the maximum likelihood estimate for an exponential trial with censored data,

$$\hat{\bar{t}} = \frac{\sum t_i}{N - N_c}, \tag{3.7}$$

where t_i is the persistence time for the i^{th} trial carcass in days, N is the number of trial carcasses, and N_c is the number of censored observations. Observations are censored if they persisted until the end of the trial. Using G_{korner}, s is estimated as

$$\hat{s} = \int_1^\infty \frac{1}{\hat{\bar{t}}} e^{-x/\hat{\bar{t}}} dx \tag{3.8}$$

3.3.3 Comparing the estimates of G

Two sets of simulations were preformed to assess the performance of G_{binom} to G_{huso}, G_{shoen}, and G_{korner} $\big($see (3.3)-(3.6)$\big)$. The first set satisfies the assumptions, in terms of carcass persistence and detection probability, made by the commonly used methods in the form they are presented above, and the second set tampers with these assumptions to demonstrate the flexibility of the G_{binom} without the need to alter its form.

The true value for G is determined by the carcass arrival distribution, the underlying distribution of carcass persistence, searcher efficiency, and the interval between searches. The simulations below were designed to mimic a study to estimate bat mortality over a 90 day period. Only one visibility class is considered, because the cake estimator of mortality is based solely on data collected on R&P.

Carcass arrival time is assigned uniformly over the 90 nights. This is accomplished by drawing from a Uniform(0,90), and accepting the proposed arrival times whose decimal values were greater than one half (i.e. [0.5,1.0), [1.5,2.0), and [2.5,3.0) represent the first, second, and third nights of the study). This assumes that every night in the study is 12 hours, carcasses are equally likely to arrive during any night over the period of interest, and arrivals occur uniformly throughout a night.

Carcass persistence is assigned using a distribution with mean 2, 4, 8, or 16 days (Figure 3.2). These are a subset of the combination of average carcass persistences considered by Huso [2010] and Korner-Nievergelt et al. [2011] in their simulations when introducing their estimators. The exponential distribution is used to simulate carcass persistence in the first set of simulations, designed to satisfy the assumptions imposed

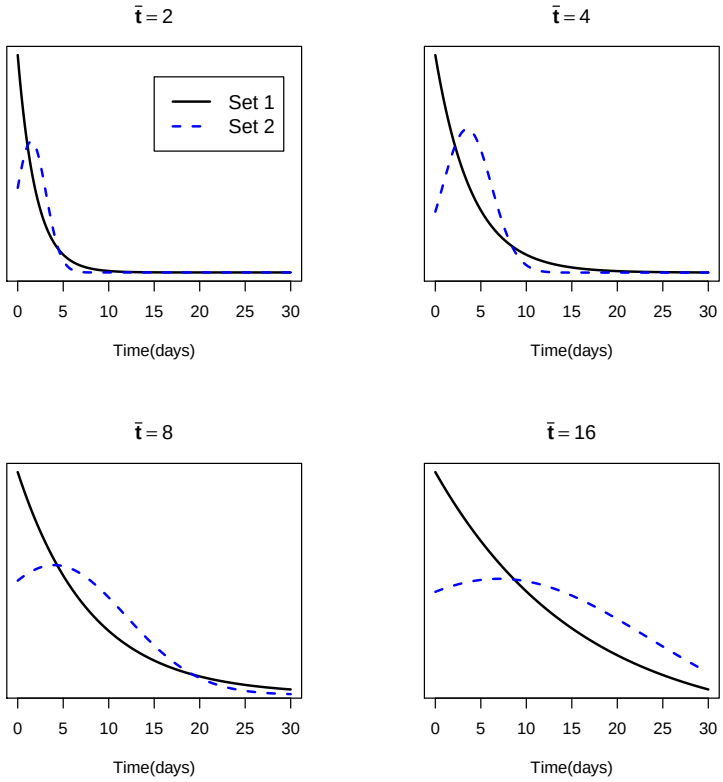

Figure 3.2: Distributions used to assign carcass persistence. $\bar{t}$ represents the average persistence time in days. Set 1 is based off the exponential distribution. Set 2 is based off normal distributions with means (standard deviations) equal to 1.5 (1.603), 3.5 (2.673), 4.0 (7.904) and 7.0 (16.43), truncated so that all persistence times are positive.

when using (3.4), (3.5), and (3.6). The second set of simulations uses a normal distribution, truncated so that persistence times are all positive. The use of a truncated normal is based on the idea that carcasses may be less likely to be removed from the searched area when the first arrive, if the scavenger removing them relies predominately on scent. The reasoning is that carcasses become more pungent a few days after dying. Therefore the

distributions used to assign carcass persistence in the second set of simulations are normal distribution with means (standard deviations) 1.5 (1.603), 3.5 (2.673), 4.0 (7.904) and 7.0 (16.43), truncated so that all persistence times are positive. The means of the Normal distributions that were truncated were selected to push the mode away from zero. This creates a difference between the exponential and truncated normal distribution to make the effect of changing the carcass persistence distribution more noticeable. The standard deviations were then calculated so that the mean of the truncated normal distribution used to assign persistence times was equal to the mean of the analogous exponential distribution.

In both sets of simulations the probability a carcass is observed given it persisted to the first search after arriving into the searched area is 0.85, which is the estimated probability of detection on R&P by Good et al. [2011]. The two sets differ in the probability of detection for carcasses that go unobserved in a given search and persist to the next search. The idea that probability of detecting a carcass decreases after each search it goes unobserved was first introduced by Huso [2010], who reasoned that carcasses missed in one search could be in a position or location making them more challenging to find. Carcasses that remain in the searched area between successive searches may also become covered in dirt, or shrivel from desiccation making them blend into the surroundings and decreasing the probability they are observed.

Detection probability can be modeled as $k^m p$, where $k \in [0,1]$, m is the number of searches a carcass has gone unobserved, and p is the probability of detection for a carcass on the first survey it is available. In the first set of simulations, $k = 1$, which assumes the probability of detecting a carcass remains constant in every simulated survey

it is available. In the second set of simulations $k = 0.5$, implying that detection probability decreases by 50% for every trial the carcass goes unobserved, and remains to the next search. As mentioned, $p = 0.85$ in all settings.

Both sets of simulations consider search intervals of 1, 4, 7, and 14 days. As with mean persistence times these are a subset of the combination of search intervals considered by Huso [2010] and Korner-Nievergelt et al. [2011] in their simulations when introducing their estimators. These values also encompass the range of all search intervals described in the mortality reports read for the literature review of this research. Simulated carcass surveys take place at noon each day. As mentioned above, nights pertain to times with decimal values in $[0.5, 1)$, therefore noon occurs at decimal value of 0.25 (i.e. 1.25 represents noon on the first day, 2.25 represents noon on the second day, and so on).

Monte Carlo estimation was utilized to calculate the true value of G for each simulation. 100,000 carcasses were assigned an arrival time, a persistence time, and the number of surveys it took to find the carcass. These values along with the search interval of the simulation were used to calculate the removal time and discovery time for each carcass. G is taken to be the proportion of carcasses where the discovery time is less than the removal time.

Estimates of G using $\hat{G}_{binom}$, $\hat{G}_{huso}$, $\hat{G}_{shoen}$, and $\hat{G}_{korner}$ are based 1000 simulated trials which use 60 carcasses. 60 is the average number of carcasses used for any one carcass size and season in the nine publicly available reports that were read for the literature review. The values in individual reports ranged from 20 (Erickson et al. [2004]) to 141 (Good et al. [2011]) carcasses.

To estimate G with $\hat{G}_{binom}$, the 60 trial carcass are randomly assigned a placement time at sunrise or sunset during any day of the study using the discrete uniform distribution on $\{0.5, 1, 1.5, ..., 89.5\}$. Each carcass is then assigned a persistence time and the number of surveys it takes to find it. As with the Monte Carlo estimate of the true value of G, these quantities along with the search interval can be used to calculate a removal and discovery time. The estimate, $\hat{G}_{binom}$, is calculated as the proportion of the 60 trial carcasses that are discovered before removed.

For $\hat{G}_{huso}$, $\hat{G}_{shoen}$ and $\hat{G}_{korner}$ the 60 carcasses are partitioned into two sets of 30, one set is used for the searcher efficiency trial and the other is used for the carcass persistence trials. It is possible to use the same carcasses in the searcher efficacy and persistence trial, but it does not appear to be standard protocol. Fiedler et al. [2007] marked trial carcasses with a discrete tag underneath the carcass, so that searchers left the trial carcasses in place after finding them. Carcasses were placed just before the search was conducted, and afterwards the searchers were asked to make sure unobserved carcasses where still present. The searchers then examined the carcasses every five days when regular searches were conducted, and recorded when the trial carcasses were no longer available. This was the only mention of a study that used the same carcasses for both searcher efficiency and carcass persistence in the literature review. No study explicitly stated that different carcasses were used, but sometimes it was inferred by the design of the studies. For instance, Johnson et al. [2003] used ten bats per season in the carcass persistence trials, and then mentions there were not enough bats for the searcher efficiently trials, so they used small birds instead. For the simulations provided in this section, it is assumed that carcasses can only be used in the searcher efficiency trial or

carcass persistence trial, but not both.

For $\hat{G}_{huso}$, $\hat{G}_{shoen}$ and $\hat{G}_{korner}$, the searcher effeiciency, p, is estimated as $\frac{X}{30}$ for $X \sim \text{Binomial}(30, 0.85)$. To estimate $\bar{t}$ (mean persistence time), in $\hat{G}_{huso}$ and $\hat{G}_{shoen}$, or s (probability of persisting 24 hours), in $\hat{G}_{korner}$, the 30 carcasses used in the carcass persistence trial are assigned a persistence time according to the distribution used in that simulation. The observed persistence in the trial was taken to be the minimum of the smallest integer greater than or equal to the simulated persistence minus one half or 15 (i.e. Observed persistence = min($\lceil$simulated persistence$\rceil - 0.5$,15), where $\lceil\cdot\rceil$ is the ceiling function). This mimics the protocol where carcasses were placed in the field and examined daily for 15 days to determine if they were still observable. The same design used by Johnson et al. [2003] for their carcass persistence trial, only with 10 carcasses. Given the observed persistence times, $\hat{\bar{t}}$ and $\hat{s}$ were calculated using (3.7) and (3.8).

After obtaining simulated outcomes from the carcass trials, G was estimated using (3.3), (3.4), (3.5), and (3.6), with the estimates $\hat{p}, \hat{\bar{t}}$ and $\hat{s}$. To verify the calculations were performed correctly, the functions perickson(), phuso() and pkorner(), which are equivalent to (3.4), (3.5) and (3.6) respectively, were used from the *carcass* package in R (Korner-Nievergelt et al. [2015]). These functions would have been used in the calculations had the author been aware they existed while performing the simulations.

The results from all the simulations suggest that $\hat{G}_{binom}$ binomial provides unbiased estimates of G regardless of the carcass persistence distribution, changes in searcher efficiency, or the search interval (Figure 3.3 and Figure 3.4). With few exceptions, the spread of the $\hat{G}_{binom}$ is comparable to any of commonly used estimators when they too are relatively unbiased. The relative error of $\hat{G}_{binom}$ is large relative to some, or all,

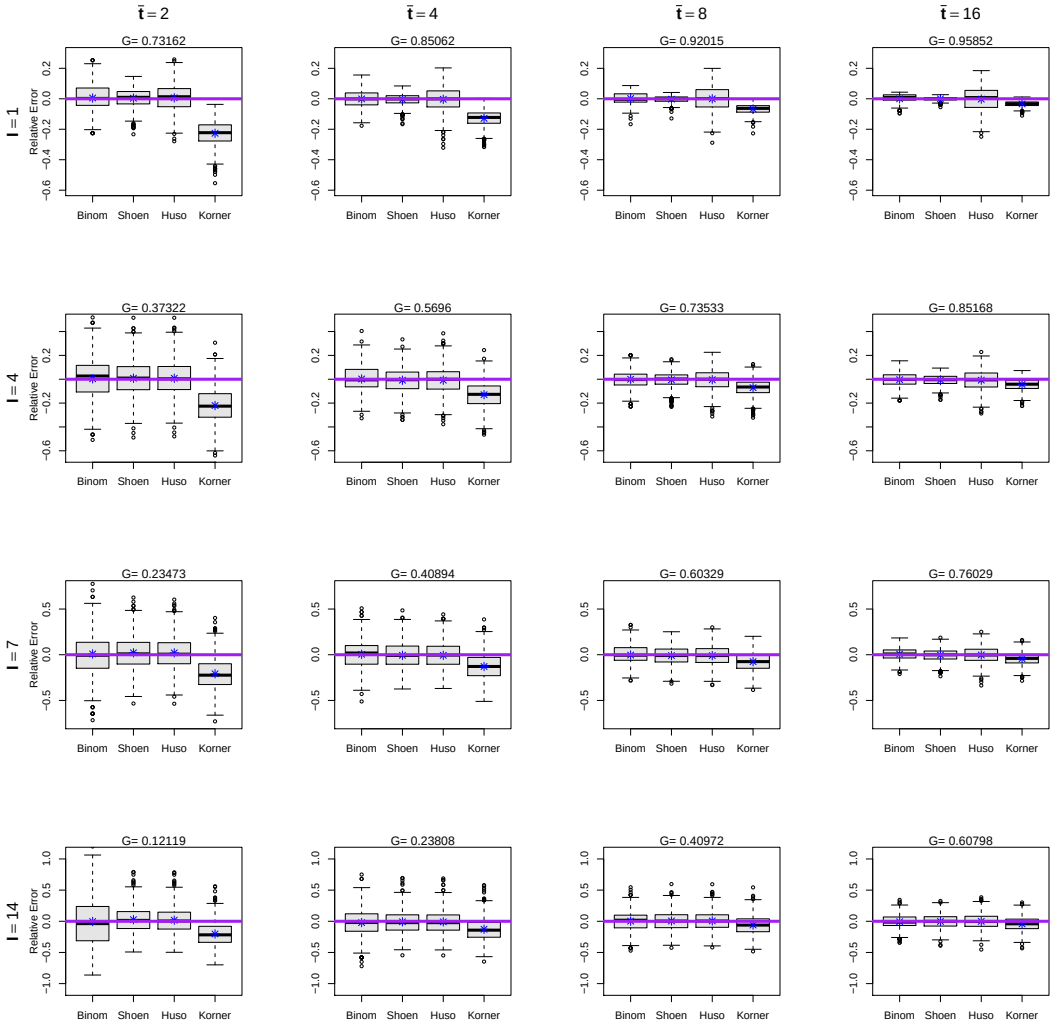

Figure 3.3: Relative error for each method used to estimate G, the probability a carcass that lands on R&P is observed, given the average persistence time ($\bar{t}$) and days between searches (I). Persistence is assigned using an exponential distribution. Probability of observing a carcass is 0.85 for every survey where the carcass is available. This implies that probability of detection is constant.

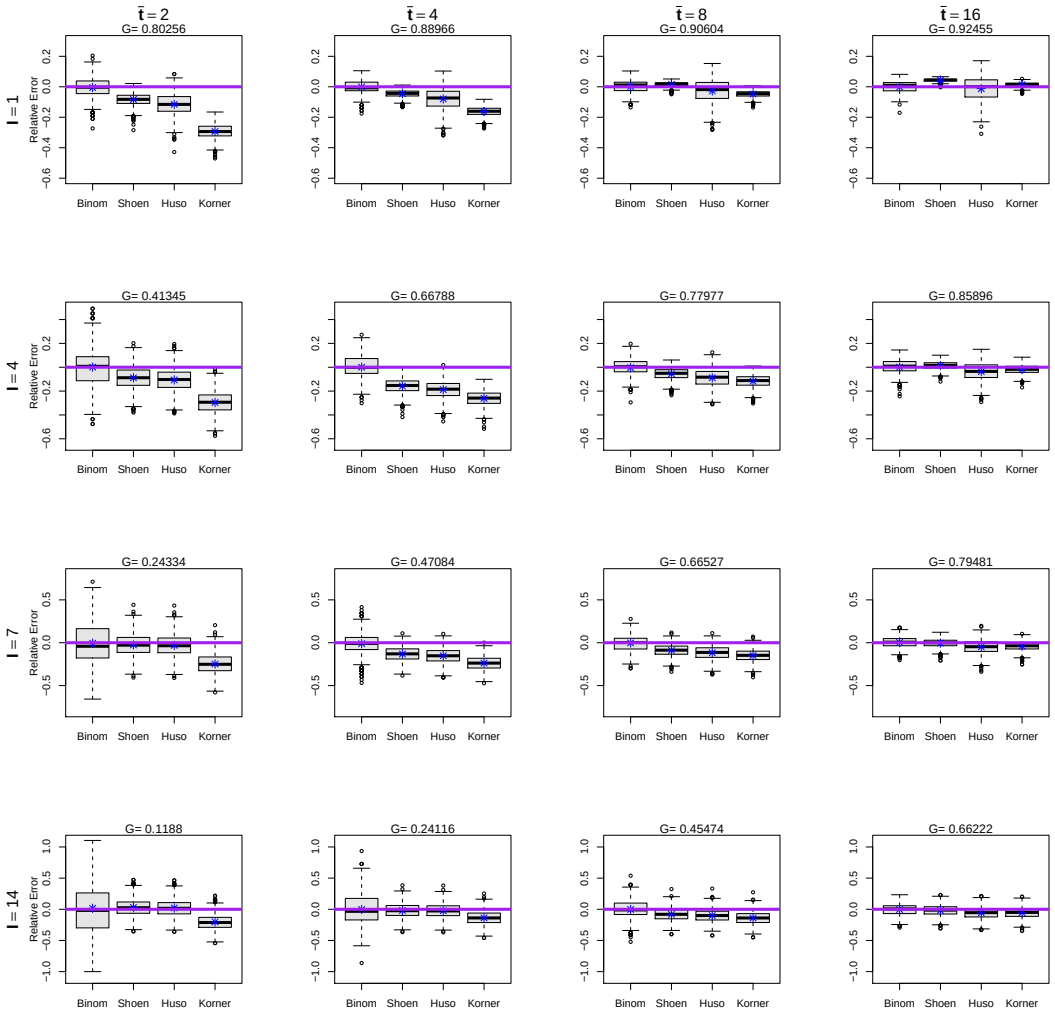

Figure 3.4: Relative error for each method used to estimate G, the probability a carcass that lands on R&P is observed, given the average persistence time ($\bar{t}$), and days between searches (I). Persistence is assigned using a truncated normal distribution. Probability of observing a carcass that is present during a survey is $0.5^m \cdot 0.85$, where m is the number of surveys the carcass was present and unobserved. This implies that detection probability decreases by 50% for each trial the carcass goes unobserved.

of the methods considered when search intervals are short and persistence is long, or when search intervals are long and persistence is short. Both of these circumstances, however, are unrealistic. If the average persistence time is 14 days, then there is no need to perform carcass surveys every day (simulation depicted in upper right corner of Figure 3.3 and Figure 3.4). Similarly if the average carcass persistence time is just two days, searches would likely be performed more often than twice a month, which leads to a 0.1212 probability of detection (simulation depicted in lower left corner of Figure 3.3).

When the assumptions of exponential persistence and constant probability of detection are met, $\hat{G}_{shoen}$ appears unbiased and has the smallest variation in most trials. When the truncated normal distribution is used to simulate carcass persistence and probability of detection decreases, $\hat{G}_{shoen}$ often underestimates G. The method proposed by Shoenfeld [2004] assumes probability of detection remains constant for all carcasses in the searched area. Therefore, the decrease in probability actually causes $\hat{G}_{shoen}$ to overestimate G, implying that truncated normal carcass persistence distribution causes $\hat{G}_{shoen}$ to underestimate.

In most of the settings considered in the first set of simulations, $\hat{G}_{binom}$ and $\hat{G}_{huso}$ produce similar results (Figure 3.3). The relative error in $\hat{G}_{huso}$ is less than $\hat{G}_{binom}$ in the unrealistic situation where the average persistence time is two days and searchers are conducted every other week. When searches are performed daily the relative error in $\hat{G}_{binom}$ is less than $\hat{G}_{huso}$. It is worth noting that the standard deviation of these methods is actually very similar when the search interval is short, and the difference in relative error occurs because $\hat{G}_{huso}$ estimates a smaller value than $\hat{G}_{binom}$ and the other meth-

ods. The method introduced by Huso [2010] assumes carcasses that go unobserved in the first search they are available are never found. This implies that $\hat{G}_{huso}$ estimates the probability a carcass that landed in the searched area is found at the next survey, while the other three methods estimate the probability a carcass that landed in the searched area is observed in any survey. The probability a carcass is observed in the first trial is obviously less than the probability a carcass is observed in any trial. This difference is the most noticeable when the probability of observing a carcass past the first trial is relatively high, which happens when average persistence is long and searches are performed often. Therefore, even though $\hat{G}_{binom}$ and $\hat{G}_{huso}$ have similar standard deviations when the search interval is short and persistence is long, $\hat{G}_{huso}$ has a larger relative error, because the value used in the denominator of the relative error calculation is smaller.

In many of the settings considered in the second set of simulations, the form of $\hat{G}_{huso}$ when assuming an exponential persistence distribution, (3.5), is biased (Figure 3.4). Since this method estimates the probability a carcass is found on the first survey it is available, it is completely unaffected by the decrease in detection probability for carcasses that go unobserved in one trial and persist to the next trial. This implies the bias emanates from not accounting for the non-exponential distribution of carcass persistence.

In almost every setting, in both sets of simulations, the form of $\hat{G}_{korner}$ in (3.6) underestimates G. This estimate assumes that carcasses arrive immediately after a search is conducted. In the simulations above searches are conducted at noon and carcasses arrive uniformly from sunset to sunrise, implying the assumption that carcasses arrive immediately after a search is conducted is invalid and leads to an underestimate of G.

3.3.4 Findings

The simulation results in this section suggest that the use of a Binomial trial to estimate G, produces unbiased results under various carcass persistence distributions, changes in probability of detection, and different search intervals.

The method proposed by Shoenfeld [2004] performs well when carcass persistence follows an exponential distribution and probability of detection is independent of carcass age; however, this estimator is not robust to carcass persistence distributions other than the exponential distribution, or changes in detection probability. With no alternative form that can account for differences from the assumed model, this method is not as robust as the binomial method.

When assuming carcass persistence follows an exponential distribution, the method proposed by Huso [2010] performs well when carcass persistence is simulated from an exponential distribution, and produces biased results when the carcass persistence is simulated from a truncated normal distribution. This method is completely unaffected by decreases in detection probability, because it assumes carcasses that go unobserved in the first survey are never found (i.e. $\hat{G}_{huso}$ estimates the probability a carcass is observed in the first survey after arrival). This is reasonable in practice, because carcasses that are found and deemed to have arrived prior to the previous search, can be excluded from the estimation. This relies on a searcher's ability to identify when carcasses arrived into the searched area. Excluding observed carcasses from estimation can be dissatisfying, especially if they are carcasses of threatened or endangered species, because it neglects information that can be used to estimate mortality.

Since the method in the form proposed by Huso [2010] is unaffected by changes in the probability of detection, the bias observed under the second set of simulations is attributed to use of a truncated normal distribution to simulate carcass persistence. In the simulations, estimates were obtained using the form of $\hat{G}_{huso}$ presented in Huso [2010], which assumes an exponential. Contrary to the implications of Bernardino et al. [2013], this method does not require the assumption of an exponential distribution. In the user's manual (Huso et al. [2012]) for software developed to implement $\hat{G}_{huso}$, users are promoted to use AICc to determine the most appropriate distribution (exponential, Weibull, log-logistical, or log-normal) to model carcass persistence. This suggests that $\hat{G}_{huso}$ can be altered to account for non-exponential carcass persistence distributions. This was not taken into account in the simulations, because Huso [2010] does not state the generalized from, which may have lead to confusion of Bernardino et al. [2013]. Also, the generalized form is not in a publicly available report, but can be found by examining the code associated with the software described in Huso et al. [2012].

The estimator proposed by Korner-Nievergelt et al. [2011] produced biased results in nearly all simulations. When carcass persistence follows an exponential distribution and probability of detection is constant, the bias is the results of the assumption that carcasses enter the searched area immediately after a search is conducted. In the simulation, searches were conducted at noon, and carcasses arrived uniformly between sunset and sunrise. In the R package *carcass* (Korner-Nievergelt et al. [2015]) adjustments can be made to assume a uniform arrival, which may increase the accuracy. The simulations did not consider the uniform method, because the form of this estimate is not provided in Korner-Nievergelt et al. [2011], and the function used to obtain $\hat{G}_{korner}$ in the *carcass*

package $\big($pkorner()$\big)$ does not provide an option to assume uniform arrival. The function estimateN() allows for uniform arrival and could have been used to obtain results for $\hat{G}_{korner}$, but a single trial took 27 seconds to run. If this method had been used for all 32,000 trials considered, it would have required 240 hours.

In the second set of simulations, the bias in the form of $\hat{G}_{korner}$ considered in the simulations is also attributed to the non-exponential carcass persistence distribution and non-constant probability of detection, both of which can be accounted for in theory using the general form of $\hat{G}_{korner}$. In the R package *carcass* (Korner-Nievergelt et al. [2015]), the carcass persistence can be estimated using Kaplan-Meier survival function, which may provide better results under the truncated normal distribution. This was not used because Korner-Nievergelt et al. [2015] state, "[I]f data for only one site is available, or sample size is small, we recommend a parametric model such as an exponential."

Korner-Nievergelt et al. [2011] also provide an alternative form to include a multiplicative decrease (k) in probability of detection for carcasses that go unobserved in one search and persist to the next search, but does not suggest a method to estimate k. Theoretically, this can be done using carcasses from the searcher efficiency trial that go unobserved, are left in the field, and persist the length of the search interval. This happened so infrequently in a majority of settings considered in the simulations, that often one or zero carcasses would have been used to estimate k. In practice estimating k is also challenging. Take for example the case where persistence follows an exponential distribution with mean equal to four (i.e. $\bar{t} = 4$), and searches are performed everyday four days (i.e. $I = 4$). In this setting, the probability a carcass that is set out immediately before a search is conducted, goes unobserved, and persist to the next trial is 0.0948.

Implying that 105 carcasses would have to be set out to expect just 10 carcasses can be used to estimate the decrease in the probability of interest. Therefore the simulations used the form of $\hat{G}_{korner}$ presented in (3.6) and in Korner-Nievergelt et al. [2011] which assumes $k = 1$.

Along with desirable statistical properties, the binomial method is also easy to implement. When using the methods proposed by Shoenfeld [2004], Huso [2010], and Korner-Nievergelt et al. [2011] carcasses have to be placed for the searcher efficiency trials, then the carcasses that went unobserved have to be revisited to ensure they were available for observation at the time of the search. In the carcass persistance trial, carcasses have to be placed and then revisited every day, or every few days depending on the protocol, to determine when they are no longer available. With the binomial method, carcasses are placed in the field, and they are either returned to the researcher or they are not. Researchers can identify trial carcasses using tags or clipping toes, but are never required to revisit the carcass after placement.

Placing trial carcasses at sunrise or sunset uniformly during the entire period of interest, may be considered more challenging than conducting a searcher efficiently trial and carcass persistence trail where carcasses are all placed at once; however, if trial carcass placement mimics the true arrival process, then this protocol is capable of capturing changes in G if they occur. If researchers are willing to assume G is constant, then carcasses do not need to be placed uniformly during the entire period of interest. Instead trial carcasses can be placed uniformly between two successive searches, which produces similar results theoretically.

Estimation using the binomial method is straight forward. Researches do not have

identify the most appropriate method to model persistence, or risk selecting an inappropriate model. The form of the binomial method never changes, and is robust to any carcass persistence distribution. The methods introduced by Huso [2010] and Korner-Nievergelt et al. [2011] in their generalized forms are valuable tools, and necessary for answering research questions that compare G in different visibility classes, seasons, and wind projects; but, when the goal of a study is to estimate mortality based on data from a single visibility class (e.g. roads and pads), over one season, the binomial method provides robust accurate estimates, with easy implementation and calculation. Therefore, it is recommended that a Binomial trial be used to estimate G when implementing the cake estimator of mortality.

3.4 Estimating the Variance of $\frac{1}{\hat{G}}$

The previous section proposed using a Binomial trial to estimate G, the probability a carcass that landed in the search area is observed. G is pivotal for estimation of turbine induced bird and bat fatalities, but it is not the focus. The goal of these studies is to estimate mortality, and G is used to adjust the number (C) of observed carcasses to the estimated number of carcasses that fell in the searched area ($\frac{C}{\hat{G}}$). Therefore mortality estimation requires an estimate for $\frac{1}{G}$.

No unbiased estimate of $\frac{1}{G}$ exists when using a Binomial(N,G) trial to estimate G, but the maximum likelihood estimate is given by $\frac{1}{\hat{G}}$, where $\hat{G} = \frac{X}{N}$, $X \sim$ Binomial(N,G). Estimating Var$[\hat{M}_{cake}]$ using the results from Theorem 2, requires estimation of Var $\left[\frac{1}{\hat{G}}\right]$. The Var $\left[\frac{1}{\hat{G}}\right]$ cannot be easily calculated using the definition of Var$[\cdot]$, because Var $\left[\frac{1}{\hat{G}}\right]$

(and even $\mathrm{E}\left[\frac{1}{\hat{G}}\right]$) is undefined, since $\hat{G}=0$ with positive probability. In this section four candidate methods for estimating $\mathrm{Var}\left[\frac{1}{\hat{G}}\right]$ are introduced and compared via a simulation to develop $\widehat{\mathrm{Var}\left[\frac{1}{\hat{G}}\right]}$.

The first proposed approach for estimating $\mathrm{Var}\left[\frac{1}{\hat{G}}\right]$ utilizes asymptotic results and the delta method (Ver Hoef [2012]). If $X \sim \mathrm{Binomial}(N,G)$ and $\hat{G}=\frac{X}{N}$, then

$$\sqrt{N}(\hat{G}-G) \xrightarrow{d} \mathrm{N}(0, G(1-G)),$$

as $N \to \infty$, by the Central Limit Theorem. Using the delta method,

$$\sqrt{N}\Big(\frac{1}{\hat{G}}-\frac{1}{G}\Big) \xrightarrow{d} \mathrm{N}\Big(0, \frac{1-G}{G^3}\Big),$$

as $N \to \infty$. Therefore $\hat{G}=\frac{X}{N}$ can be estimated using the asymptotic variance with

$$\widehat{\mathrm{Var}\left[\frac{1}{\hat{G}}\right]} = \frac{1-\hat{G}}{N\hat{G}^3}. \tag{3.9}$$

The next two methods consider a function, $f(\cdot)$, of $Y \sim$Binomial$(N,\hat{G})$ that is strictly positive on $\{0,1,...,\mathrm{N}\}$, and estimate $\mathrm{Var}\left[\frac{1}{\hat{G}}\right]$ as $\mathrm{Var}[f(Y)]$. Huso et al. [2012] obtains confidence intervals for mortality by performing independent bootstraps for the searcher efficiency, carcasses persistence, and the observed number of carcasses at individual turbines. Results are then combined across the bootstrapped values to understand uncertainty in the mortality estimate. Searcher efficiency (p), using the methods proposed by Huso [2010], is estimated by placing N_p trial carcasses in the field and recording the number observed by the searchers (X_p). The uncertainty due to this process is in-

cluded into mortality estimates by drawing from a Binomial$(N_p, \hat{p})$ distribution where $\hat{p} = \frac{X_p}{N_p}$. When a bootstrap value from the proposal distribution is zero, the estimate of $\hat{p}$ is calculated as $\frac{0.5}{N_p}$. Using this idea take $Y \sim \text{Binomial}(N, \hat{G})$, and define

$$Z = \begin{cases} \frac{N}{0.5} & \text{if } Y = 0, \\ \frac{N}{Y} & \text{otherwise.} \end{cases}$$

Then the the estimate of $\text{Var}\left[\frac{1}{\hat{G}}\right]$ can be calculated as

$$\widehat{\text{Var}\left[\frac{1}{\hat{G}}\right]} = \text{Var}[Z]. \tag{3.10}$$

While developing a confidence interval for the probability of a success in a Binomial experiment, Agresti and Coull [1998] proposed adding two successes and two failures to the result of the experiment. This idea can be utilized by letting $Y \sim \text{Binomial}(N, \hat{G})$, and calculating the estimate of $\text{Var}\left[\frac{1}{\hat{G}}\right]$ as

$$\widehat{\text{Var}\left[\frac{1}{\hat{G}}\right]} = \text{Var}\left[\frac{N+4}{Y+2}\right]. \tag{3.11}$$

The final approach that will be considered in this section is a Bayesian approach. Let X be the number of observed carcasses from the binomial trial. Suppose,

$$G \sim \text{Uniform}(0,1) \qquad \text{and} \qquad X|G \sim \text{Binomial(N,G)}.$$

Then

$$G|X \sim \text{Beta}(X+1, N-X+1).$$

For $X > 1$, $\text{Var}\left[\frac{1}{\hat{G}}\right]$ can be estimated as

$$\widehat{\text{Var}\left[\frac{1}{\hat{G}}\right]} = \text{Var}\left[\frac{1}{G}\middle|X\right] = \frac{(N+1)N}{X(X-1)} - \left(\frac{N+1}{X}\right)^2. \tag{3.12}$$

When $X \leq 1$, then $\text{Var}\left[\frac{1}{G}\middle|X\right]$ does not exist. Note when $X = 0$, (3.9) is also undefined, and (3.10) and (3.11) estimate $\text{Var}\left[\frac{1}{\hat{G}}\right]$ is zero.

The simulation used to evaluate and compare (3.9), (3.10), (3.11), and (3.12) considers values of G in $\{0.2, 0.3, ..., 0.9\}$ and values of N in $\{20, 60, 140\}$, where N is the number of carcasses placed in the field. The values for N represent the minimum (Erickson et al. [2004]), mean, and maximum (Good et al. [2011]) number of carcasses used to estimate G in the nine publicly available reports of mortality estimation at wind projects read in the literature review. Ten thousand trials were generated for each combination of G and N. Each trial consisted of a draw (X) from a Binomial(N, G), $\hat{G}$ was calculated as $\frac{X}{N}$, and $\widehat{\text{Var}\left[\frac{1}{\hat{G}}\right]}$ was calculated using (3.9), (3.10), (3.11), and (3.12).

The true value for $\text{Var}\left[\frac{1}{\hat{G}}\right]$ was estimated using the variance of the 10,000 simulated values for $\frac{1}{\hat{G}}$,

$$\text{Var}\left[\frac{1}{\hat{G}}\right] = \frac{\sum_i \left(\frac{1}{\hat{G}_i} - \sum \frac{1/\hat{G}}{10{,}000}\right)^2}{10{,}000 - 1}.$$

The methods were compared using the relative error,

$$\frac{\widehat{\text{Var}\left[\frac{1}{\hat{G}}\right]}_i - \text{Var}\left[\frac{1}{\hat{G}}\right]}{\text{Var}\left[\frac{1}{\hat{G}}\right]},$$

of the individual estimates (Figure 3.5 and Figure 3.6), and mean squared error (MSE),

$$\frac{\sum_i \left[\left(\widehat{\text{Var}\left[\frac{1}{\hat{G}}\right]}_i - \text{Var}\left[\frac{1}{\hat{G}}\right] \right)^2 \right]}{10,000},$$

(Table 3.5). Results for the simulation where 20 carcasses were used to estimate G, when G equals 0.2 or 0.3, were excluded, because a Monte Carlo estimate of $\text{Var}\left[\frac{1}{\hat{G}}\right]$ could not be obtained. In both cases there was a significant number of trials where $\frac{1}{\hat{G}}$ was undefined because $X = 0$. Without an estimate for $\text{Var}[\frac{1}{\hat{G}}]$, the relative error and MSE could not be calculated. None of the other combinations of settings produced cases where $X = 0$, except for the simulation with $N = 20$ and $G = 0.4$, where 1 of 10,000 trials had to be excluded in obtaining the Monte Carlo estimate of $\text{Var}\left[\frac{1}{\hat{G}}\right]$, relative errors, and MSE. Three additional trials, where $X = 1$, were also excluded from the results for the Bayesian method, (3.12), when $N = 20$ and $G = 0.4$.

The estimates of $\text{Var}\left[\frac{1}{\hat{G}}\right]$ using (3.9) and (3.11) tend to be the least biased, least variable (Figure 3.5 and Figure 3.6), and therefore have the lowest MSE (Table 3.5). In the cases where G is relatively high (e.g. 0.6 to 0.9) (3.9) and (3.11) produce similar results, with (3.9) typically yielding a slightly lower MSE when the number of trial carcasses is 60 or 140, and (3.11) yielding a slightly lower MSE when 20 trial carcasses are used. When G is relativity low (e.g. 0.2 to 0.5), (3.9) and (3.11) tend to produce similar results when 140 trial carcasses are used, but (3.11) produces a lower MSE when 20 or 60 trial carcasses are used.

The method given by (3.11) produced a lower MSE than (3.9) when G was less than 0.6 and 20 trial carcasses are used to estimate G, but to some extent researchers can

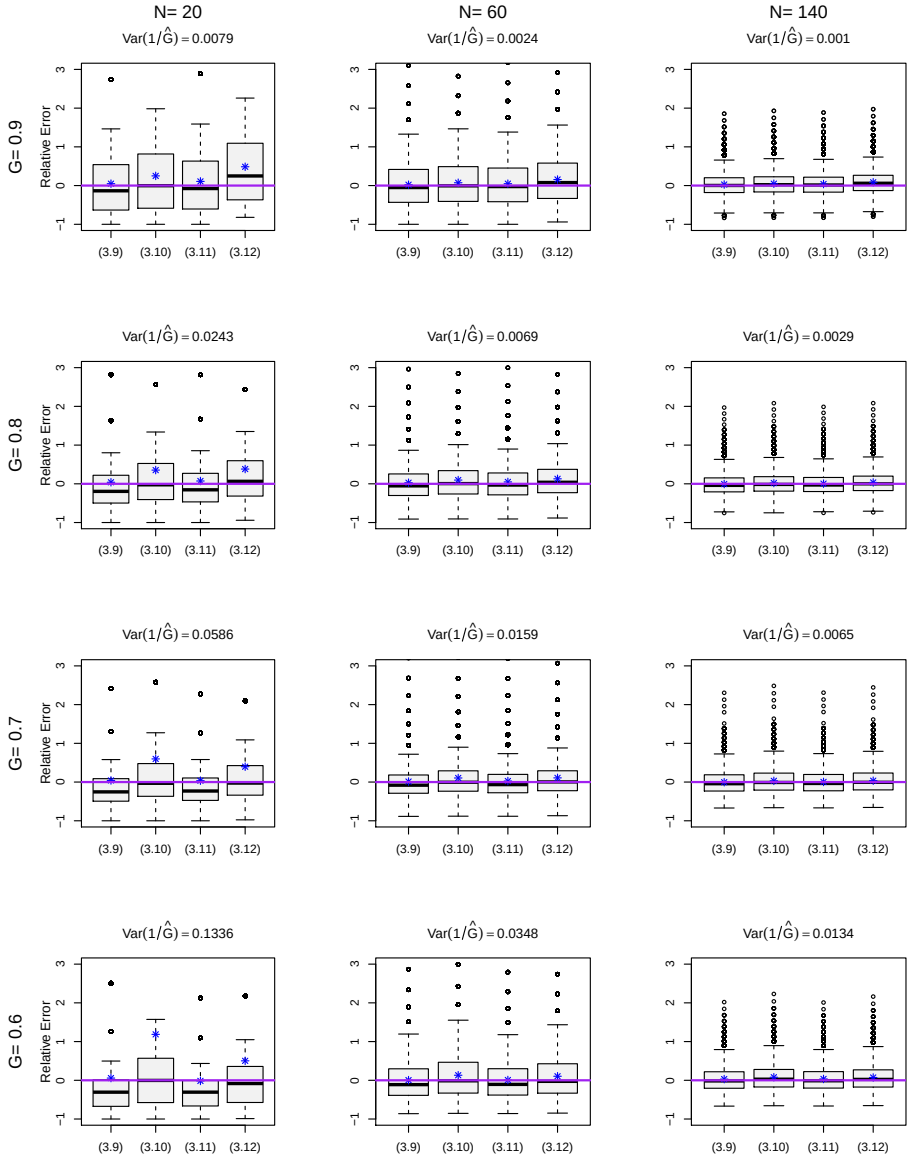

Figure 3.5: Relative error of the four proposed methods for estimating Var $\left[\frac{1}{\hat{G}}\right]$, when N trial carcasses are used to estimate G, the probability a carcass is observed given it landed in the searched area, with $\hat{G} = \frac{X}{N}$, $X \sim \text{Binomial}(N, G)$.

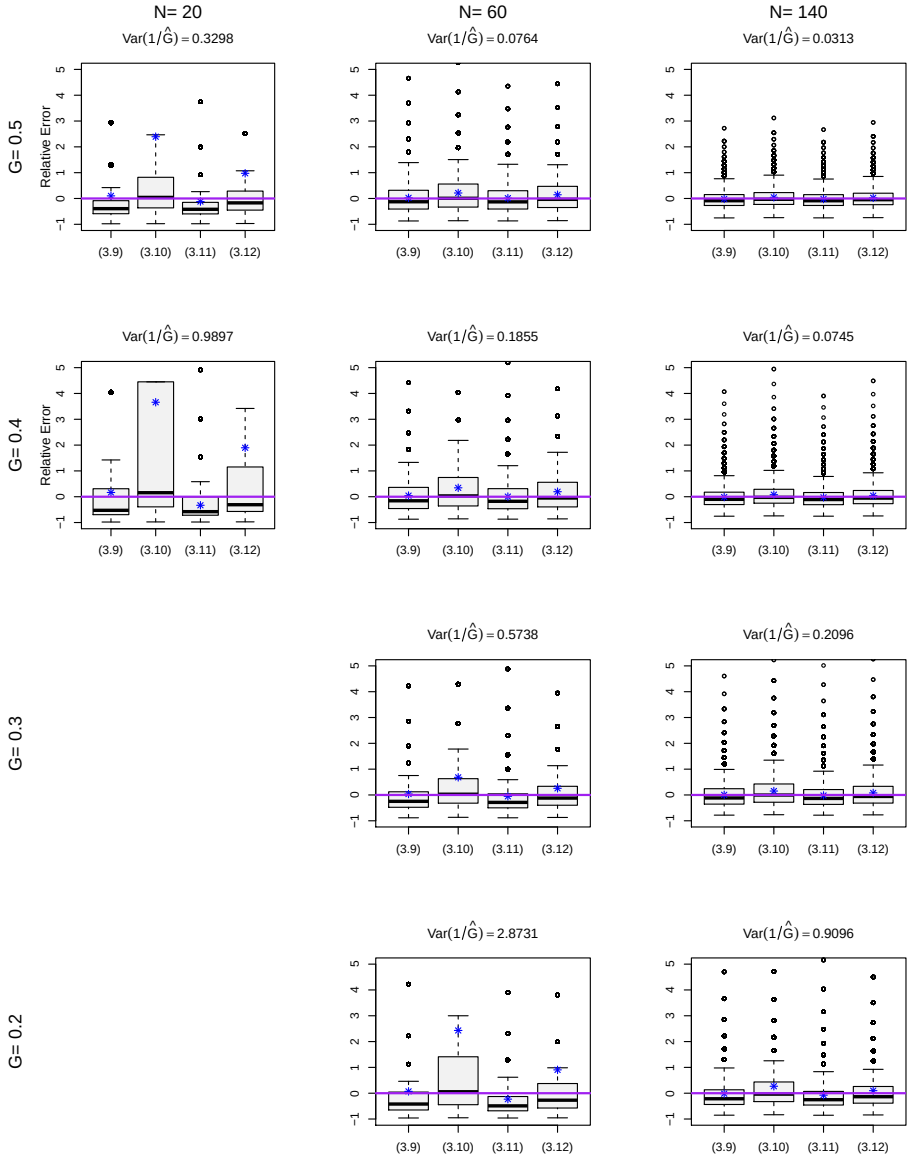

Figure 3.6: Relative error of the four proposed methods for estimating Var $\left[\frac{1}{\hat{G}}\right]$, when N trial carcasses are used to estimate G, the probability a carcass is observed given it landed in the searched area, with $\hat{G} = \frac{X}{N}$, $X \sim \text{Binomial}(N, G)$.

Table 3.5: Mean squared error (MSE) of the four proposed methods for estimating $\text{Var}\left[\frac{1}{\hat{G}}\right]$, when N trial carcasses are used to estimate G, the probability a carcass is observed given it landed in the searched area, with $\hat{G} = \frac{X}{N}$, $X \sim \text{Binomial}(N, G)$.

		G			
N	Equation	0.9	0.8	0.7	0.6
20	(3.9)	$6.7\text{x}10^{-5}$	0.0005	0.0047	0.0490
	(3.10)	$1.2\text{x}10^{-4}$	0.0013	0.0518	1.0338
	(3.11)	$7.2\text{x}10^{-5}$	0.0005	0.0035	0.0202
	(3.12)	$1.2\text{x}10^{-4}$	0.0010	0.0116	0.2435
60	(3.9)	$1.6\text{x}10^{-6}$	$1.1\text{x}10^{-5}$	$6.3\text{x}10^{-5}$	0.0003
	(3.10)	$1.9\text{x}10^{-6}$	$1.4\text{x}10^{-5}$	$8.4\text{x}10^{-5}$	0.0005
	(3.11)	$1.7\text{x}10^{-6}$	$1.2\text{x}10^{-5}$	$6.3\text{x}10^{-5}$	0.0003
	(3.12)	$2.0\text{x}10^{-6}$	$1.4\text{x}10^{-5}$	$7.9\text{x}10^{-5}$	0.0004
140	(3.9)	$1.2\text{x}10^{-7}$	$7.5\text{x}10^{-7}$	$3.9\text{x}10^{-6}$	$2.0\text{x}10^{-5}$
	(3.10)	$1.3\text{x}10^{-7}$	$8.1\text{x}10^{-7}$	$4.3\text{x}10^{-6}$	$2.4\text{x}10^{-5}$
	(3.11)	$1.2\text{x}10^{-7}$	$7.6\text{x}10^{-7}$	$3.9\text{x}10^{-6}$	$2.0\text{x}10^{-5}$
	(3.12)	$1.3\text{x}10^{-7}$	$8.3\text{x}10^{-7}$	$4.3\text{x}10^{-6}$	$2.3\text{x}10^{-5}$

		G			
N	Equation	0.5	0.4	0.3	0.2
20	(3.9)	15.69	110.2	N/A	N/A
	(3.10)	21.45	151.2		
	(3.11)	0.14	0.8		
	(3.12)	46.28	417.3		
60	(3.9)	0.0022	0.0217	0.3827	68
	(3.10)	0.0040	0.0610	3.9202	1186
	(3.11)	0.0020	0.0179	0.2436	7
	(3.12)	0.0030	0.0331	0.7499	2120
140	(3.9)	$1.2\text{x}10^{-4}$	0.0009	0.0112	0.3511
	(3.10)	$1.5\text{x}10^{-4}$	0.0013	0.0178	0.8460
	(3.11)	$1.2\text{x}10^{-4}$	0.0009	0.0102	0.2862
	(3.12)	$1.4\text{x}10^{-4}$	0.0011	0.0139	0.4942

control the variation in their estimate of G and therefore $\text{Var}\left[\frac{1}{\hat{G}}\right]$. Korner-Nievergelt et al. [2013] demonstrated that searcher efficiency and carcass persistence for bats and mice are similar. Therefore mice can be used as a supplement to achieve the desired samples size. Researchers do not have the same control over G, but if G is low they could consider decreasing the time between searches.

Along with the statistical performance, ease of implementation also needs to be taken into consideration. (3.9) does not require any understanding of statistics, while (3.11) may be more challenging to calculate for someone without a background in statistics. Taking the performance in the simulations and simplicity into account it is recommending that (3.9) is used when calculating $\text{Var}[\widehat{M}_{cake}]$ in the form provided in Theorem 2.

3.5 Estimating the Probability f_i

To calculate the standard error of $\widehat{M}_{cake}$ using the results of Theorem 2, the probability (f_i) a carcass lands in the i^{th} annulus needs to be estimated. Let $f(r)$ be probability density function (pdf) for carcass distance from the turbine, and r_i be the distance from the inner diameter for the i^{th} annulus to the turbine, then

$$f_i = \int_{r_i}^{r_{(i+1)}} f(x)\mathrm{d}x.$$

Under a R&P search protocol, the observed distances cannot be used directly to estimate $f(r)$, because only a portion of each annulus is searched, and the proportion of area searched decreases with distance. This means that carcasses landing further

from the turbine where proportion of area searched is low, are less likely to be observed relative to carcasses that land closer to the turbine, where proportion of area searched is high. Therefore, any method used to estimate f_i must account for the proportion of area searched for the i^{th} annulus (A_i). In this section three methods for estimating $f(r)$, or f_i, are introduced and compared via a simulation.

The cake and *glm* methods of adjusting for unsearched areas discussed in Chapter 2 can be utilized to obtain estimates for $f(r)$. The cake method indirectly estimates the number of carcasses in the i^{th} annulus as $\frac{C_i}{GA_i}$, where C_i is the number of observed carcasses in the i^{th} annulus, and G is the probability a carcass is observed given it landed in the searched area. Using the same logic f_i can be estimated as

$$\hat{f}_i = \frac{\frac{C_i}{GA_i}}{\sum_i \frac{C_i}{GA_i}} = \frac{\frac{C_i}{A_i}}{\sum_i \frac{C_i}{A_i}}. \tag{3.13}$$

The *glm* method adjusted for unsearched areas by estimating the spatial fall distribution of carcasses using Poisson regression. Utilizing the spatial carcass distribution, the marginal distribution for distance can estimated by integrating over the angle from the turbine. It is also possible, and computationally less expensive, to estimate the marginal distance distribution directly while still using Poisson regression. This can be accomplished by modeling

$$C_i \sim \text{Poisson}(\lambda_i) \qquad \log(\lambda_i) = \beta_0 + \beta_1 r_i + \beta_2 r_i^2 + \log(O_i),$$

where O_i is the amount of area searched for the i^{th} annulus. The pdf of carcass distance

can be estimated using the fitted model as,

$$\hat{f}_{pois}(r) = \frac{r\exp(\hat{\beta}_0 + \hat{\beta}_1 r + \hat{\beta}_2 r^2)}{\int r\exp(\hat{\beta}_0 + \hat{\beta}_1 r + \hat{\beta}_2 r^2)\mathrm{d}r}.$$

The estimate of f_i is

$$\hat{f}_i = \int_{r_i}^{r_{(i+1)}} \hat{f}_{pois}(x)\mathrm{d}x. \tag{3.14}$$

The idea and R code for the third approach considered in this section was provided by Daniel Dalthorp (personal communications). The method fits a parametric distribution to carcass distance by relating an assumed parametric family of distribution functions, $f(r|\Theta)$, indexed by Θ, to the observed carcass distribution function, $f_o(r|\Theta)$. Dalthorp recognized that if the spatial fall distribution is isotropic, then

$$f_o(r|\Theta) = \frac{f(r|\Theta)A(r)}{\int f(r|\Theta)A(r)\mathrm{d}r},$$

where $A(r)$ is a known function representing the proportion of the circumference defined by the circle with radius r in the searched area. The heuristic justification is that the probability a carcass is observed in a given area is the product of the probability it falls into that area times the proportion of that area that was searched. Given $f_o(r|\Theta)$, the log-likelihood function for the observed carcass distances (Δ) is given by

$$l(\Theta) \propto \sum_{r\in\Delta} \log(f(r|\Theta)) - [\log(\int f(r|\Theta)A(r)\mathrm{d}r)].$$

The maximum likelihood estimate (mle) of Θ can be obtained by maximizing the log-

likelihood over Θ, and f_i can be calculated as

$$\hat{f}_i = \int_{r_i}^{r_{i+1}} \hat{f}(x|\hat{\Theta}_{mle})\mathrm{d}x. \tag{3.15}$$

In the simulations that follow, this method is applied assuming that carcass distance follows a gamma distribution ($\Theta = (\alpha, \beta)$ and $f(r|\alpha,\beta) = (\Gamma(\alpha)\beta^{\alpha})^{-1} r^{\alpha-1} e^{-r/\beta}$), but any parametric family of distributions could be used.

The simulations used to evaluate and compare the performance of (3.13), (3.14), and (3.15) in estimating f_i consider the R&P configurations of two wind projects, three isotropic spatial carcass distributions, and four average carcass per turbine rates, all of which were used in the simulations of Chapter 2. The wind projects are referred to as WP2, which has 355 turbines located on agricultural land, and WP3, which has 23 turbines located on a forested ridge. The average rate of carcasses per turbine is set to either 2, 10, 25, or 70. The three carcass distance distributions are displayed in Figure 3.7. In all trials it was assumed that carcasses which landed on R&P were found with probability 0.85. For more justification on why these R&P configurations, rates, and distributions were chosen, and how each simulated trial is performed, refer to Section 2.3.

For each combination of settings, 1000 trials were performed, and $\hat{f}_i$ for i in {2,3, ..., 119} was calculated using each of (3.13), (3.14), and (3.15). The values for i are based on the annuli used to partition the area beneath turbines when applying the cake method of adjusting for unsearched areas. Since the purpose of obtaining $\hat{f}_i$ is to estimate $SD(\widehat{M}_{cake})$ using the results of Theorem 2, and each of the three methods provide

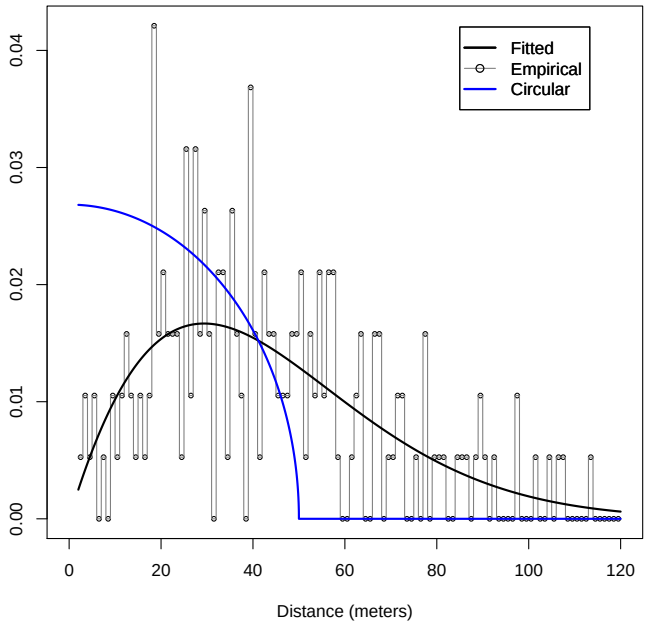

Figure 3.7: Probability density functions (pdf) of the distributions used for assigning carcass distance from the turbine tower. The fitted and empirical functions are based on data collected at WP1. The circular distribution was calculated under the implausable assumption that carcasses are struck uniformly in the rotor swept area, and fall straight down after colliding with the blades.

estimates for 118 f_i's in every trial, the performance was compared using

$$\frac{1}{T}\sqrt{\frac{M}{G}\sum_i \frac{(1-GA_i)\hat{f}_i}{A_i}}, \tag{3.16}$$

where T is the number of turbines. This is the estimate of the standard deviation of the estimated number of fatalities per turbine using the cake method, when M and G are assumed known (Corollary 2.1). Of course, if M is known there is no need to estimate

it, but using (3.16) for the comparison isolates the variation attributed to estimating f_i.

To compare the performance of the three methods proposed to estimate f_i, consider the relative error in calculating (3.16) (Figure 3.8 and Figure 3.9). The true value for the relative error calculation was obtained by substituting the true value for f_i in place of $\hat{f}_i$ in (3.16).

The results suggest that the empirical estimates for f_i using (3.13) provide relatively unbiased estimates, regardless of the R&P configurations, underlying distance distribution, $f(r)$, and average carcasses per turbine rate. The fitted distribution was obtained using Poisson regression, and therefore should give an advantage to Poisson regression technique (3.14); however, the relative error of (3.16) appears similar for the empirical and Poisson methods at both WP2 and WP3 under the fitted distribution. This suggests there is no advantage to using the Poisson regression method, even when it provides a good approximation of the underlying distribution.

Modeling carcass distance using maximum likelihood estimates from a Gamma distribution (3.15) shows promising results. This method produced the smallest relative error in a majority of the settings considered. The estimates obtained using (3.15) in (3.16) produced accurate results under the fitted distribution, for both R&P configurations, and under the empirical distribution at WP3. At WP2, under the empirical distribution, (3.15) over estimates the standard deviation on average by 4.5% when the rate is 2, to 6.8% when the rate is 70. Under the circular distribution, (3.15) overestimates by about 30% at WP2 for every rate, and by about 2% at every rate at WP3. It is not surprising that (3.15) performs poorly under the circular distribution, because the circular distribution is poorly approximated by a Gamma distribution.

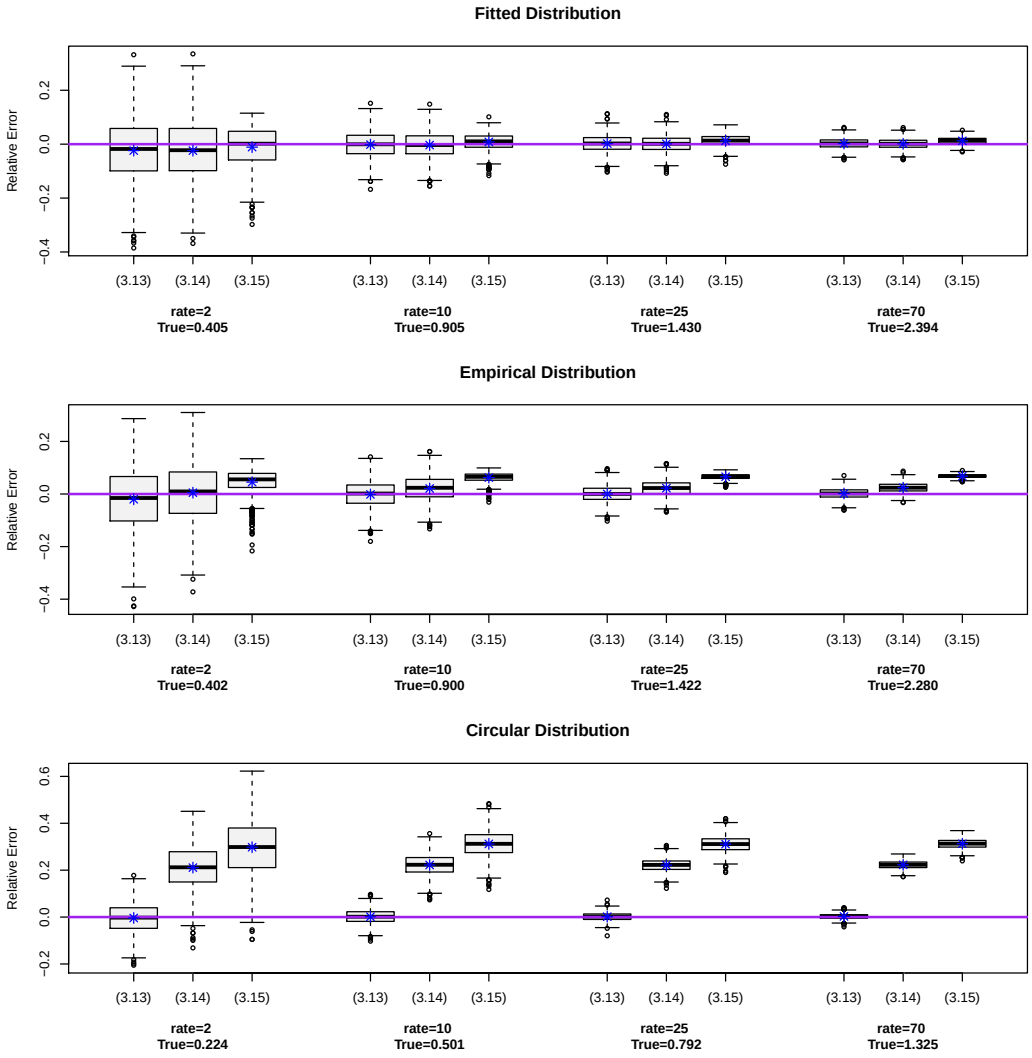

Figure 3.8: Relative error of the estimated standard deviation of the estimated average number of carcasses per turbine, using (3.13), (3.14), and (3.15) and the R&P configurations at WP2. The title of each plot displays the name of the distribution used to assign distance, $f(r)$ (Figure 3.7). "Rate" refers to the average number of carcasses per turbine. "True" refers to the value of the standard deviation when $\hat{f}_i = f_i$ in (3.16) used to calculate the relative error for each trial.

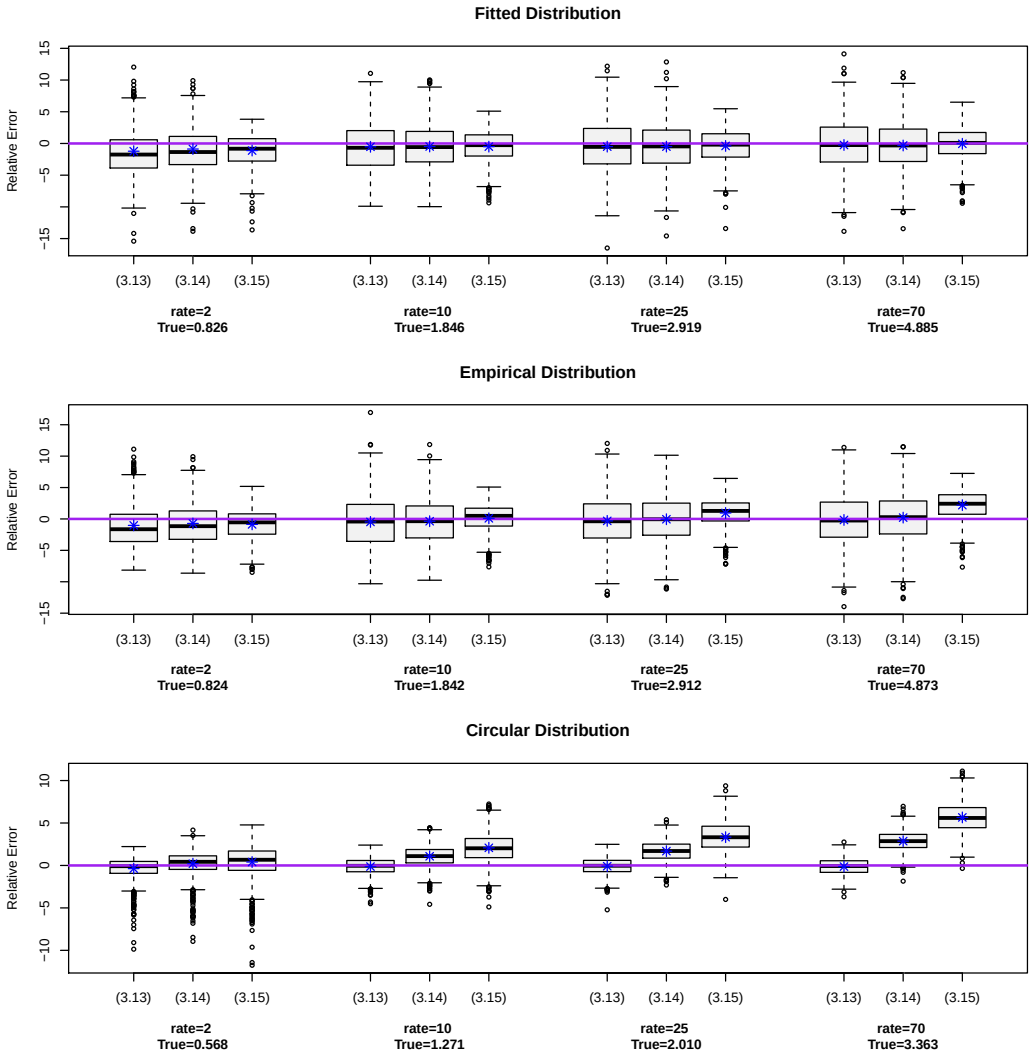

Figure 3.9: Relative error of the estimated standard deviation of the estimated average number of carcasses per turbine, using (3.13), (3.14), and (3.15) and the R&P configurations at WP3. The title of each plot displays the name of the distribution used to assign distance, $f(r)$ (Figure 3.7). "Rate" refers to the average number of carcasses per turbine. "True" refers to the value of the standard deviation when $\hat{f}_i = f_i$ in (3.16) used to calculate the relative error for each trial.

Given the similarity to the cake method of accounting for unsearched areas, the empirical method, (3.13), is a natural choice to estimate f_i. These estimates are obtained using the same principles as the cake method and estimator, and it is robust to the underlying carcass distance distribution, which was pivotal in the decision to use the cake method to estimate mortality under an isotropic fall distribution using data solely collected on R&P.

3.6 Estimating Variation of $\widehat{M}_{cake}$

In Section 3.4 and Section 3.5 methods were proposed to estimate quantities that are unknown in practice and influence the standard deviation of $\widehat{M}_{cake}$. The proposed methods are implemented in this section to develop parametric (Subsection 3.6.1), and bootstrap (Subsection 3.6.2) method for standard error calculation and confidence interval creation. The methods are compared in Subsection 3.6.3.

3.6.1 Parametric Estimate of Var$\left[\widehat{M}_{cake}\right]$

Theorem 2 and the simulations performed in sections 3.3, 3.4, and 3.5 lay a foundation for estimating the standard deviation of $\widehat{M}_{cake}$ parametrically. Under the conditions of Theorem 2,

$$SD[\widehat{M}_{cake}] = \sqrt{\text{Var}\left[\frac{GM}{\hat{G}}\right] + \text{E}\left[\frac{GM}{\hat{G}^2}\right]\sum_i \frac{(1-GA_i)f_i}{A_i}}.$$

When G is estimated using a binomial trial with N carcasses, as outlined in Section 3.3, this quantity can be estimated to form

$$SE(\widehat{M}_{cake}) = \sqrt{\hat{G}^2\widehat{M}^2_{cake}\widehat{\text{Var}\left[\frac{1}{\hat{G}}\right]} + \hat{G}\widehat{M}_{cake}\widehat{\text{E}\left[\frac{1}{\hat{G}^2}\right]}\sum_i \frac{(1-\hat{G}A_i)\hat{f}_i}{A_i}}$$

$$= \sqrt{\hat{G}^2\widehat{M}^2_{cake}\left(\frac{1-\hat{G}}{N\hat{G}^3}\right) + \hat{G}\widehat{M}_{cake}\left(\frac{1}{\hat{G}^2}\right)\sum_i \frac{(1-\hat{G}A_i)\frac{C_i}{A_i}}{\sum_i \frac{C_i}{A_i}}}{A_i}}$$

$$= \sqrt{\frac{\widehat{M}^2_{cake}(1-\hat{G})}{N\hat{G}} + \frac{\widehat{M}_{cake}}{\hat{G}\sum_i \frac{C_i}{A_i}}\sum_i \frac{(1-\hat{G}A_i)C_i}{A_i^2}}$$

$$= \sqrt{\frac{\widehat{M}^2_{cake}(1-\hat{G})}{N\hat{G}} + \frac{1}{\hat{G}^2}\sum_i \frac{(1-\hat{G}A_i)C_i}{A_i^2}} \tag{3.17}$$

In (3.17), $\text{Var}\left[\frac{1}{\hat{G}}\right]$ is estimated using asymptotic results and the delta method given in Section 3.4, $E\left[\frac{1}{\hat{G}^2}\right]$ is estimated using asymptotic results, and the f_i are estimated using the empirical method in Section 3.5.

3.6.2 Bootstrap Estimate of Var $\left[\widehat{M}_{cake}\right]$

If G is estimated using any method other than a Binomial trial, the estimate for $\text{Var}\left[\frac{1}{\hat{G}}\right]$ in deriving (3.17) does not apply, making the equation invalid for estimating the standard deviation of $\widehat{M}_{cake}$. Under this circumstance it is still possible to account for the variation in $\widehat{M}_{cake}$ attributed to adjusting for unsearched area by using a para-

metric bootstrap method. The use of a bootstrap conforms to the standard methods for calculating the standard error for mortality estimates of turbine induced bird and bat fatalities (Huso et al. [2012] and Korner-Nievergelt et al. [2015]).

Accounting for the uncertainty in the estimate of mortality (M) due to the adjustment for unsearched areas requires simulating observed carcass counts for each annulus. The number (C) of observed carcasses can be modeled as a binomial random variable with M (=Mortality) trials and probability of success, or finding a carcass, equal to the probability (G) a carcass is observed given it landed in the searched area times the probability (a) a carcass lands in the searched area (i.e. $C \sim \text{Binom}(M, aG)$). The location ($\Delta$) of the C carcasses is a sample from the observed distribution ($f_0(r, \theta)$), which is a function of the carcass distribution ($f(r, \theta)$), and the searched areas (i.e. R&P configuration).

A bootstrapped observed carcass distribution can be obtained by simulating an observed count (C_{boot}) from a Binom($\hat{M}, \hat{a}\hat{G}$) distribution. Then C_{boot} locations can be obtained by sampling with replacement form the observed carcass locations (Δ).

Estimating the the uncertainty of $\widehat{M}_{cake}$ using a bootstrapping method also requires a bootstrapped value for $\hat{G}$. Obtaining $\hat{G}_{boot}$ depends on the method used to estimate G. If a Binomial(N, G) trial was used to estimate G, then $\hat{G}_{boot}$ can be obtained by simulating from a Binomial($N, \hat{G}$) and dividing by N. If G was estimated using independent trials for searcher efficiency and carcass persistence, then Huso et al. [2012] obtains $\hat{G}_{boot}$ by sampling with replacement from both data sets and applying the formula used to obtain $\hat{G}$ (e.g. Shoenfeld [2004], Huso [2010],Korner-Nievergelt et al. [2011]) to the bootstrapped values.

Researchers should avoid conducting trials where $\hat{G}_{boot}$ can take on the value of

zero by placing enough trial carcasses while estimating G, or decreasing the interval between searches to increase G. In the event, however, that some values of simulated binomial trials are zero, researchers can add two pseudo successes and failures to every simulated trial (Agresti and Coull [1998]). This method is recommended based on the performance of (3.11) in Section 3.4.

Given $(C_{1,boot}, C_{2,boot}, ..., C_{n_a,boot})$ and $\hat{G}_{boot}$, a bootstrap value of $\widehat{M}_{cake}$ can be calculated as

$$\widehat{M}_{boot} = \frac{1}{\hat{G}_{boot}} \sum_i \frac{C_{i,boot}}{A_i}.$$

The bootstrapped estimate of SD $\left[\widehat{M}_{cake}\right]$ is obtained by simulating B bootstrapped values of $\widehat{M}_{cake}$ and taking

$$\text{SE}\left[\widehat{M}_{cake}\right] = \text{SD}(\widehat{M}_{1,boot}, ..., \widehat{M}_{B,boot}). \tag{3.18}$$

The set of B bootstrapped values for $\widehat{M}_{cake}$ can also be used to calculate bias, confidence intervals and other desired statistics of $\widehat{M}_{cake}$.

3.6.3 Simulating $\widehat{\text{SD}}\left[\widehat{M}_{cake}\right]$

The final simulation presented in this chapter was designed to test the validity and performance of the parametric and bootstrap methods for standard error calculation and confidence interval creation when estimating mortality with $\widehat{M}_{cake}$. The simulations were performed using the same techniques outlined in Chapter 2, under a subset of the settings that have been used throughout this chapter, and considered the R&P configu-

rations of WP2 and WP3, the fitted and empirical fall distributions from Figure 3.7, two values for the average number of carcasses per turbine (10 and 70), and two values for G, the probability a carcass is observed given it landed on R&P (0.50 and 0.85). In short, mortality (M) is held constant for a set of conditions and determined by the number of turbines and average number of fatalities per turbine. Carcass location was assigned independently to each carcass based on the assumed fall distribution. Carcasses were assigned an indicator to determine if they were on R&P according to the configurations used in that trial. Carcasses that landed on R&P were assigned a random value from a Bernoulli(G) distribution to determine if they were observed. This process produces a data set designed to mimic the random process observed in practice when implementing a R&P search protocol. Ten-thousand trials were performed for each combination of settings. In each simulated trial, G was estimated using a binomial trial with 60 carcasses, and both (3.17) and (3.18) were applied to estimate SD$[\widehat{M}_{cake}]$, and form a 95% confidence interval for mortality.

In each trial the estimate for $\widehat{M}_{cake}$ was recorded to obtain the Monte Carlo estimate for the true of SD$\left[\widehat{M}_{cake}\right]$ (Table 3.6). For each estimate of $\widehat{M}_{cake}$, (3.17) and (3.18) were used to calculate the standard error. These methods are compared using the error, relative to Monte Carlo estimate (Figure 3.10). In each trial, the parametric and bootstrap methods were also used to obtain 95% confidence intervals for M. The parametric 95% confidence interval was obtained using,

$$\widehat{M}_{cake} \pm 1.96 \cdot \text{SE}(\widehat{M}_{cake}),$$

Table 3.6: Monte Carlo mean (standard deviation) estimates for the average number of carcasses per turbine calculated as $\widehat{M}_{cake}$ divided by the number of turbines (355 at WP2 and 23 at WP3). Results are based on 10,000 trials for each combination of wind project, fall distribution, average rate of carcasses per turbine, and probability (G) of observing a carcass that landed on the R&P.

		Rate =10		Rate=70	
Wind Project	Distance Distribution	G=0.50	G=0.85	G=0.50	G=0.85
WP2	Fitted	10.2 (1.9)	10.1 (1.1)	71.6 (10.2)	70.6 (4.6)
	Empirical	10.2 (1.8)	10.0 (1.1)	71.2 (10.3)	70.3 (4.6)
WP3	Fitted	10.2 (2.9)	10.0 (1.9)	71.2 (11.8)	70.1 (5.5)
	Empirical	10.2 (2.9)	10.0 (2.0)	71.2 (12.3)	71.1 (11.9)

where SE($\widehat{M}_{cake}$) was calculated using (3.17). The critical value is taken from the standard normal distribution using the central limit theorem, because the cake method is the sum of random variables with a small negative dependence that goes to zero as the distance between the inner and outer diameter of the annuli goes to zero. $\hat{G}$ converges in probability to G as the number of trial carcasses goes to infinity. Therefore, Slutsky's theorem can be applied to argue that the cake estimator asymptotically follows a normal distribution. The 95% confidence interval using the bootstrap method was obtained by taking the 0.025 and 0.975 quantile from the 1000 bootstrapped estimates of $\widehat{M}_{cake}$. These two methods for creating 95% confidence intervals are compared using coverage probability, and mean length (Table 3.7).

The results for the parametric, (3.17), and bootstrap, (3.18), methods of estimating SD($\widehat{M}_{cake}$) suggest that both techniques produce similar results. The bootstrap method appears to be slightly more accurate and precise than the parametric method, specifically

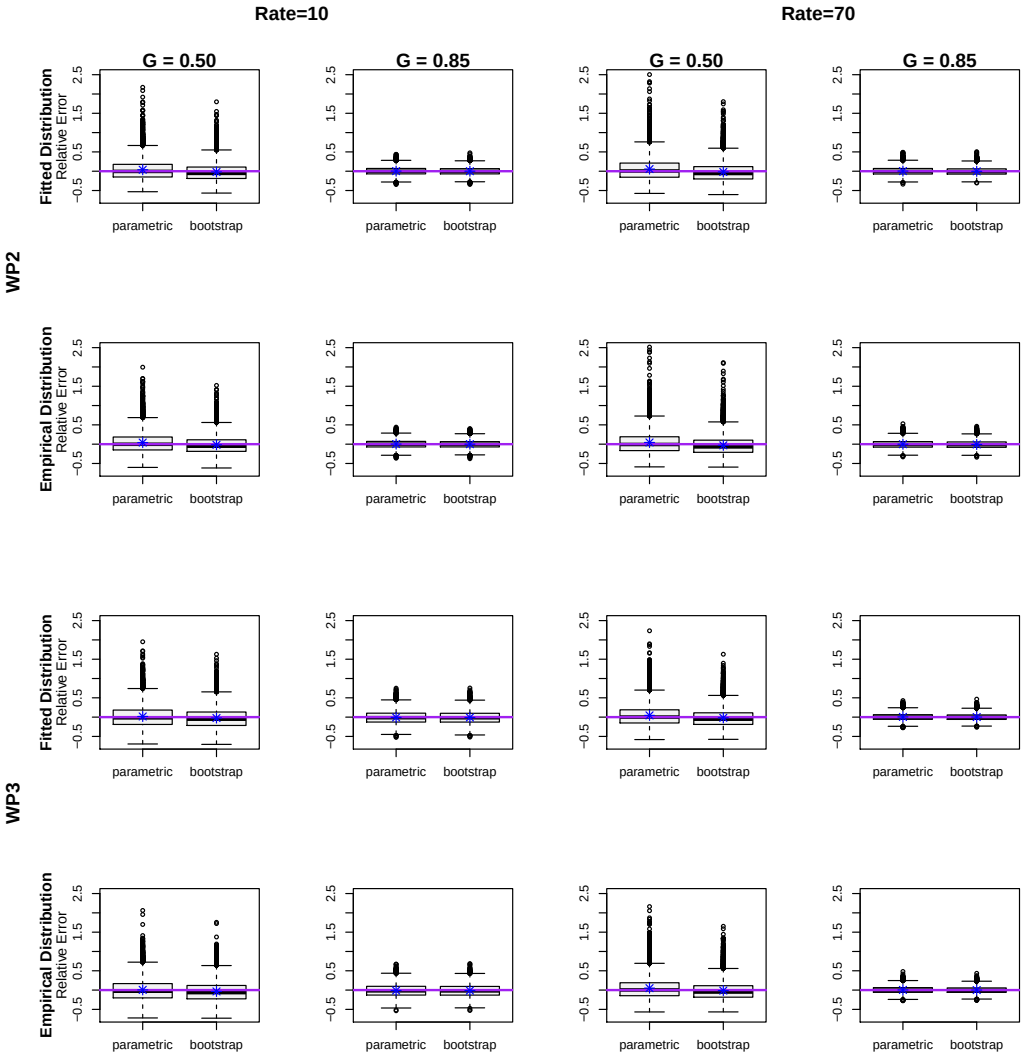

Figure 3.10: Estimates for SD[$\widehat{M}_{cake}$] using the parametric (3.17) and bootstrap (3.18) methods. Results are based on 10,000 trials for each combination of setting and considered the R&P configurations at WP2 and WP3, the fitted and empirical distance distributions displayed in Figure 3.7, two values for the probability of detecting a carcass in the searched area (G), and two average carcass per turbine rates.

Table 3.7: Coverage probability (and length) of the 95% confidence intervals for mortality (M) created using the parametric and bootstrapping methods for estimating uncertainty of $\widehat{M}_{cake}$. Results are based on 10,000 trials for each combination of wind project, fall distribution, average rate of carcasses per turbine, and probability (G) of observing a carcass that landed on the R&P.

			Rate =10		Rate=70	
Wind Project	Distance Distribution	Method	G=0.50	G=0.85	G=0.50	G=0.85
WP2	Fitted	para	94.6 (7.5)	94.6 (3.8)	94.7 (41.7)	94.4 (13.7)
		boot	94.7 (7.3)	95.3 (3.9)	95.1 (40.1)	95.6 (13.9)
	Empirical	para	94.4 (7.4)	94.7 (3.8)	94.5 (41.5)	94.3 (13.6)
		boot	94.5 (7.2)	94.9 (3.9)	95.0 (39.8)	95.0 (13.8)
WP3	Fitted	para	93.7 (11.3)	93.6 (7.3)	94.4 (47.6)	94.9 (21.5)
		boot	92.8 (11.2)	93.9 (7.4)	94.6 (46.1)	95.4 (21.9)
	Empirical	para	93.4 (11.4)	93.6 (7.2)	94.8 (47.7)	94.7 (21.5)
		boot	92.8 (11.2)	93.9 (7.4)	94.9 (46.2)	95.2 (22.0)

when $G = 0.50$; But the conclusions obtained from either method, will likely produce the same practical results.

The results for coverage probability and mean length of the 95% confidence intervals, are also similar for both methods. Both tend to have better coverage and shorter lengths when the average carcass per turbine rate increases or the probability of observing a carcass that landed on R&P increases.

When M is is estimated from R&P searches using the cake method of adjusting for unsearched area, and a binomial trial to estimate G, the results for the parametric and bootstrap techniques are similar from a practical view, and therefore the suggestion is for the researcher to use the method that is the most convenient for them. The bootstrapping method may likely be easier to integrate into the statistical software suggested by Huso

et al. [2012] and Korner-Nievergelt et al. [2015], as these softwares already bootstrap to estimate the uncertainty around mortality estimates. The parametric method may be easier if estimation is performed by hand. If G is estimated using independent trials for carcass persistence and searcher efficiency then the uncertainty in $\widehat{M}_{cake}$ should only be calculated using the bootstrapping techniques, because (3.17) assumes G was estimated with a binomial trial and is invalid otherwise.

3.7 Conclusions

This chapter utilized the cake method of adjusting for unsearched areas introduced in Chapter 2, to develop the cake estimator of mortality (3.1). Theoretical results were provided in Section 3.2, and give a set of conditions that show when estimation of mortality using the cake estimator is appropriate from a theoretical perspective. The most restrictive of these conditions is the need for uniform carcass density within an annulus. This condition implies the spatial carcass distribution is isotropic, meaning carcasses are distributed uniformly with respect to angle from the turbine. When isotropy is a reasonable assumption, it is still unlikely the carcass distribution is perfectly uniform within every annulus, because carcass density tends to decrease with distance. This assumption becomes more reasonable when the buffer, the difference between the inner and outer diameters of the annuli, is decreased. For this reason a one meter buffer was used throughout Chapter 2 and Chapter 3, opposed to the ten meter buffer used by Jain [2005] when developing this method of adjusting for unsearched areas. In practice researchers should use the smallest buffer possible given the accuracy of the equipment

used to record carcass location.

The cake estimator of mortality requires an estimate for G, the probability a carcass is observed given it landed on R&P. In Section 3.3 the performance of estimating G with a binomial trial was compared to the commonly used methods that form an estimate of G by estimating carcass persistence and searcher efficiency independently. The results suggests that the Binomial method for estimating G is as or more accurate than the commonly used methods. The results also suggests that without altering its simple form, the binomial method can accommodate a variety of carcass persistence distributions and reductions in probability of detection for carcasses that go unobserved and persist to the next trial.

The results given in Table 3.6 are not exhaustive but provide insight to understanding how the cake estimator of mortality is affected by different R&P configurations, carcass fall distributions, average rate of carcasses per turbine, and probabilities of observing a carcass that landed on R&P. Recall in all of these simulations, G was estimated using a binomial trial with 60 carcasses. These results show that the estimator is biased, and the bias becomes more noticeable when the rates are low or G decreases. This was expected. When conducting a binomial trial $\hat{G}$ yields an unbiased estimate of G, but $\frac{1}{\hat{G}}$ is biased for $\frac{1}{G}$. Further research is needed to determine if the the bias can be accounted for. Given the accuracy of the bootstrapping method in estimating the standard deviation of the mortality estimate, it may be possible to use bootstrapped mortality estimates, to quantify the bias and adjust the estimate provided by $\widehat{M}_{cake}$.

Sections 3.4 and 3.5 explored methods for estimating Var $\left[\frac{1}{\hat{G}}\right]$, when G is estmimated from a binomial trial, and the underlying distribution of carcass distance from the

turbine, which are needed to calculate the standard error of $\widehat{M}_{cake}$. Methods were suggested based on their performance relative to each other, ease of use, and how well they aligned with the empirical theme of the cake estimator. The proposed methods were applied to form parametric and bootstrapping procedures for estimating the standard deviation of $\widehat{M}_{cake}$ and form confidence intervals for mortality. Both procedures yielded similar results, and it will be left up to researchers to determine which method is best for them.

Along with testing if the bootstrapping methods provide a means of accounting for the bias in $\widehat{M}_{cake}$, future work will be focused on developing an R package to implement the cake estimator of mortality. An R package would provide researchers the opportunity to deviate from suggested methods provided in this chapter, but more importantly it will provide assistance to researchers interested in estimating mortality of birds or bats at wind projects from data only collected on R&P.

4 Accounting for Anisotropy

4.1 Introduction

The results in Chapter 2 demonstrated that the cake and generalized linear model (*glm*) methods of accounting for unsearched areas are capable of producing accurate and precise estimates for the proportion of carcasses that land on the roads leading up to turbines and pads beneath the turbines (R&P) as long as the spatial carcass distribution is isotropic. Under an anisotropic distribution the cake and *glm* methods produce biased estimates depending on the R&P configurations. The purpose of this chapter is to determine if the cake and *glm* methods can be adjusted to accurately account for unsearched areas under anisotropic fall distributions.

Section 4.2 motivates the need for estimators that maintain desirable properties under anisotropic carcass fall distributions. In Section 4.3 adjustments are proposed for the cake and *glm* methods, along with corresponding hypothesis tests to aid in determining if anisotropy is present. Section 4.4 assesses the proposed methods via a simulation. Section 4.5 gives the results of the simulations, and Section 4.6 summarizes the findings of the chapter.

4.2 Evidence of Anisotropy

Researchers as early as Howell and DiDonato [1991] have commented that carcass distributions may be a function of wind, with carcasses being found more often and further from the turbine in the direction the wind is moving. Intuitively, it seems carcasses would be more likely to fall with the wind, opposed to against the wind. Therefore anisotropic spatial carcass distributions are likely at projects where the wind direction does not vary uniformly.

Searches for bat fatalities at WP1, introduced in Chapter 2, in 2013 were conducted daily within a 90 meter radius, cleared of all vegetation surrounding 15 turbines, enabling researchers to obtain the location of 200 carcasses determined to have been killed on the previous night (Figure 4.1a). The average direction from which the wind was blowing on the night of arrival for each of the 200 carcasses was calculated using data from two on-site meteorological towers (Figure 4.1b). The largest proportion (35%) of fatalities arrived on nights where the wind originated from the southwest quadrant. The largest proportion (33.5%) of bats fell in the northeast quadrant, providing evidence that wind direction influences carcass location.

The effect of wind on bat carcass location becomes even more apparent when all 200 carcass locations are displayed relative to a northern originating wind (Figure 4.1c). Only 20% of carcasses were observed upwind relative to the average nightly wind direction, and carcasses landed further from the turbine in the downwind direction.

Figure 4.1 was created using the average wind direction for the night, because the exact time the carcass arrived is unknown. The average wind direction for a night was

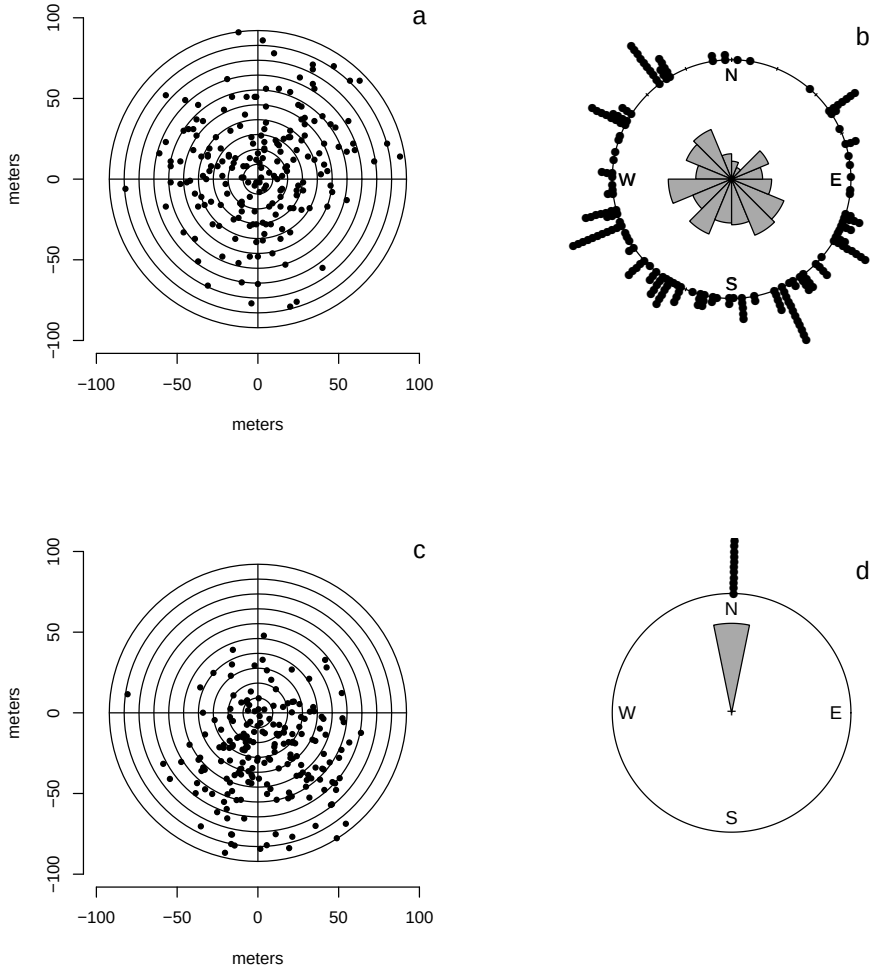

Figure 4.1: Fall distribution relative to nearest turbine and average nightly wind direction for 200 carcasses at WP1 in April to November 2013. (a) Carcass location relative to the nearest turbine (y-axis oriented N-S). (b) Rose plot of the average nightly wind direction (dots display the direction from which the wind originates) on the night the fatalities occurred. (c) Carcass location relative to the nearest turbine, rotated to a northern originating average nightly wind direction. (d) Rose plot showing rotated average wind direction.

calculated by averaging across measurements produced every 10 minutes by two meteorological towers. On average the ten minute interval wind direction measurements spanned 122^{o} per night, implying the wind direction at the time the bat collided with the turbine could differ substantially from the average. If the true wind direction at the time of the collision was known and used to display carcass location, or if the circular standard deviation of wind directions was less, it is likely anisotropy would be even more severe than it appears in Figure 4.1c.

Wind direction influences carcass location, and it is reasonable to suspect that spatial carcass distributions at wind projects with little variation in wind direction may be anisotropic. In the forms they were presented in Chapter 2, the cake and *glm* methods of accounting for unsearched areas under a R&P search protocol where not robust to anisotropic fall distributions. Therefore adjustments must be made to these methods in order to accurately and precisely estimate mortality at wind projects using data solely obtained from R&P searches when anisotropy is present.

4.3 Accounting and Testing for Anisotropy

In this section modifications to the cake and *glm* methods of accounting for unsearched areas, presented in Chapter 2, are proposed to enhance performance under anisotropic fall distributions. Both methods give rise to hypothesis tests to determine if anisotropy is present. The performance of the methods and tests are compared via simulations in Section 4.4.

4.3.1 Anisotropic Cake Method

The cake method, based on the ideas of Jain [2005], accounts for unsearched areas by partitioning the fall zone into concentric annuli, indexed by i. Mortality (M) is estimated by summing over the number of observed carcasses (C_i) in each annulus divided by the probability (G) a carcass is observed given it landed in the searched area, and the proportion (A_i) of area searched.

$$\widehat{M}_{cake} = \frac{1}{\hat{G}} \sum_i \frac{C_i}{A_i},$$

where $\hat{G}$ is an estimate of G.

The cake method performs well under isotropic fall distributions, because it partitions the area beneath a turbine into annuli. Under an isotropic distribution carcass density is uniform for a fixed distance, and therefore relatively uniform within an annulus. Under anisotropy, carcass density is not uniform for a given distance; however, the premise of the cake method can still be applied to obtain reasonable results as long as the fall zone is partitioned into areas where carcass density is relatively uniform within each element. Potentially, this can be accomplished by: (1) further dividing the annuli used in the traditional cake method into quadrants or eighths, or (2) dividing the fall area into squares or rectangles. There are numerous reasonable partitions that can be implemented using the empirical idea of the cake method, but researchers must ensure that at least some portion of every element in the partition is searched (i.e. $A_i \neq 0$ for all i). Researchers can achieve this by clearing and searching the entire area beneath one or more turbines, although this does deviate from a true R&P search protocol.

Section 4.4 tests how the partition obtained by further dividing the annuli into quadrants accounts for various anisotropic spatial carcass distributions. Let j in $\{1, 2, 3, 4\}$ index the quadrant. Under this partition the anisotropic cake method can be expressed as

$$\widehat{M}^{(a)}_{cake} = \frac{1}{\hat{G}} \sum_i \sum_{j=1}^{4} \frac{C_{ij}}{A_{ij}}, \tag{4.1}$$

where C_{ij} and A_{ij} are the observed number of carcasses found and proportion of area searched in the j^{th} quadrant of the i^{th} annulus. Ideally, the quadrant lines should be constructed to partition upwind areas together and downwind areas together. This means that the quadrant lines should be drawn 45^o clockwise and counterclockwise from the average wind direction (Figure 4.2). This requires estimating the average wind direction at the time of collision with the turbine over all the fatalities that took place during

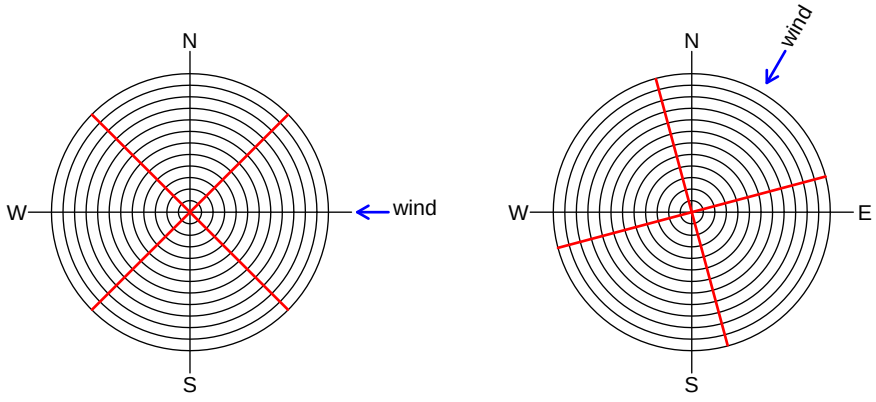

Figure 4.2: Examples of the proposed method for determining quadrant lines for the anisotropic cake method of adjusting for unsearched areas.

the period of interest. If the carcass distribution is anisotropic because there is little variation in wind direction, then the average wind direction should yield an adequate estimate. If anisotropy is present and there is no predominant wind direction, then averaging the average nightly wind directions weighted by the number of observed fatalities on each night may provide a reasonable estimate; although, it could be misleading if the probability of observing a fatality is not constant across nights. The probability of observing a fatality that took place may change if the carcass fall distribution is a function of wind speed, or if certain weather conditions influence carcass persistence or searcher efficiency.

4.3.2 The χ^2-test of Anisotropy

Partitioning the fall zone using annuli divided into quadrants can also be used to test if an equal proportion of carcasses fall into each quadrant for every distance. If carcasses are more or less likely to fall in some quadrants, then there is evidence for an anisotropic spatial carcass distribution. Let $p_{j|i}$ be the proportion of carcasses that fall into the j^{th} quadrant conditioned on landing in the i^{th} annulus. Then, the data obtained to estimate mortality using the anisotropic cake method introduced in the previous subsection can be utilized to test

$$\begin{array}{ll} H_0 : p_{1|i} = p_{2|i} = p_{3|i} = p_{4|i} = 0.25 & \text{vs.} \\ H_1 : p_{j|i} \neq 0.25 \text{ for some } j \text{ in } \{1,2,3,4\} & \end{array}$$

for every annulus (indexed by i). For fixed i, this can be accomplished with a χ^2 goodness-of-fit test using the observed counts in each quadrant, and the proper hypoth-

esized proportions. Simply hypothesizing 25% of the carcasses should be observed in each quadrant could produce misleading results if the proportion (A_{ij}) of area searched in each quadrant differs. If the carcass distribution is isotropic and relatively uniform within an annulus, then the expected proportion ($p_{0,j|i}$) of observed carcasses in the j^{th} quadrant conditioned on landing in the i^{th} annulus is equal to the proportion of area searched in annulus i contained in quadrant j. This can be calculated as $p_{0,j|i} = \frac{A_{ij}}{\sum_j A_{ij}}$. Letting $(C_{i1}, C_{i2}, C_{i3}, C_{i4})$ be the observed counts in each quadrant, and $\dot{C} = \sum_{j=1}^{4} C_{i,j}$, the χ^2 test statistic can be calculated as

$$X_i^2 = \sum_{j=1}^{4} \frac{(C_{ij} - p_{0,j|i}\dot{C})^2}{p_{0,j|i}\dot{C}},$$

with a corresponding p-value obtained by calculating $\mathrm{P}(X > X_i^2)$ with $X \sim \chi_3^2$. Testing if an equal proportion of carcasses fall in each quadrant for every annulus simultaneously is achieved using the test statistic $X^2 = \sum_i X_i^2$ and p-value $\mathrm{P}(X > X^2)$ with $X \sim \chi_{3n}^2$, where n is the total number of distance bins considered.

When performing a χ^2-test there are numerous rules of thumb imposed on the expected cell count to ensure valid conclusions. A majority of introductory statistics textbooks reference Cochran [1954] which suggests that no expected cell count be less than one, and at most 20% of the expected cell counts be less than five. In this setting the expected cell count is $p_{0,j|i}\dot{C}$ for a fixed i and j. Satisfying the suggestion put forth by Cochran [1954] will likely require aggregating across annuli used in calculating $\widehat{M}_{cake}^{(a)}$. In the simulations described in Section 4.4 one meter annuli divided into four quadrants are used to calculate $\widehat{M}_{cake}^{(a)}$, and ten meter distance bins also divided into quadrants

are used to calculate the χ^2 statistic. In practice researchers should choose reasonable bin sizes, before conducting the test, that ensure the conditions suggested by Cochran [1954] are satisfied.

As previously mentioned, this test is capable of identifying anisotropic distributions where the proportion of carcasses falling in a quadrant differs at some distance. Depending on the orientation of the two lines used to define the quadrants, it is possible for a fall distribution to be anisotropic and have an equal probability on landing in any quadrant for every distance. In fact, any distribution with a reflective symmetry across both quadrant lines will satisfy this conditions (Figure 4.3).

Anisotropic distributions that are symmetric across both quadrant axes can still be

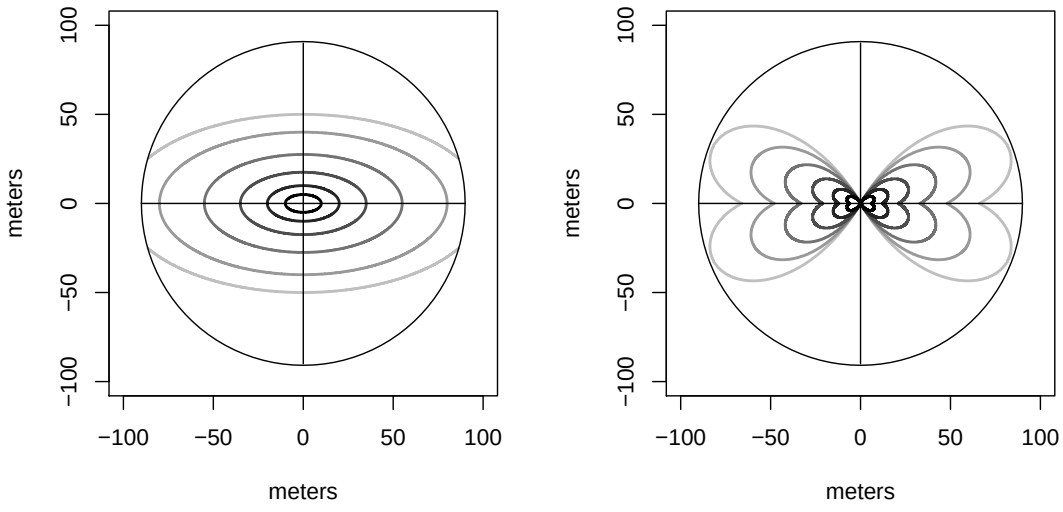

Figure 4.3: Contour plot of anisotropic distributions where an equal number of carcasses are expected to fall in each quadrant if quadrant lines are defined by the x and y axes.

identified by rotating the quadrant lines 45°, and performing the χ^2-test in the same fashion on the new quadrants. It is possible to contrive distributions that are anisotropic and would not be captured by either χ^2-test, but such examples are even more hypothetical than those given in Figure 4.3. Performing the test using multiple partitions requires a multiple comparisons adjustment, such as the Šidák correction (Šidák [1967]), to preserve the desired type-I error rate.

The χ^2 test for anisotropy of

$$\begin{aligned} &H_0\text{: Isotropic Fall Distribution} \qquad \text{vs.} \\ &H_1\text{: Anisotropic Fall Distribution} \end{aligned}$$

is performed by conducting the χ^2 test described above using both the quadrant lines used in calculating $\widehat{M}^{(a)}_{cake}$, and those lines rotated 45°. Implementing the Šidák correction, H_0 is rejected in favor of H_1 at level α if either test statistic is greater than the $1-(1-\alpha)^{\frac{1}{2}}$ quantile from a χ^2_{3n} distribution, where n is the number of distance bins that were used to calculate the test statistics.

4.3.3 Anisotropic *glm* Method

The *glm* method presented in Chapter 2, based on the ideas of Huso and Dalthorp [2014], partitions the fall zone into one meter square cells indexed by distance (r) and direction (θ), and models the carcass distribution by normalizing the fitted Poisson regression model on the observed counts ($C_{r,\theta}$) in each cell,

$$\begin{aligned} C_{r,\theta} &\sim \text{Poisson}(\lambda_{r,\theta}) \\ \log(\lambda_{r,\theta}) &= \beta_0 + \beta_1 r + \beta_2 r^2 + \log(O_{r,\theta}), \end{aligned} \tag{4.2}$$

where $O_{r,\theta}$ is the number of turbines that contain cell (r,θ) in R&P. In order to account for anisotropic carcass distributions, θ must be taken into account to allow carcass density to depend on direction. Inclusion of θ into the Poisson regression model requires accounting for its circular nature. Circular variables have a cyclical pattern (e.g. direction on a compass, time of day, day of year), and cannot be integrated into statistical models as traditional numerical variables, because high values are close to small values. For example, in azimuth 355^o is closer to 5^o than 340^o. Methods have been derived to incorporate circular variables into linear and generalized linear models (Pewsey et al. [2013]). For a simple linear regression model with a continuous response (y) and circular predictor (θ), the most basic model is given by

$$y_i = \beta_0 + \beta_1 \cos(\theta) + \beta_2 \sin(\theta) + \varepsilon_i \tag{4.3}$$

where ε_i is the random error term and typically assumed to be independent and identically distributed according to some distribution with mean zero. (4.3) works well when the mean of the response follows a true sinusoidal pattern as a function of θ. Pewsey et al. [2013] gives numerous extensions of (4.3) that can be used when a sinusoidal function of θ is not appropriate, one of which is modeling y as a K^{th} order Fourier series of θ,

$$y_i = \beta_0 + \sum_{k=1}^{K} \beta_{2k-1} \cos(k\theta) + \beta_{2k} \sin(k\theta) + \varepsilon_i. \tag{4.4}$$

Incorporating the circular variable direction into (4.2) requires modeling the natural logarithm of carcass density as a quadratic function of distance that can depend on the

angle. This can be achieved by including an interaction between the distance and angle when modeling $\log(\lambda_{r,\theta})$. The proposed anisotropic *glm* model assumes the observed carcass count ($C_{r,\theta}$) in the cell indexed distance r and direction θ follows a Poisson distribution with mean $\lambda_{r,\theta}$ with

$$\begin{aligned}\log(\lambda_{r,\theta}) &= \beta_0 + \beta_1 r + \beta_2 r^2 \\ &\quad + \sum_{k=1}^{K} \beta_{4k-1} r\cos(k\theta) + \beta_{4k} r\sin(k\theta) + \beta_{4k+1} r^2\cos(k\theta) + \beta_{4k+2} r^2\sin(k\theta) \\ &\quad + \log(O_{r,\theta}), \end{aligned} \tag{4.5}$$

where θ is the clockwise angle form the average wind direction. Again this requires estimating the average wind direction which is discussed in Subsection 4.3.1.

The main effects for angle (i.e. $\sin(\theta)$ and $\cos(\theta)$) are not incorporated into (4.5), because it seems reasonable to assume a common intercept for each direction. In this application no carcass can land within two meters of the turbine, but theoretically the generalized linear model used to estimate the spatial carcass distribution produces an estimated carcass density at the origin. If the main effects for angle were included in the model, the estimated density at the origin could change depending on the value for θ that is used, providing multiple density estimates for a single location. To avoid this issue, the main effects are not included in (4.5).

The value of K represents the order of the Fourier expansion on θ. Higher values of K allow for more flexible models; however, increasing K by one requires estimation of four additional coefficients. An excess of terms in the model could potentially in-

crease the variation in mortality estimates. In the simulations described in Section 4.4, estimates are calculated using K equal to one through four, to determine if an optimum value exists.

After obtaining the fitted equation of (4.5), denoted $\widehat{\log(\lambda_{r,\theta})}$, the estimates for the probability (a) a carcass lands in the searched area and mortality (M) are obtained using the equivalent procedure to the analogous isotropic method introduced in Chapter 2. The estimated fall distribution is calculated as

$$\hat{f}^{(a)}(r,\theta) = \frac{re^{\widehat{\log(\lambda_{r,\theta})}}}{\sum_{r,\theta} re^{\widehat{\log(\lambda_{r,\theta})}}}.$$

Using $\hat{f}^{(a)}(r,\theta)$, a is estimated as

$$\hat{a}^{(a)}_{glm} = \sum_{r,\theta} \hat{f}^{(a)}(r,\theta)\frac{O_{r,\theta}}{T}, \tag{4.6}$$

where T is the total number of turbines at the wind facility. Given the estimated proportion of carcasses that land on R&P, M is estimated as,

$$\widehat{M}^{(a)}_{glm} = \frac{\frac{C}{\hat{G}}}{\hat{a}^{(a)}_{glm}}. \tag{4.7}$$

4.3.4 Likelihood Ratio Test for Anisotropy

The anisotropic glm method of adjusting for unsearched areas presents another method that can be used to test for anisotropy. If the fall distribution is isotropic then the coefficients for the terms with θ should all be zero. Testing

$$\begin{array}{ll} \mathrm{H}_0\text{: } \beta_3 = ... = \beta_{4k+2} = 0 & \text{vs.} \\ \mathrm{H}_1\text{: } \beta_i \neq 0 \text{ for } i \in 3, ..., 4k+2\ , & \end{array}$$

where k is the order of the Fourier expansion, can be accomplished using a likelihood ratio test. The loglikelihood function assuming a Poisson distribution is given by

$$\ell(\lambda_{r,\theta}) = \sum_{r,\theta}[C_{r,\theta}\log(\lambda_{r,\theta}) - \lambda_{r,\theta} - \log(C_{r,\theta}!)].$$

Let $\hat{\lambda}_{r,\theta}^{(0)}$ be the maximum likelihood estimate (mle) of $\lambda_{r,\theta}$ obtained from the fitted model to (4.5) when $K = 0$ (i.e. the isotropic *glm* model given in Chapter 2), and $\hat{\lambda}_{r,\theta}^{(k)}$ be the mle of $\lambda_{r,\theta}$ obtained from the fitted model to (4.5) when $K = k$ for some k in {1, 2, 3, ...}. Let

$$\Lambda = 2[\ell(\hat{\lambda}_{r,\theta}^{(k)}) - \ell(\hat{\lambda}_{r,\theta}^{(0)})].$$

In practice, Λ can be approximated numerically. For instance, in R it can be obtained by calculating the difference in "Residual Deviance" between the isotropic and anisotropic fitted models. H_0 is rejected in favor of H_1 at level α if $\mathrm{P}(X > \Lambda) < \alpha$ with $X \sim \chi^2_{4k}$. When H_0 is rejected, there is evidence that the carcass distribution depends on θ, implying the carcass distribution is anisotropic.

4.4 Simulations

Simulations were designed to evaluate the performance of the methods of adjusting for unsearched areas under anisotropic carcass distributions proposed in Section 4.3,

and used to compare the methods to each other. The simulations were also utilized to evaluate and compare the tests for determining if anisotropy is present. Each trial of every simulation produces a data set of observed carcasses designed to mimic the random process observed in practice. Two R&P configurations, three spatial carcass distributions, and four average carcass per turbine rates were considered.

The two R&P configurations were obtained from anonymous wind projects referred to as WP2 and WP4. WP2, which was used in Chapter 2, is utilized again; however, WP3 was not used in these simulations. Under the anisotropic carcass distribution considered in Chapter 2, the isotropic cake and *glm* methods produced reasonable results at WP3, because the amount of area searched for every angle was similar. The R&P configurations of WP4 are used instead. Like WP3, WP4 has 23 turbines and is located on a ridge-line. As the results below demonstrate, the bias in the estimates obtained using the isotropic cake and *glm* methods under anisotropic carcass distributions is more apparent at WP4 relative to WP3.

Three carcass distributions were considered in the simulations: one isotropic and two anisotropic (Figure 4.4). The distributions were used to create four settings: Isotropy, Anisotropy 0, Anisotropy 5.5, and Anisotropy EMP.

The Isotropy setting simulates carcass location from an isotropic distribution, derived from a Poisson regression model fit on the carcass distances to the nearest turbine observed at WP1 in 2013. This distributions was referred to as the fitted distribution in Chapter 2.

The same anisotropic distribution used in Chapter 2 (Figure 4.4 (left)) is considered again. It was developed to mimic a circumstance where the wind predominately

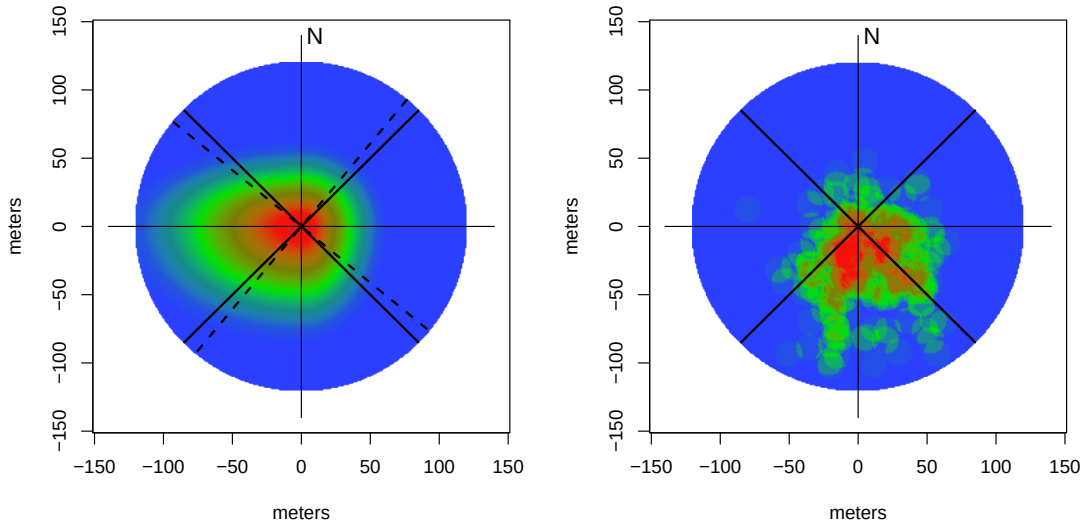

Figure 4.4: Heatmaps of the anisotropic distributions used in the simulations with quadrant lines for the anisotropic cake method. Anisotropic distributions used in Anisotropy 0 (Left), Anisotropy 5.5 (Left), and Anisotropy EMP (Right). Solid lines indicated the quadrants for the anisotropic cake method in Anisotropy 0 and Anisotropy EMP. The dashed lines indicate the quadrant in Anisotropy 5.5.

originates in the east. Carcasses are twice as likely to land west of the turbine, where they also tend to be the most dispersed. This single anisotropic distribution was used to create two estimation scenarios: Anisotropy 0 and Anisotropy 5.5. In Anisotropy 0 researchers correctly assume the average wind directions originates from the east. In Anisotropy 5.5 researchers incorrectly assumed the wind originates from the 5.5^{o} counterclockwise from due east. This affects the orientation of the quadrant lines used when implementing the anisotropic cake method (Figure 4.4), and the direction used for $\theta = 0$ when implementing the anisotropic *glm* methods.

The distribution used in the Anisotropy EMP (Figure 4.4 (right)), is based off the location of the carcasses observed at WP1 relative to a the nearest turbine a northern average wind direction (Figure 4.1c). To simulate carcass location, the coordinates from one of the 200 locations displayed in Figure 4.1c is selected, and then shifting uniformly to any cell within 10 meters of the original selected coordinates. Some restrictions were needed when selecting the locations within 10 meters of the original coordinates to ensure the simulated carcasses location was at least two meters from the turbine. In Anisotropy Emp it is assumed the wind originates north of the turbines.

The simulations used the same four average carcass per turbine rates considered in Chapter 2 (2, 10, 25, and 70), except at WP4, where the rate of 2 carcasses per turbine was excluded. At WP4 only eight carcasses are expected to be observed when the average rate is 2, which makes estimation using the anisotropic methods unfeasible. Therefore, this case was excluded from the results. In practice, if eight carcasses are observed, researchers should avoid using the anisotropic techniques discussed in this chapter.

Simulated carcass searches were performed to or past the maximum assignable distance from the turbine, 120 meters. The probability (G) of observing a carcass that landed on R&P was held constant at 0.85 and assumed known. One thousand trials where performed for every combination of R&P configuration, anisotropic setting, and average rate of carcasses per turbine.

In each trial an estimate for the probability a carcass lands on R&P ($\hat{a}$), and a pseudo estimate for mortality ($\widetilde{M}$) were recorded for the isotropic and anisotropic cake methods, and the isotropic and anisotropic glm methods ($K = 1,2,3,4$). As in Chapter 2, the

expression "pseudo" is used, because G is assumed known, meaning that G was used in place of $\hat{G}$ in (4.1) and (4.7). For the *glm* methods, the value for the AIC of the Poisson regression model was recorded. In every trial the p-value for the χ^2 and *LR* ($K = 1, 2, 3, 4$) tests were recorded.

4.5 Results

The results are based on the pseudo estimates, $\bar{M} = \frac{\tilde{M}}{T}$, of the average mortality per turbine. Estimates denoted with $^{(a)}$, were calculated using a method designed to account for anisotropy. The value of K for the *glm* methods denotes the order of the Fourier expansion on θ when fitting the Poisson regression model, (4.5).

In some circumstances at WP4, the anisotropic *glm* models associated with the third and fourth order Fourier expansions were calculated excluding trials with unreasonable estimates (Table 4.2). For example, 31 trials with estimates greater than 100 carcasses per turbine were excluding in calculating the mean and standard deviation of $\bar{M}^{(a)}_{glm}(K = 4)$ at WP4 under the isotropic carcass distribution with an average rate of 10 carcasses per turbine. Unreasonable estimates for M occur when the leading coefficient of the Poisson regression model is positive for some direction, causing predicted carcass density to actually increase with distance from the turbine. Restricting this from happening is not trivial, because the leading coefficient of the *glm* used to model carcass density as a function of distance, r, for a fixed value of θ is the sum of nine terms when $K = 4$. To ensure predicted density does not increase with distance in any direction requires fitting a model where the sum of the nine coefficients associated with terms

Table 4.1: Mean (and standard deviation) for the estimated average number of carcasses per turbine at WP2, calculated as $\widetilde{M}$ divided by the number of turbines (355). An $^{(a)}$ indicates anisotropic methods. The value of K for the *glm* methods gives the order of the Fourier expansion. Values in bold indicate that method was within 1% of the lowest MSE amongst the models considered for a given setting.

		rate=2	rate=10	rate=25	rate=70
Isotropy	$\bar{M}_{cake}$	2.03 (0.39)	10.0 (0.9)	25.1 (1.5)	70.4 (2.4)
	$\bar{M}^{(a)}_{cake}$	2.03 (0.40)	10.0 (0.9)	25.1 (1.5)	70.4 (2.5)
	$\bar{M}_{glm}$	**2.00 (0.38)**	**10.0 (0.9)**	**24.9 (1.4)**	**70.0 (2.4)**
	$\bar{M}^{(a)}_{glm}(K=1)$	1.99 (0.39)	9.9 (0.9)	24.9 (1.4)	70.0 (2.4)
	$\bar{M}^{(a)}_{glm}(K=2)$	2.05 (0.42)	10.0 (1.0)	25.0 (1.5)	70.1 (2.4)
	$\bar{M}^{(a)}_{glm}(K=3)$	2.10 (0.46)	10.2 (1.0)	25.2 (1.5)	70.3 (2.5)
	$\bar{M}^{(a)}_{glm}(K=4)$	1.95 (0.53)	9.9 (1.2)	24.8 (2.0)	69.8 (3.3)
Anisotropy 0	$\bar{M}_{cake}$	2.27 (0.48)	11.4 (1.1)	28.5 (1.6)	80.0 (2.7)
	$\bar{M}^{(a)}_{cake}$	**2.12 (0.43)**	10.7 (1.0)	26.8 (1.5)	75.1 (2.5)
	$\bar{M}_{glm}$	2.26 (0.48)	11.4 (1.1)	28.4 (1.6)	80.0 (2.7)
	$\bar{M}^{(a)}_{glm}(K=1)$	2.13 (0.44)	10.7 (1.0)	26.7 (1.5)	74.8 (2.5)
	$\bar{M}^{(a)}_{glm}(K=2)$	**2.08 (0.45)**	10.6 (1.0)	25.9 (1.5)	72.5 (2.5)
	$\bar{M}^{(a)}_{glm}(K=3)$	2.04 (0.48)	**10.1 (1.0)**	**25.2 (1.6)**	**70.3 (2.6)**
	$\bar{M}^{(a)}_{glm}(K=4)$	1.93 (0.53)	9.9 (1.2)	24.9 (1.9)	70.0 (3.1)
Anisotropy 5.5	$\bar{M}_{cake}$	2.27 (0.48)	11.4 (1.1)	28.5 (1.6)	80.0 (2.7)
	$\bar{M}^{(a)}_{cake}$	**2.13 (0.43)**	10.8 (1.0)	26.8 (1.5)	75.2 (2.5)
	$\bar{M}_{glm}$	2.26 (0.48)	11.4 (1.1)	28.4 (1.6)	80.0 (2.7)
	$\bar{M}^{(a)}_{glm}(K=1)$	2.13 (0.44)	10.7 (1.0)	26.7 (1.5)	74.8 (2.5)
	$\bar{M}^{(a)}_{glm}(K=2)$	**2.08 (0.45)**	10.6 (1.0)	25.9 (1.5)	72.5 (2.5)
	$\bar{M}^{(a)}_{glm}(K=3)$	2.04 (0.48)	**10.1 (1.0)**	**25.2 (1.6)**	**70.3 (2.6)**
	$\bar{M}^{(a)}_{glm}(K=4)$	1.93 (0.53)	9.9 (1.2)	24.9 (1.9)	70.0 (3.1)
Anisotropy Emp	$\bar{M}_{cake}$	**1.90 (0.37)**	**9.6 (0.8)**	23.9 (1.4)	67.0 (2.1)
	$\bar{M}^{(a)}_{cake}$	1.85 (0.36)	9.3 (0.8)	23.3 (1.3)	65.1 (2.1)
	$\bar{M}_{glm}$	**1.90 (0.37)**	**9.6 (0.8)**	**24.0 (1.3)**	67.3 (2.3)
	$\bar{M}^{(a)}_{glm}(K=1)$	1.83 (0.37)	9.1 (0.8)	22.8 (1.3)	63.8 (2.0)
	$\bar{M}^{(a)}_{glm}(K=2)$	1.87 (0.40)	9.1 (0.8)	22.5 (1.3)	62.8 (2.0)
	$\bar{M}^{(a)}_{glm}(K=3)$	1.96 (0.49)	9.7 (1.1)	24.0 (1.7)	67.1 (2.7)
	$\bar{M}^{(a)}_{glm}(K=4)$	1.94 (0.53)	9.8 (1.2)	24.5 (1.9)	**68.8 (3.1)**

Table 4.2: Mean (and standard deviation) for the estimated average number of carcasses per turbine at WP4, calculated as $\widetilde{M}$ divided by the number of turbines (23). An $^{(a)}$ indicates anisotropic methods. The value of K for the *glm* methods gives the order of the Fourier expansion. Values in bold indicate that method was within 1% of the lowest MSE amongst the models considered for a given setting.

		rate=10	rate=25	rate=70
Isotropy	$\bar{M}_{cake}$	10.1 (2.2)	24.9 (3.3)	70.1 (5.7)
	$\bar{M}^{(a)}_{cake}$	10.1 (2.6)	24.9 (4.1)	70.0 (7.0)
	$\bar{M}_{glm}$	**10.1 (2.1)**	**25.0 (3.3)**	**70.1 (5.6)**
	$\bar{M}^{(a)}_{glm}(K=1)$	10.2 (2.5)	25.1 (3.9)	70.3 (6.6)
	$\bar{M}^{(a)}_{glm}(K=2)$	10.3 (4.1)	25.1 (4.2)	70.3 (7.0)
	$\bar{M}^{(a)}_{glm}(K=3)$	11.5 (8.0)†	25.6 (5.6)	70.5 (7.1)
	$\bar{M}^{(a)}_{glm}(K=4)$	11.8 (8.5)*	26.2 (6.6)†	71.0 (7.7)
Anisotropy 0	$\bar{M}_{cake}$	**8.3 (1.9)**	20.6 (3.0)	58.0 (5.1)
	$\bar{M}^{(a)}_{cake}$	10.0 (3.7)	24.9 (5.9)	70.0 (10.0)
	$\bar{M}_{glm}$	**8.4 (1.9)**	20.7 (2.9)	58.2 (5.0)
	$\bar{M}^{(a)}_{glm}(K=1)$	10.1 (3.1)	**25.0 (4.8)**	**69.5 (8.3)**
	$\bar{M}^{(a)}_{glm}(K=2)$	10.5 (3.6)	25.6 (5.3)	71.2 (8.6)
	$\bar{M}^{(a)}_{glm}(K=3)$	11.2 (6.5)†	26.0 (6.7)	70.8 (9.2)
	$\bar{M}^{(a)}_{glm}(K=4)$	11.9 (9.1)*	27.1 (8.9)†	71.7 (10.7)
Anisotropy 5.5	$\bar{M}_{cake}$	**8.3 (1.9)**	20.6 (3.0)	58.0 (5.1)
	$\bar{M}^{(a)}_{cake}$	10.5 (4.1)	26.4 (6.5)	73.6 (10.9)
	$\bar{M}_{glm}$	**8.4 (1.9)**	20.7 (2.9)	58.2 (5.0)
	$\bar{M}^{(a)}_{glm}(K=1)$	10.1 (3.1)	**25.0 (4.8)**	**69.5 (8.3)**
	$\bar{M}^{(a)}_{glm}(K=2)$	10.5 (3.6)	25.6 (5.3)	71.2 (8.6)
	$\bar{M}^{(a)}_{glm}(K=3)$	11.2 (6.5)†	26.0 (6.7)	70.8 (9.2)
	$\bar{M}^{(a)}_{glm}(K=4)$	11.9 (9.1)*	27.1 (8.9)†	71.7 (10.7)
Anisotropy Emp	$\bar{M}_{cake}$	11.7 (2.5)	29.4 (3.8)	82.4 (6.5)
	$\bar{M}^{(a)}_{cake}$	9.7 (2.1)	**24.3 (3.2)**	**68.4 (5.3)**
	$\bar{M}_{glm}$	11.7 (2.5)	29.2 (3.7)	81.9 (6.4)
	$\bar{M}^{(a)}_{glm}(K=1)$	**9.7 (2.0)**	**23.9 (3.1)**	66.7 (5.0)
	$\bar{M}^{(a)}_{glm}(K=2)$	9.7 (2.4)	24.1 (3.7)	67.3 (5.6)
	$\bar{M}^{(a)}_{glm}(K=3)$	10.1 (4.4)	24.6 (4.2)	68.4 (5.7)
	$\bar{M}^{(a)}_{glm}(K=4)$	10.2 (4.5)†	24.9 (4.4)	69.2 (6.1)

† Calculated excluding 10-15 trials where $\bar{M} > 100$

* Calculated excluding 30-45 trials where $\bar{M} > 100$

that include r^2 are negative for every value of θ. In these 31 trials, between 20 and 36 observed carcass were used to fit the 19 parameter model, which is a relatively small sample size for such a complicated model. In practice, researchers should avoid using the higher order *glm* methods when sample sizes are relatively small, and can use graphical displays to identify fitted carcass distributions that suggest carcass density increases with distance. Therefore researchers should be able to identify situations that lead to these unreasonable estimates which justifies the exclusion of these trials from Table 4.2.

Isotropy

Under the isotropic setting, the average estimates obtained by $\bar{M}_{cake}$ and $\bar{M}^{(a)}_{cake}$ are almost identical at both wind projects for all the rates considered (Table 4.1, Table 4.2, and Figure 4.5). At WP2, there is negligible increase in standard deviation for the anisotropic cake method relative to the isotropic method. At WP4, the standard deviation increases by about 22%.

Under the isotropic setting, the anisotropic *glm* methods display bias which increases with the order of the Fourier expansion, K. The bias never exceeds 3% at WP2, and is the most noticeable at WP4 when the rate is 10 carcasses per turbine, which is also when the number of observed carcasses is at its lowest (Table 4.3). The bias stems from estimates for the non-zero coefficients, β_1 and β_2 in (4.5), that define the carcass distributions. As the number of terms in the model increases, so does the bias of $\hat{\beta}_1$ and $\hat{\beta}_2$ (Figure 4.6). Coefficient estimates when fitting a Poisson regression model are obtained using maximum likelihood estimates, which may be biased. In this setting the bias in $\hat{\beta}_1$ and $\hat{\beta}_2$ becomes more noticeable as more non-significant terms are introduced to the model.

Like the bias, the variability of the anisotropic *glm* methods also increases as K

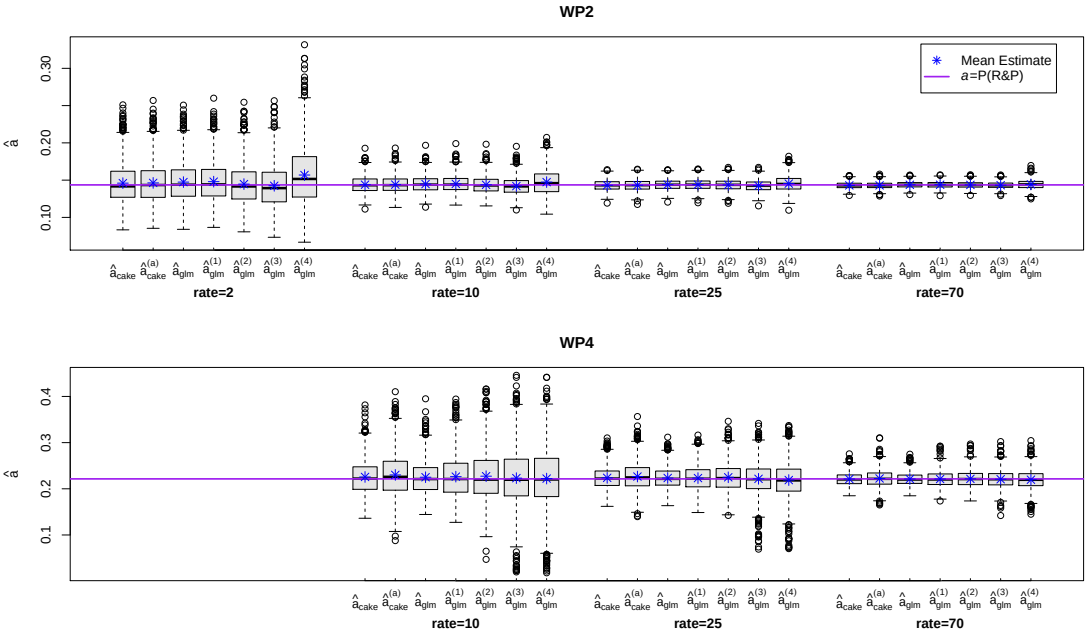

Figure 4.5: Estimates for $\hat{a}$ using isotropic and anisotropic methods under the Isotropy setting for every average rate of carcasses per turbine considered at WP2 (top) and WP4 (bottom). Anisotropic methods are indicated with a superscript. The superscript for the *glm* methods gives the order of the Fourier expansion used when fitting the Poisson regression model.

Table 4.3: Expected number of observed carcasses for each setting under the two R&P configurations considered in the simulation for each average rate of carcasses per turbine.

	WP2				WP4		
Setting	rate=2	rate=10	rate=25	rate=70	rate=10	rate=25	rate=70
Isotropy	87	433	1083	3033	43	108	303
Anisotropy0	90	451	1126	3155	40	101	281
AnisotropyEMP	85	425	1062	2974	44	110	307

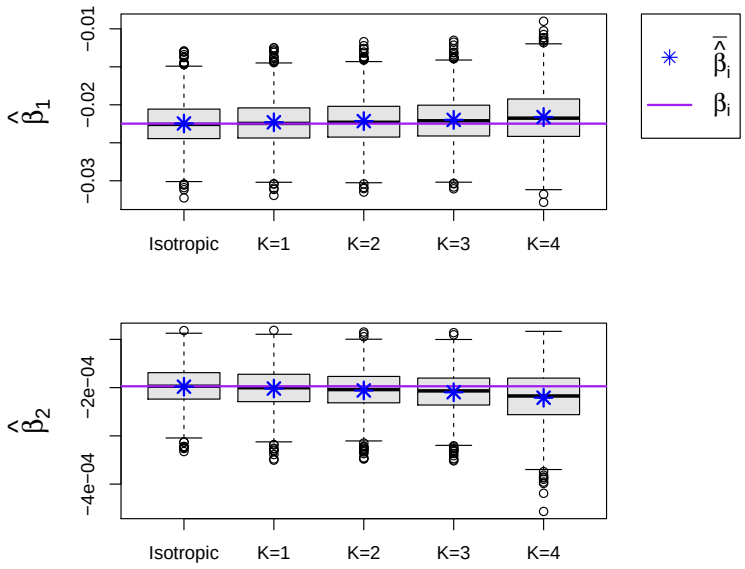

Figure 4.6: Estimates of β_1 and β_2 in (4.5) for the *glm* methods at WP2, under the isotropic fall distribution with an average of 70 carcasses per turbine.

increases. At WP2, the standard deviation of $\bar{M}$ for the anisotropic *glm* methods when $K = 1, K = 2, K = 3$, and $K = 4$ ranges from 1%-2%, 1%-10%, 4%-21%, and 33%-42% greater than the standard deviation of the isotropic *glm* method, respectively, with the relative percentage typically at its lowest when the rate is 70, the maximum rate considered. At WP4 the standard deviation of $\bar{M}$ for the anisotropic *glm* methods when $K = 1, K = 2, K = 3$, and $K = 4$ ranges from 18%-19%, 25%-95%, 27%-280%, and 38%-304% greater than the standard deviation of the isotropic *glm* method. The increase in the standard deviation of the mortality estimates as K increases can be attributed to the increase in variability of $\hat{\beta}_1$ and $\hat{\beta}_2$ as the number of non-significant terms in the Poisson regression model increases (Figure 4.6).

Anisotropy 0

Under Anisotropy 0, carcass location was simulated using an anisotropic distribution (Figure 4.4 (left)), and researchers correctly identified that carcasses were struck under an eastern wind on average. This is the same distribution used in Chapter 2 to display the sensitivity of the isotropic cake and *glm* methods to anisotropic carcass distributions. The results of the isotropic methods at WP2 are tantamount to those seen in Chapter 2, with a consistent 14% positive bias for both methods across all rates considered (Table 4.1 and Figure 4.7). At WP4 the isotropic methods underestimate the average number of carcasses per turbine by about 17% for each rate (Table 4.2).

When it is known that the wind originates from due east, the quadrants of the anisotropic cake method are defined using lines rotated 45^{o} clockwise and counterclockwise of the east-west line (Figure 4.4 (left)). At WP2, the anisotropic cake method reduces the bias by about 50% for every rate, relative to the isotropic methods (Table 4.2). The standard deviation also decreases, which is probably attributed to the decrease in the average estimates and the mean-variance relationship. The anisotropic cake method has the lowest mean square error (MSE) of all methods considered when there are 2 carcasses per turbine on average.

At WP4, the anisotropic cake method eliminates the bias of the isotropic method, producing the least biased results of all the methods considered when the rate is 10 or 70 carcasses per turbine; however, due to a relatively high standard deviation it does not produce this lowest MSE at any rate.

For the anisotropic *glm* methods, θ is set equal to zero due east of the turbine under Anisotropy 0. In general, at WP2, the bias decreases, and the standard deviation

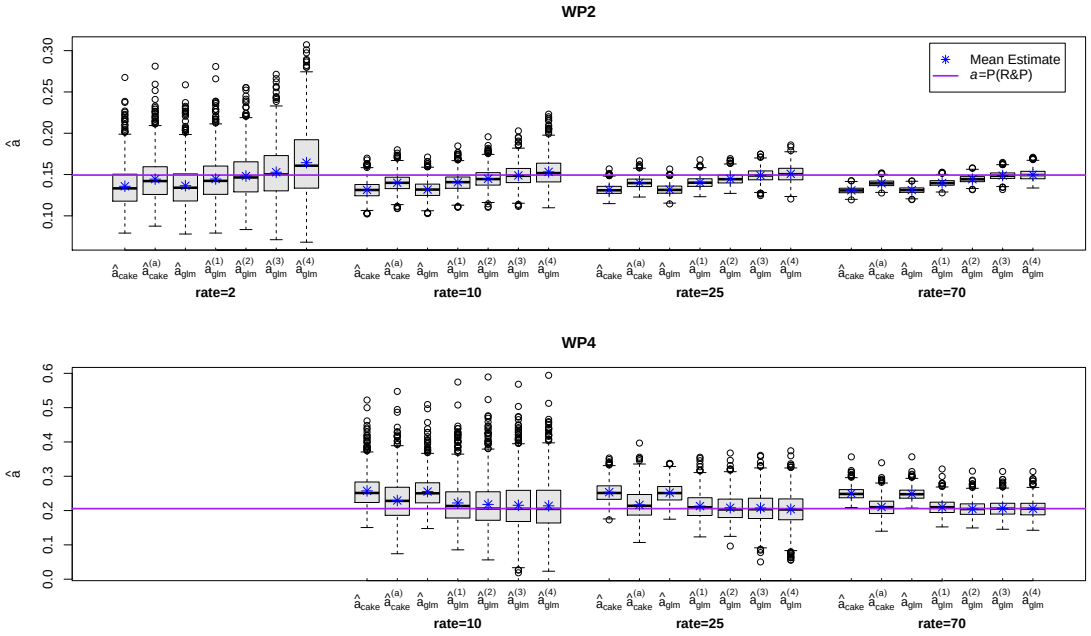

Figure 4.7: Estimates for $\hat{a}$ using isotropic and anisotropic methods under the Anisotropy 0 setting for every average rate of carcasses per turbine considered at WP2 (top) and WP4 (bottom). Anisotropic methods are indicated with a superscript. The superscript for the *glm* methods gives the order of the Fourier expansion used when fitting the Poisson regression model.

increases as the order (K) of the Fourier expansion increases (Figure 4.7). When $K = 1$, the *glm* method produces similar results to the anisotropic cake method, reducing the bias by about 50% and the standard deviation by 8% relative to the isotropic *glm* method for every rate. When $K = 2$ the bias is reduced to about 4% for every rate, the standard deviation is comparable to $K = 1$, and the MSE is the lowest for all methods considered when the rate is 2 carcasses per turbine. The *glm* method with $K = 3$ produces the lowest MSE under Anisotropy 0 for average rates of 10, 25, and 70 carcasses per turbine. The bias ranges from 2% when the rate is 2, to a mere 0.4% when the rate is 70. The

standard deviation when $K = 3$ is 6% greater than when $K = 1$ or 2 when the rate is 2, and comparable to $K = 1$ or 2 when the rate is 10, 25 or 70. When $K = 4$ the *glm* method produces the least biased results of all methods considered when the rate is 10 or more, but the standard deviation increases by about 20% relative to $K = 3$.

At WP4, under Anisotropy 0, the bias of the *glm* method with $K = 1$ is decreased to about 0.5% for every rate, producing the least biased results of all the *glm* methods considered (Table 4.2). The *glm* method with $K = 1$ also produces the lowest MSE of all methods considered at WP4 when the rate is 25 or 70. When the rate is 10 the MSE of the *glm* method with $K = 1$ is 9.62, while the MSE of the isotropic *glm* method is 6.33. Therefore, even with a 17% bias, the isotropic *glm* method produces the lowest MSE when the rate is 10 carcasses per turbine, and on average 40.2 carcasses are observed (Table 4.3). In general, at WP4, the bias and the standard deviation of the *glm* methods increase as K increases past one (Figure 4.7), with some trials excluded as unreasonable when tabulating the results for $K = 3$ or $K = 4$.

Anisotropy 5.5

The results for Anisotropy 5.5 are based on the same set of trials used for Anisotropy 0, but with the false assumption that on average wind originates from 5.5^{o} counterclockwise of due east. This affects orientation of the quadrant lines for the anisotropic cake method (Figure 4.4 (left)), and the value for θ assigned to each cell for the *glm* method. Anisotropy 5.5 is intended to show the effects of miscalculating the average wind direction by 5.5 degrees, relative to Anisotropy 0 where the correct wind direction was assumed.

The isotropic cake and *glm* methods do not take into account wind direction, and

therefore produce the same results regardless of the assumed average wind direction (Table 4.1 and Table 4.2). The anisotropic cake method produced similar results at WP2 for both of the assumed originating wind directions, but differed at WP4. Under Anisotropy 0, at WP4, the anisotropic cake method had at most a 0.5% bias, but the bias ranged from 5% to 6% under Anisotropy 5.5. This indicates that the anisotropic cake method is sensitive to the orientation of quadrant lines, and performs better when the average originating wind direction is correctly identified.

The results for the anisotropic *glm* methods are identical in Anisotropy 0 and Anisotropy 5.5. This is because changing the value of $\theta = 0$ only reparametrizes the model. Under this circumstance, 5.5^{o} was added to every value of θ, relative to Anisotropy 0, and

$$\big(\sin(\theta+\phi),\cos(\theta+\phi)\big) = \big([\cos(\phi)-\sin(\phi)]\cos(\theta),[\sin(\phi)+\cos(\phi)]\sin(\theta)\big).$$

This implies that the explanatory variables from *glm* models fit under Anisotropy 5.5 are a linear combination of the explanatory variables used in Anisotropy 0. Therefore, the predicted values from the two models will be identical. Thus, the choice for $\theta = 0$ is arbitrary when using the anisotropic *glm* method. In practice, it may still be beneficial to identify the average wind direction for interpretation of the model, or to compare distributions across wind projects, but mis-identifying the wind direction has no effect on the estimates using the anisotropic *glm* method.

Anisotropy EMP

At WP2, under the Anisotropy EMP setting, the bias of the isotropic cake and *glm* methods ranges from 4% to 5% (Figure 4.8). The bias actually becomes worse under

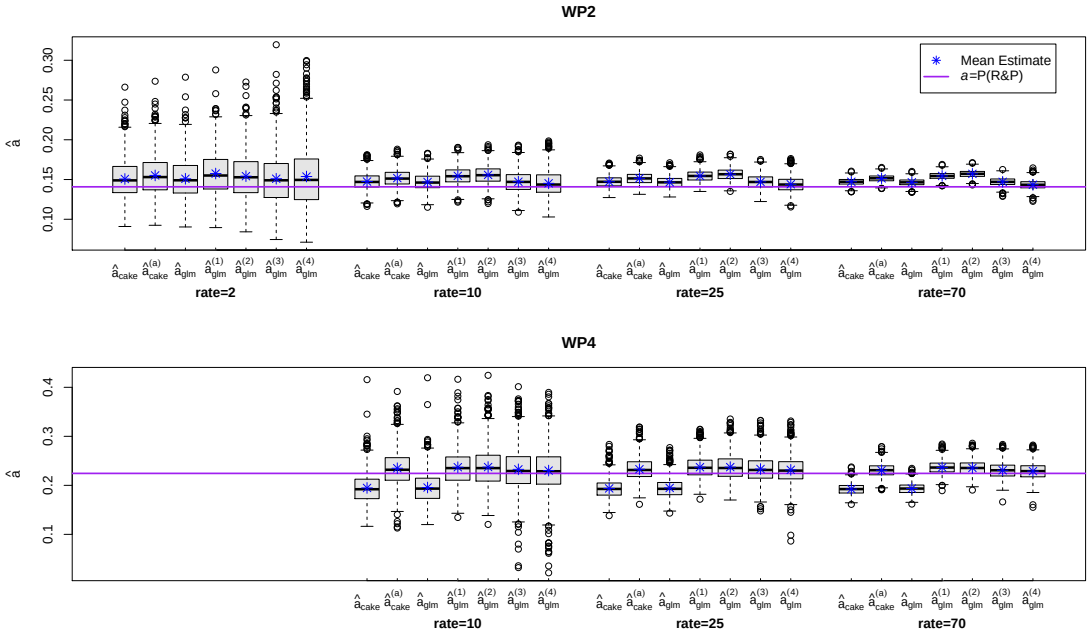

Figure 4.8: Estimates for $\hat{a}$ using isotropic and anisotropic methods under the Anisotropy EMP setting for every average rate of carcasses per turbine considered at WP2 (top) and WP4 (bottom). Anisotropic methods are indicated with a superscript. The superscript for the *glm* methods gives the order of the Fourier expansion used when fitting the Poisson regression model.

the anisotropic cake method and *glm* methods for $K = 1$ or 2. The bias decreases for the *glm* methods when $K = 3$ or $K = 4$ relative to the isotropic methods. However, due to increases in standard deviation for both of these anisotropic methods, the isotropic methods produce the lowest MSE of all methods considered except when the rate is 70, in which case the *glm* method with $K = 4$ has the lowest MSE.

At WP4, under the Anisotropy EMP setting, the isotropic cake and *glm* overestimate mortality by about 17% on average, for every rate. All of the anisotropic methods significantly decrease the bias with the anisotropic cake method or *glm* method with $K = 1$

producing the lowest MSE amongst the methods considered.

In practice, researchers will not know which anisotropic method produces the lowest MSE, but anisotropic *glm* methods can be compared using AIC (Akaike [1998]). In every trial the AIC of each *glm* method was recorded (Table 4.4).

Under the isotropic carcass distribution, the isotropic *glm* method produced the lowest AIC in at least 85% of the trials for every rate at both wind projects. Under the

Table 4.4: Proportion of trials where a given *glm* method produced the lowest AIC. Underlined values produced the lowest AIC in the largest proportion of trials for a setting and rate. Bold values indicate the method that produced the lowest MSE. The results for Anisotropy 5.5 are not displayed, because they are identical to Anisotropy 0.

		WP2				WP4		
		rate=2	rate=10	rate=25	rate=70	rate=10	rate=25	rate=70
Isotropy	$\bar{M}_{glm}$	**0.859**	**0.875**	**0.880**	**0.876**	**0.851**	**0.851**	**0.901**
	$\bar{M}^{(a)}_{glm}(K=1)$	0.092	0.091	0.084	0.084	0.088	0.093	0.068
	$\bar{M}^{(a)}_{glm}(K=2)$	0.025	0.025	0.025	0.023	0.038	0.028	0.016
	$\bar{M}^{(a)}_{glm}(K=3)$	0.014	0.005	0.010	0.014	0.013	0.016	0.009
	$\bar{M}^{(a)}_{glm}(K=4)$	0.010	0.004	0.001	0.003	0.010	0.012	0.006
Anisotropy 0	$\bar{M}_{glm}$	0.312	0.000	0.000	0.000	**0.590**	0.294	0.018
	$\bar{M}^{(a)}_{glm}(K=1)$	0.541	0.681	0.496	0.062	0.296	**0.561**	**0.742**
	$\bar{M}^{(a)}_{glm}(K=2)$	**0.097**	0.219	0.336	0.472	0.061	0.095	0.155
	$\bar{M}^{(a)}_{glm}(K=3)$	0.036	**0.079**	**0.144**	**0.400**	0.030	0.035	0.062
	$\bar{M}^{(a)}_{glm}(K=4)$	0.015	0.021	0.024	0.066	0.023	0.015	0.023
Anisotropy Emp	$\bar{M}_{glm}$	**0.040**	**0.000**	**0.000**	0.000	0.061	0.000	0.000
	$\bar{M}^{(a)}_{glm}(K=1)$	0.695	0.339	0.031	0.000	**0.721**	**0.707**	**0.468**[†]
	$\bar{M}^{(a)}_{glm}(K=2)$	0.129	0.064	0.002	0.000	0.125	0.141	0.134
	$\bar{M}^{(a)}_{glm}(K=3)$	0.090	0.502	0.761	0.494	0.060	0.103	**0.258**[†]
	$\bar{M}^{(a)}_{glm}(K=4)$	0.046	0.095	0.206	**0.506**	0.033	0.049	0.140

[†] Lowest MSE of the *glm* methods

anisotropic carcass distributions, at WP2, the models which produced the lowest AIC the most often do not correspond to the model with the lowest MSE, with only one exception. Under the distribution used in Anisotropy EMP when the average rate of carcasses per turbine is 70, the anisotropic *glm* with $K = 4$ had the lowest MSE and produced the lowest AIC in 50.6% of the trials.

The results using AIC are more promising at WP4, where the *glm* method that produced the lowest MSE also produced the lowest AIC in a majority of the trials. Under the anisotropic settings, the model with the lowest MSE had the lowest AIC between 56% and 74% of the trials for every setting.

Determining if the anisotropic methods need to be utilized, requires identifying if anisotropy is present. The χ^2-test proposed in Subsection 4.3.2 and likelihood ratio (*LR*) test proposed in Subsection 4.3.4 provide an opportunity to accomplish this. Determining the level of a test requires careful thought about the consequences of a Type-I or Type-II error. In this setting using an isotropic method when anisotropy is present (Type-I error), produced poor results in general, while using an anisotropic method under an isotropic setting (Type-II error) usually produced accurate estimates that were slightly more variable than the equivalent isotopic method. Therefore, I recommend setting α to 0.10. The performance of the χ^2 and *LR* tests are compared by examining the proportion of trials where the result of the test suggested the carcass distribution was not isotropic at level 0.10 (Table 4.5).

The results under the Isotropic setting provide the opportunity to examine the calibration of the hypothesis tests when the null hypothesis is true (i.e. the fall distribution is isotropic). At WP2, the χ^2-test appears conservative when the average rate of carcasses

Table 4.5: Proportion of trials where the χ^2-test and likelihood ratio (*LR*) tests rejected the null hypothesis that the carcass distribution is isotropic at nominal level 0.10. The value for K in the LR test gives the order of the Fourier expansion of direction, θ, associated with the Poisson regression model.

		WP2				WP4		
		rate=2	rate=10	rate=25	rate=70	rate=10	rate=25	rate=70
Isotropy	χ^2	0.056	0.060	0.074	0.093	0.099	0.106	0.103
	$LR(K=1)$	0.120	0.112	0.104	0.095	0.114	0.118	0.094
	$LR(K=2)$	0.124	0.110	0.108	0.094	0.150	0.119	0.098
	$LR(K=3)$	0.121	0.101	0.104	0.111	0.162	0.150	0.096
	$LR(K=4)$	0.152	0.118	0.115	0.110	0.178	0.150	0.101
Anisotropy 0	χ^2	0.099	0.901	1.000	1.000	0.317	0.533	0.852
	$LR(K=1)$	0.680	1.000	1.000	1.000	0.372	0.706	0.983
	$LR(K=2)$	0.614	1.000	1.000	1.000	0.336	0.630	0.967
	$LR(K=3)$	0.542	1.000	1.000	1.000	0.326	0.588	0.950
	$LR(K=4)$	0.511	1.000	1.000	1.000	0.346	0.539	0.928
Anisotropy Emp	χ^2	0.521	1.000	1.000	1.000	0.215	0.732	1.000
	$LR(K=1)$	0.963	1.000	1.000	1.000	0.937	1.000	1.000
	$LR(K=2)$	0.934	1.000	1.000	1.000	0.881	0.998	1.000
	$LR(K=3)$	0.923	1.000	1.000	1.000	0.854	0.999	1.000
	$LR(K=4)$	0.900	1.000	1.000	1.000	0.827	0.997	1.000

per turbine is 2, rejecting the null hypothesis at the nominal level 0.10 in 5.6% of the trials. The test approaches the nominal level as the rate increase to 70, rejecting the null hypothesis in 9.3% of the trials. At WP4 the χ^2-test appears relatively exact for each rate.

Under the isotropic distribution, at WP2, the *LR* tests are anti-conservative rejecting the null hypothesis more than 10% of the time. In general, the proportion of p-values less than 0.10 increases as K increases, and decreases closer to the nominal level as the rate increases. A similar patter is observed at WP4.

The results using the two anisotropic distributions evaluates the power of the tests.

At both wind projects, all of the *LR* tests are more powerful than the χ^2-test, except when the rate is 25 or 70 at WP2 where all methods rejected the assumption of isotropy at level 0.10 in every trial. The *LR* test with $K = 1$ was the most powerful test amongst the tests that were considered, and, in general, power decreased as K increased.

4.6 Summary and Conclusions

In Section 4.2, results from carcass surveys at WP1 indicated that wind direction influences carcass location, with carcasses landing more often and further from the turbine in the downwind direction, as suggested by Howell and DiDonato [1991]. This gives reason to suspect that the spatial distribution of carcasses may be anisotropic at wind projects that have little variation in wind direction, which can lead to biased results when using the isotropic cake and *glm* methods of accounting for unsearched areas.

In this chapter, methods were proposed to adjust the cake and *glm* methods to account for anisotropic carcass distributions. The anisotropic cake method further divides the annuli of the isotropic cake method into quadrants, and estimates mortality as the sum of the observed number of carcasses divided by the proportion of area searched in each quadrant of each annulus and the estimated probability of observing a carcass that landed on R&P, (4.1). The anisotropic *glm* model integrates direction using a Fourier expansion into the Poisson regression model that is normalized to estimate the spatial carcass distribution, (4.5). This method estimates the probability a carcass lands on R&P using the estimated carcass distribution, and then estimates mortality as the number of observed carcasses divided by the estimated probabilities that a carcass lands on R&P

and that a carcass is observed given it landed on R&P, (4.7).

Formulating the anisotropic cake and *glm* methods gave rise to techniques that can be utilized to test if the anisotropy is present. The data collected when implementing the anisotropic cake method can be utilized to test for evidence of anisotropy by conducting a χ^2-test to determine if an equal proportion of carcasses fell in each quadrant (Subsection 4.3.2). When implementing the anisotropic *glm* method, the Poisson regression model, (4.5), can be utilized to test for evidence of anisotropy by testing if coefficients that include direction terms are significant to the model with a likelihood ratio test (Subsection 4.3.4).

Simulations were designed to test the accuracy and precision of the proposed anisotropic methods relative to their isotropic counterparts, and to compare the two methods to each other (Section 4.4). The simulations were also used to compare the performances of the hypothesis tests that were proposed in Section 4.3.

Before estimating mortality, researchers have to decide on the appropriate method to account for unsearched areas, which requires identifying if anisotropy is present. Amongst the likelihood ratio tests considered in this chapter, which compared Poisson regression models that differed by the order of the Fourier expansion of direction, θ, the test using the model with the first order expansion produced best results. Under the isotropic fall distribution considered, the test corresponding to the first order expansion was the closest to rejecting the null hypothesis at the nominal level; and under the anisotropic distributions the test had the best power. When compared to the χ^2-test, neither seem to be better in terms of calibration, but in terms of power the likelihood ratio test corresponding to the first order expansion clearly outperformed the χ^2-test (Table

4.5). Based on the results of these simulations, I suggest that researchers determine if the fall distribution is anisotropic by using the likelihood ratio test which compares the Poisson regression model using the first order Fourier expansion of direction to the Poisson regression model of the isotropic method.

Under the Isotropy setting, the recommended hypothesis test was slightly anticonservative, but still produced reasonable results concluding that anisotropy was present in at most 12% of trials at level 0.10. Therefore, in a majority of trials, the test correctly concludes the carcass distribution is isotropic. In these cases the isotropic methods would be used, which produce accurate and precise estimates in this setting (Chapter 2). The results from the anisotropic methods under the Isotropy setting were still reasonable, particularly when the expected number of observed carcasses was 85 or more (Table 4.3). Therefore, when the test falsely concludes the carcass distribution is anisotropic, the practical conclusions would likely remain similar.

When the carcass distribution is identified as anisotropic, it is possible to obtain accurate estimates of mortality based on data collected only on roads and pads. Under the circumstances where the carcass distribution is anisotropic, and the isotropic cake and *glm* methods are biased, the anisotropic cake and *glm* methods displayed promising results. For example, under the anisotropy in Figure 4.4 the anisotropic *glm* methods reduce the biased of the isotropic cake and *glm* methods from 14% to 1% using the third order Fourier expansion at WP2, and from 17% to 0.06% using the first order Fourier expansion at WP3, while maintaining reasonable standard deviations.

When an anisotropic carcass distribution is present, the isotropic methods may produce reasonable results. Under the Anisotropy EMP setting, at WP2, the isotropic esti-

mates where only biased by about 4.5% for every rate. The isotropic methods produce reasonable results at WP2 under this distribution, because the observed carcass density at each distance is representative of the marginal density. This can be attributed to the combination of the specific anisotropic distribution and the R&P configurations at WP2. When observed carcass densities at each distance are representative of the underlying average density, the isotropic methods will perform well even under an anisotropic distribution. This was also observed in Chapter 2 at WP3 when the same distribution used in Anisotropy 0 and Anisotropy 5.5 only induced a 1.5% bias. Unfortunately there is no hard rule that can be used to determine when an isotropic method is going to produced reasonable results. However, the results in this chapter suggested that when an isotropic method produces reasonable results, so does an anisotropic method; and when the isotropic methods produce unreasonable results, there is an anisotropic that produces better results. Therefore researchers can error on the side of caution, and always use an anisotropic method when there is evidence to suggest anisotropy is present.

In almost every setting at both wind projects, one of the *glm* methods produced the lowest MSE (Table 4.1 and Table 4.2). Perhaps better partitions of the fall zone can be constructed to implement the idea of the cake methods that better accounts for anisotropy, but in the form tested in this chapter, the results for the anisotropic cake method were not as satisfactory as the anisotropic *glm* methods. In many settings the results for the anisotropic cake method and the first order Fourier expansion anisotropic *glm* method were almost identical. Further research is needed to determine if these two methods will typically produce similar results, but if this trend continues there would be no reason consider the anisotropic cake method.

Furthermore there are some circumstances where the anisotropic cake method requires correctly identifying the average wind direction. At WP4, under Anisotropy 0, the bias was reduced to from 17% to less than 0.5% for all three rates considered if the average wind direction is correctly identified, but the bias was 5.2% when the assumed average wind direction is just 5.5^{o} off from the truth. If the carcass distribution is anisotropic because the wind typically originates from the same direction, then it should be easy to estimate the average wind direction; however, if the wind direction is correlated with fatalities, then the average wind direction at the time of the collision may be more difficult to estimate. For example, this could happen if bats are more likely to be in the rotor swept area if the the wind originates from the southwest, or if another weather variable (e.g. temperature, precipitation, barometric pressure) is correlated with both fatalities and wind direction. In both of these examples, bats would more likely be struck when the wind is blowing in a certain direction. Without knowledge of the wind direction when the fatalities happened, estimating average wind direction at the time of collision could be problematic. The anisotropic *glm* methods, on the other hand, produced the same results regardless of identification of the average wind direction. Given the anisotropic cake method produced similar results to the first order anisotropic *glm* method, and the sensitivity of the anisotropic cake method to correctly identifying the average wind direction, I recommend using the *glm* methods when the *LR* ratio test concludes anisotropy is present.

In this chapter, five *glm* methods where considered, and each one of them produced the lowest MSE in at least one setting which used an anisotropic fall distribution (Table 4.1 and Table 4.2). The *glm* that produced the lowest MSE also produced the lowest AIC

in a majority of the trials for every setting at WP4, but the same did not hold at WP2 where the model with the lowest MSE only produced the lowest AIC in the majority of trials in one setting. AIC does not always identify the model with the lowest MSE, but in almost every set of conditions considered, the model with the lowest AIC in a majority of the trials produced reasonable results given the applications. Therefore, researchers should take AIC into account when trying to decide which *glm* should be used. The number of observed carcasses should also be taken into account when deciding on the appropriate order to the Fourier expansion in the Poisson regression model. Researchers should avoid fitting higher order models when the number of observed carcasses is small (< 40), and should use graphical displays to ensure estimated carcass density does not increase with distance from the turbine.

Regardless of the ability to identify the best order for the Fourier expansion when utilizing the the anisotropic *glm* method, the results of this chapter demonstrate that when the isotropic cake and *glm* methods produce unsatisfactory biased results, the anisotropic *glm* method is capable of producing accurate estimates with a reasonable precision, making mortality estimation possible from R&P searches even when the underlying spatial fall distribution is anisotropic.

5 Discussion

5.1 Summary

Wind turbines pose a threat to birds and bats, and post-construction monitoring at wind projects is necessary to assess impacts to species at risk of colliding with turbine blades (Kunz et al. [2007b], Arnett et al. [2008]). Mortality at individual wind projects is typically estimated by conducting carcass surveys, where human observers are sent to predetermined areas to search for carcasses (Gauthreaux [1995], U.S. Fish and Wildlife Service [2012]), and then adjusting the observed counts for imperfect detection due to unsearched areas, searcher efficiency, and carcass persistence (Shoenfeld [2004], Huso [2010], Korner-Nievergelt et al. [2011]). Traditionally, the searched area is obtained by taking a random sample of turbines and searching as much of a predetermined shape (e.g. square or circle) as possible (Gauthreaux [1995]). Areas within the predetermined shape that cannot be searched due to thick vegetation, crop fields, steep terrain, or rivers can be accounted for using the methods proposed by Jain [2005], Good et al. [2011], and Huso and Dalthorp [2014]. This thesis utilized the ideas of the aforementioned methods to develop methodology for mortality estimation from carcass surveys performed entirely on roads leading up to turbines and pads beneath turbines (R&P).

In Chapter 2 the cake, ratio, and *glm* methods of accounting for unsearched areas, which are based off the ideas presented by Jain [2005], Good et al. [2011], and Huso and Dalthorp [2014], respectively, were introduced (Section 2.2). A simulation was

preformed to determine the plausibility of, and the most appropriate method for, estimating the probability a carcass lands in the searched area (i.e. R&P), which is a pivotal quantity for mortality estimation (Section 2.3). The simulations considered various R&P configurations, average carcass per turbine rates, spatial carcass distributions, and search protocols.

The results of the simulations suggested that the cake and *glm* methods are more accurate and precise than the ratio method when the spatial carcass fall distributions is isotropic (Section 2.4). Furthermore, the cake and *glm* methods are less expensive to implement, because estimates are based solely on data collected on R&P; while the ratio method requires additional data collected at turbines cleared of vegetation, and additional trials to estimate detection rates off R&P.

When the spatial carcass distribution is isotropic, the cake and *glm* methods produced similar results if a Poisson process provides a good approximation to the underlying process determining carcass location (Section 2.4). When the Poisson process provides a poor approximation, the *glm* method produces slightly biased results, while the cake method appears relatively robust to any reasonable isotropic spatial carcass distribution.

In Chapter 3, The cake method of adjusting for unsearched areas was utilized to develop an estimator of mortality based on R&P carcass surveys under isotropic carcass distributions, which required a method to estimate the probability (G) a carcass is observed given it landed on R&P. It was suggested G be estimated using a single Binomial trial, that accounts for both searcher efficiency and carcass persistence simultaneously by placing trial carcasses on the R&P uniformly at sunrise and sunset throughout the

period of interest (Section 3.3). Simulation results suggested that this simple method produces accurate estimates, that are robust to various carcass persistence distributions and changes in probability of detection, and often as precise as commonly used methods that estimate searcher efficiency and carcass persistence separately to form an estimate of G. Theoretical results of the cake estimator (Section 3.2) were utilized to obtain a parametric method for calculations of standard error and confidence interval creation (Section 3.6), which can also be calculated using a parametric bootstrap.

Simulation results suggest the cake estimator of mortality provides accurate and precise estimates under isotopic fall distributions (Section 3.6), but researchers must be able to identify when the assumption of isotropy is appropriate. If unaccounted for, the cake (and *glm*) method of accounting for unsearched areas produces biased results under anisotropic fall distributions at some wind projects (Section 2.4 and Section 4.5). The degree of bias under these circumstances depends on the interaction of the R&P configurations and the orientation of the specific anisotropic spatial carcass distribution. Researchers can test for anisotropic distributions using a likelihood ratio test between Poisson regression models (Section 4.3). When the result of the test suggests that the assumption of an isotropic carcass distributions is inappropriate, the *glm* method can be expanded to include terms for direction (Section 4.3), and used to accurately and precisely estimate the probability a carcass lands on R&P under anisotropic distributions (Section 4.5).

5.2 Limitations

The simulations performed throughout this thesis were designed to capture a wide variety of settings, representative of conditions that may be encountered during implementation. As with most statistical procedures, the methods presented in this document have limitations. The cake and *glm* methods, in both isotropic and anisotropic forms, account for unsearched areas by estimating the spatial carcass distribution, which requires a reasonable number of observed carcasses. In simulations where only eight carcasses were observed on average (Section 2.4: WP3, Rate=2, Isotropy), the coefficient of variation for the pseudo estimates of mortality was almost 50% for the cake and *glm* methods, which can lead to undesirable confidence intervals even when mortality and the standard deviation of the method are accurately estimated. When 40 carcasses were observed on average (Section 4.5: WP4, Rate=10, Anisotropy0), the recommended likelihood ratio test only identified the anisotropic fall distribution in 38% of trials. Under this circumstance the isotropic methods underestimated mortality by 17%, on average. The proposed methods performed well when at least 85 carcasses where observed on average. To determine the minimum number of carcasses that have to be observed to ensure valid inference requires examining a finer range of expected carcass counts, under numerous R&P configurations.

The areas searched when implementing a R&P protocol are not selected randomly, which forces the assumption that the observed carcass density at a location and/or distance from the turbine is representative. As a committee member pointed out, engineers take wind into account when building roads. If roads were placed in areas with less

wind, then the sample collected on R&P may not be representative, which could result in biased estimates.

Certain R&P configurations may preclude the implementation of a R&P search protocol, especially if anisotropy is present. For instance, if every road to all turbines came in from the east, there would be no way of testing or accounting for an anisotropic fall distribution, because of the lack of information in the other directions.

Lastly, R&P searches may not be appropriate if there is an interaction between wind direction and R&P configuration. In all of the simulations considered in this thesis, it was assumed that spatial distribution of carcasses was constant among turbines. If this does not hold, it could be problematic. For instance if all the turbines with roads that come in from the east have wind that originates in the east, and all turbines that with roads come in from the north have wind that originates in the north, estimates based on R&P searches may be biased.

With the exception of low observed carcass counts, researchers should be able to identify the circumstances where observed carcass densities may not be representative, and avoid estimating mortality based on data solely from R&P searches.

5.3 Future Work

Continued research will attempt to address the limitation imposed by the observed sample size. By performing similar simulations at additional R&P configurations it may be possible to provide general guidelines for the observed carcass counts required to confidently estimate mortality from R&P searches, under isotropic and anisotropic

settings.

The cake estimator of mortality displayed promising results in Chapter 3. The statistical methods were proposed to make calculations easy, but writing an R package would make implementation of the ideas from Chapter 3 even easier.

In Chapter 4, the *glm* method of accounting for unsearched areas was adjusted to accurately and precisely estimate the probability a carcass lands on R&P under anisotropic fall distributions. Implementing this method to estimate mortality would require formulating an approach for standard error calculation and confidence interval creation.

6 Appendix

6.1 Justification for normality of $\widehat{M}_{cake}$

Let

M	=True mortality
G	=Probability a carcass is observed given it landed on R&P
i	=Index for the annuli (1, ..., K)
A_i	=Proportion of the i^{th} annulus contained in R&P (known)
f_i	=Probability a carcass lands in the i^{th} annulus
$f_{i,o}$	=Probability a carcass lands in the R&P of the i^{th} annulus (=$\frac{A_i f_i}{\sum_i A_i f_i}$)
a	=Probability a carcass lands on R&P (=$\sum_i f_{i,o} = \sum_i A_i f_i$)
C	=Number of observed carcasses (=$\sum_i C_i$) $C \sim$Binom(M, aG)
C_i	=Observed number of carcasses in the i^{th} annulus $(C_1, ..., C_K)\|C \sim$Multinomial$(C, f_{1,o}..., f_{K,o})$

Observe

$$\mathrm{E}(C_i) = E[E(C_i)|C] = E(Cf_{i,o}) = MGaf_{i,o} = MGA_i f_i,$$

$$\begin{aligned}
\mathrm{Var}(C_i) &= \mathrm{Var}[\mathrm{E}(C_i)|C] + \mathrm{E}[\mathrm{Var}(C_i|C)] \\
&= \mathrm{Var}(Cf_{i,o}) + \mathrm{E}[Cf_{i,o}(1-f_{i,o})] \\
&= MGa(1-aG)f_{i,o}^2 + MGaf_{i,o}(1-f_{i,o}))
\end{aligned}$$

$$= MGaf_{i,o}(1 - Gaf_{i,o})$$
$$= MGA_i f_i(1 - GA_i f_i),$$

$$\begin{aligned}
\mathrm{Cov}(C_i, C_j) &= \mathrm{E}[\mathrm{Cov}(C_i, C_j)|C] + \mathrm{Cov}[\mathrm{E}(C_i|C), \mathrm{E}(C_j|C)] \\
&= \mathrm{E}(-Cf_{i,0}f_{j,0}) + \mathrm{Cov}(Cf_{i,0}, Cf_{j,0}) \\
&= -MGaf_{i,0}f_{j,0} + MGa(1 - Ga)f_{i,0}f_{j,0} \\
&= MG^2a^2 f_{i,0}f_{j,0} \\
&= MG^2 A_i f_i A_j f_j,
\end{aligned}$$

and,

$$\begin{aligned}
\mathrm{Corr}(C_i, C_j) &= \frac{MG^2a^2 f_{i,0}f_{j,0}}{\sqrt{MGaf_{i,o}(1 - Gaf_{i,o})MGaf_{j,o}(1 - Gaf_{j,o})}} \\
&= \sqrt{\frac{Gaf_{i,0}Gaf_{j,0}}{(1 - Gaf_{i,0})(1 - Gaf_{j,0})}}
\end{aligned}$$

As the buffer, difference between outer and inner radii, of the annuli goes to 0, $f_{i,0}$ and $f_{i,0} \to 0$, which implies $\mathrm{Corr}(C_i, C_j) \to 0$. Therefore, the central limit theorem for dependent random variables can be applied to obtain

$$\frac{1}{s_k}\sum_{i=1}^{K}\left[\frac{C_i}{GA_i} - \mathrm{E}\left(\frac{C_i}{GA_i}\right)\right] \xrightarrow{d} \mathrm{N}(0,1),$$

where

$$\begin{aligned} s_k^2 &= \sum_{i=1}^{K} \mathrm{Var}(\frac{C_i}{GA_i}) \\ &= \frac{1}{G^2} \sum_{i=1}^{K} \frac{MGA_i f_i (1 - GA_i f_i)}{A_i^2} \\ &= \frac{M}{G} \sum_{i=1}^{K} \frac{(1 - GA_i f_i) f_i}{A_i} \end{aligned}$$

This value differs from the variance of $\widehat{M}_{cake}$ in Theorem 2, because it assumes the correlation between C_i and C_j is zero, and there is no variation in estimating G, which hold asymptotically. Let N be the number of trial carcasses used in the binomial(N,G) trial to estimate G, then $\hat{G} \xrightarrow{p} G$ as $N \to \infty$ by the weak law of large numbers. Therefore,

$$\frac{\mathrm{Var}\left[\frac{GM}{\hat{G}}\right] + \mathrm{E}\left[\frac{GM}{\hat{G}^2}\right] \sum_{i=1}^{k} \frac{(1-GA_i)f_i}{A_i}}{\frac{M}{G} \sum_{i=1}^{K} \frac{(1-GA_i f_i)f_i}{A_i}} \xrightarrow{p} 1,$$

as $K, N \to \infty$. By the continuous mapping theorem $\frac{G}{\hat{G}} M \xrightarrow{p} M$. Thus,

$$\begin{aligned} &\frac{\widehat{M}_{cake} - M}{\mathrm{Var}\left[\frac{GM}{\hat{G}}\right] + \mathrm{E}\left[\frac{GM}{\hat{G}^2}\right] \sum_{i=1}^{k} \frac{(1-GA_i)f_i}{A_i}} \\ &= \frac{\sum_{i=1}^{K} \left\{ \left[\frac{C_i}{\hat{G}A_i} - \mathrm{E}\left(\frac{C_i}{\hat{G}A_i}\right) \right] + \left[\mathrm{E}\left(\frac{C_i}{\hat{G}A_i}\right) - \mathrm{E}\left(\frac{C_i}{GA_i}\right) \right] \right\}}{\frac{M}{G} \sum_{i=1}^{K} \frac{(1-GA_i f_i)f_i}{A_i}} \div \frac{\mathrm{Var}\left[\frac{GM}{\hat{G}}\right] + \mathrm{E}\left[\frac{GM}{\hat{G}^2}\right] \sum_{i=1}^{k} \frac{(1-GA_i)f_i}{A_i}}{\frac{M}{G} \sum_{i=1}^{K} \frac{(1-GA_i f_i)f_i}{A_i}} \\ &\xrightarrow{d} \mathrm{N}(0,1) \end{aligned}$$

as $K, N \to \infty$ by Slutsky's theorem, and $\widehat{M}_{cake}$ is asymptotically distributed

$$\mathrm{N}\left(M, \mathrm{Var}\left[\frac{GM}{\hat{G}}\right] + \mathrm{E}\left[\frac{GM}{\hat{G}^2}\right] \sum_{i=1}^{k} \frac{(1 - GA_i) f_i}{A_i}\right).$$

Bibliography

Alan Agresti and Brent A Coull. Approximate is better than exact for interval estimation of binomial proportions. *The American Statistician*, 52(2):119–126, 1998.

Hirotogu Akaike. Information theory and an extension of the maximum likelihood principle. In *Selected Papers of Hirotugu Akaike*, pages 199–213. Springer, 1998.

R Anderson, N Neumann, J Tom, W Erickson, MD Strickland, M Bourassa, KJ Bay, and KJ Sernka. Avian monitoring and risk assessment at tehachapi pass wind resource area. *Subcontractor Report. National Renewable Energy Laboratory*, 2004.

Edward B Arnett, W Brown, Wallace P Erickson, Jenny K Fiedler, Brenda L Hamilton, Travis H Henry, Aaftab Jain, Gregory D Johnson, Jessica Kerns, Rolf R Koford, et al. Patterns of bat fatalities at wind energy facilities in north america. *The Journal of Wildlife Management*, 72(1):61–78, 2008.

J Bernardino, R Bispo, H Costa, and M Mascarenhas. Estimating bird and bat fatality at wind farms: a practical overview of estimators, their assumptions and limitations. *New Zealand Journal of Zoology*, 40(1):63–74, 2013.

Regina Bispo, Joana Bernardino, Tiago A Marques, and Dinis Pestana. Modeling carcass removal time for avian mortality assessment in wind farms using survival analysis. *Environmental and Ecological Statistics*, 20(1):147–165, 2013.

William G Cochran. Some methods for strengthening the common χ 2 tests. *Biometrics*, 10(4):417–451, 1954.

David Drake, Susan Schumacher, and M Sponsler. Regional analysis of wind turbine-caused bat and bird fatality. *Environmental and Economic Research and Development Program of Wisconsins Focus on Energy, Madison, Wisconsin, USA*, 2012.

WP Erickson, J Jeffrey, K Kronner, and K Bay. Stateline wind project wildlife monitoring annual report, results for the period july 2001–december 2002. *Tech. Rpt. to FPL Energy, Oregon Office of Energy, and Stateline Technical Advisory Committee*, 2004.

JK Fiedler, TH Henry, RD Tankersley, CP Nicholson, and Tennessee Valley Authority. Results of bat and bird mortality monitoring at the expanded buffalo mountain windfarm, 2005. *Report prepared for the Tennessee Valley Authority*, 2007.

Sidney A Gauthreaux. Suggested practices for monitoring bird populations, movements and mortality in wind resource areas. *PNAWPPM-II, p88-110. www. nrel. gov*, 1995.

RE Good, WP Erickson, A Merrill, S Simon, K Murray, K Bay, and C Fritchman. Bat monitoring studies at the fowler ridge wind energy facility, benton county, indiana: April 13-october 15, 2010. prepared for fowler ridge wind farm. prepared by western ecosystems technology. *Inc., Cheyenne, Wyoming*, 2011.

RE Good, A Merrill, S Simon, K Murray, and K Bay. Bat monitoring studies at the fowler ridge wind farm, benton county, indiana. an unpublished report submitted to the fowler ridge wind farm by west. *Inc., Cheyenne, WY, USA*, 2012.

J Gruver, M Sonnenburg, K Bay, and W Erickson. Post-construction bat and bird fatality study at the blue sky green field wind energy center, fond du lac county, wisconsin: July 21, 2008–october 31, 2008 and march 15, 2009–june 4, 2009. western ecosystems technology. *Inc., Cheyenne, Wyoming, USA*, 2009.

Cris D Hein, Alex Prichard, Todd Mabee, and Michael R Schirmacher. Efficacy of an operational minimization experiment to reduce bat fatalities at the pinnacle wind farm, mineral county, west virginia, 2013. *Final Report. An Annual Report Submitted to Edison Mission Energy and the Bats and Wind Energy Cooperative. Bat Conservation International, Austin, Texas. February*, 2014.

Judd A Howell and Joseph E DiDonato. Assessment of avian use and mortality related to wind turbine operations, altamont pass, alameda and contra costa counties, california, september 1998 through august 1989. final report submitted to us windpower, 1991.

CL Hull and Stuart Muir. Search areas for monitoring bird and bat carcasses at wind farms using a monte-carlo model. *Australasian Journal of Environmental Management*, 17(2):77–87, 2010.

Manuela M Huso, Nicholas Som, and Lew Ladd. Fatality estimator users guide. Technical report, US Geological Survey, 2012.

Manuela MP Huso. An estimator of wildlife fatality from observed carcasses. *Environmetrics*, 22(3):318–329, 2010.

Manuela MP Huso and Dan Dalthorp. Accounting for unsearched areas in estimating wind turbine-caused fatality. *The Journal of Wildlife Management*, 78(2):347–358, 2014.

Aaftab Jain, Paul Kerlinger, Richard Curry, and Linda Slobodnik. Annual report for the maple ridge wind power project postconstruction bird and bat fatality study–2006. *Cell*, 315:560–8650, 2007.

Aaftab Ashok Jain. Bird and bat behavior and mortality at a northern iowa windfarm. Master's thesis, Iowa State University, 2005.

Gregory D Johnson, Wallace P Erickson, M Dale Strickland, Maria F Shepherd, Douglas A Shepherd, and Sharon A Sarappo. Mortality of bats at a large-scale wind power development at buffalo ridge, minnesota. *The American Midland Naturalist*, 150(2): 332–342, 2003.

Edward L Kaplan and Paul Meier. Nonparametric estimation from incomplete observations. *Journal of the American statistical association*, 53(282):457–481, 1958.

Paul Kerlinger. An assessment of the impacts of green mountain power corporations wind power facility on breeding and migrating birds in searsburg, vermont. *National Renewable Energy Laboratory Report. Golden, CO, USA*, 2002.

Jessica Kerns, Wallace P Erickson, and Edward B Arnett. Bat and bird fatality at wind energy facilities in pennsylvania and west virginia. *Relationships between bats and wind turbines in Pennsylvania and West Virginia: an assessment of fatality search protocols, patterns of fatality, and behavioral interactions with wind turbines. Edited by EB Arnett. The Bats and Wind Energy Cooperative, Bat Conservation International, Austin, Tex*, pages 24–95, 2005.

Fränzi Korner-Nievergelt, Pius Korner-Nievergelt, Oliver Behr, Ivo Niermann, Robert Brinkmann, and Barbara Hellriegel. A new method to determine bird and bat fatality at wind energy turbines from carcass searches. *Wildlife Biology*, 17(4):350–363, 2011.

Fränzi Korner-Nievergelt, Robert Brinkmann, Ivo Niermann, and Oliver Behr. Estimating bat and bird mortality occurring at wind energy turbines from covariates and carcass searches using mixture models. *PloS one*, 8(7):e67997, 2013.

Fränzi Korner-Nievergelt, Oliver Behr, Robert Brinkmann, Matthew A Etterson, Manuela MP Huso, Dan Dalthorp, Pius Korner-Nievergelt, Tobias Roth, and Ivo Niermann. Mortality estimation from carcass searches using the r-package carcassa tutorial. *Wildlife Biology*, 21(1):30–43, 2015.

Thomas H Kunz, Edward B Arnett, Brian M Cooper, Wallace P Erickson, Ronald P Larkin, Todd Mabee, Michael L Morrison, M Strickland, and Joseph M Szewczak. Assessing impacts of wind-energy development on nocturnally active birds and bats: a guidance document. *The Journal of Wildlife Management*, 71(8):2449–2486, 2007a.

Thomas H Kunz, Edward B Arnett, Wallace P Erickson, Alexander R Hoar, Gregory D Johnson, Ronald P Larkin, M Dale Strickland, Robert W Thresher, and Merlin D Tuttle. Ecological impacts of wind energy development on bats: questions, research needs, and hypotheses. *Frontiers in Ecology and the Environment*, 5(6):315–324, 2007b.

Sharon Lohr. *Sampling: design and analysis*. Nelson Education, 2009.

Peter McCullagh. Generalized linear models. *European Journal of Operational Research*, 16(3):285–292, 1984.

Michael L Morrison. *Searcher bias and scavenging rates in bird/wind energy studies*. National Renewable Energy Laboratory NREL/SR-500–30876. Golden, Colorado, 2002.

Jennie L Pearce and Mark S Boyce. Modelling distribution and abundance with presence-only data. *Journal of applied ecology*, 43(3):405–412, 2006.

Arthur Pewsey, Markus Neuhäuser, and Graeme D Ruxton. *Circular statistics in R*. Oxford University Press, 2013.

R Core Team. *R: A Language and Environment for Statistical Computing*. R Foundation for Statistical Computing, Vienna, Austria, 2015. URL `http://www.R-project.org/`.

Barry S Rowlingson and Peter J Diggle. Splancs: spatial point pattern analysis code in s-plus. *Computers & Geosciences*, 19(5):627–655, 1993.

Peter Shoenfeld. Suggestions regarding avian mortality extrapolation. *Prepared for the Mountaineer Wind Energy Center Technical Review Committee*, 2004.

Zbyněk Šidák. Rectangular confidence regions for the means of multivariate normal distributions. *Journal of the American Statistical Association*, 62(318):626–633, 1967.

Robert Suryan, Roberto Albertani, and Brian Polagye. A synchronized sensor array for remote monitoring of avian and bat interactions with offshore renewable energy facilities. 2016.

U.S. Department of Energy. *Wind Vision: A New Era for Wind Power in the United States*. CreateSpace Independent Publishing Platform, 2015. ISBN 9781508860549. URL https://books.google.com/books?id=viZNrgEACAAJ.

U.S. Department of Energy. *Electric Power Monthly*. Feburary 2017. URL https://www.eia.gov/electricity/monthly. Energy Information Administration.

U.S. Fish and Wildlife Service. *US Fish and Wildlife Service land-based wind energy guidelines*. US Fish and Wildlife Service, 2012.

Jay M Ver Hoef. Who invented the delta method? *The American Statistician*, 66(2): 124–127, 2012.

David I Warton, Leah C Shepherd, et al. Poisson point process models solve the pseudo-absence problem for presence-only data in ecology. *The Annals of Applied Statistics*, 4(3):1383–1402, 2010.

G Wobeser and AG Wobeser. Carcass disappearance and estimation of mortality in a simulated die-off of small birds. *Journal of Wildlife Diseases*, 28(4):548–554, 1992.